Mechanical behaviors and applications of shape memory polymer and its composites [F]

[iD] **Wei Zhao,** [iD] **Nan Li, Liwu Liu, et al.**

COLLECTIONS

[F]   This paper was selected as Featured

View Online   Export Citation   CrossMark

Applied Physics Reviews

Special Topic: Materials and Technologies
for Bioimaging and Biosensing

Submit Today!

Mechanical behaviors and applications of shape memory polymer and its composites Ⓕ

View Online   Export Citation   CrossMark

Wei Zhao,[1] Ⓘ Nan Li,[1] Ⓘ Liwu Liu,[1] Jinsong Leng,[2,a] Ⓘ and Yanju Liu[1,a] Ⓘ

AFFILIATIONS

[1]Department of Astronautical Science and Mechanics, Harbin Institute of Technology (HIT), P.O. Box 301, No. 92 West Dazhi Street, Harbin 150001, People's Republic of China

[2]Centre for Composite Materials, Harbin Institute of Technology (HIT), P.O. Box 3011, No. 2 YiKuang Street, Harbin 150080, People's Republic of China

[a]Authors to whom correspondence should be addressed: lengjs@hit.edu.cn and yj_liu@hit.edu.cn

ABSTRACT

Shape memory polymer (SMP) and SMP composites (SMPC) can memorize the permanent shape and recover from the temporary shape to the permanent shape when stimulated by the appropriate stimuli. Because of the unique shape memory effect, coupled with its low cost, low density, high specific strength, biodegradability, biocompatibility, and other characteristics, SMP and SMPC have become possible materials to solve the problems currently faced by space deployable structures, biomedical devices, mold manufacturing, release devices, etc. This work reviews the research and developments of SMP and SMPC, including the achievements in constitutive theory, the applications, and prospects in aerospace, biomedical medicine, intelligent mold, and release devices.

Published under an exclusive license by AIP Publishing. https://doi.org/10.1063/5.0126892

TABLE OF CONTENTS

I. INTRODUCTION

An intelligent material is a type of functional material integrating sensing, control, and actuation, which can actively perceive temperature, chemical action, electricity, light, magnetic field, and other external stimuli. By adjusting its structure and property, it can appropriately respond to the changes in the external environment through self-warning, self-diagnosis, self-adaptation, and self-repair.[1,2] Intelligent materials are the multidisciplinary product of mechanics, materials, physics, chemistry, machinery,

microelectronics, etc. Active variant materials, programmable materials, digital materials, and reconfigurable materials belong to the category of intelligent materials.

Shape memory polymer (SMP), as a branch of polymer-based intelligent material, can select and control the material system from a temporary state to an original state in a preset way under external stimuli.[3–8] The matrix of SMP includes epoxy, polyvinyl alcohol, polystyrene, polylactic acid (PLA), polyurethane (TPU), polycaprolactone (PCL), etc. According to whether the shape memory effect (SME) is reversible, SMP can be categorized as one-way or two-way SMP. Two-way SMP exhibits a reversible SME cycle, which means it can switch between the original and temporary states without external load.[9,10] Furthermore, according to the number of temporary shapes that can be memorized, SMP can be divided into double SME, triple SME, and multiple SME.

However, the modest modulus, strength, and function greatly limit the application of SMP. By combining SMP with other reinforcement materials, the fabricated shape memory polymer composites (SMPC) not only have excellent mechanical properties and large bearing capacity but also can provide a variety of actuation modes.[11–13] SMPC has many advantages, such as low cost, easy processing, lightweight, and broad application prospects. For example, a variety of long/short fiber and nanoparticle-reinforced SMPCs are proposed to improve the stiffness, recovery force, and functionality.[14–17] SMPC can be fabricated in the following methods: mechanical blending, *in situ* polymerization, chemical cross-linking, etc. According to inclusion type, SMPC can be divided into particle/short fiber-reinforced, nanomaterial-reinforced, and continuous fiber-reinforced SMPC. The addition of inclusions improves the basic mechanical properties and endows SMPC with new actuation properties, such as electric, optical, magnetic, and microwave actuation.

One of the most important properties of SMP/SMPC is its temperature-dependent stiffness. At low temperatures, SMP/SMPC is in a glassy state with high elastic modulus and small limit deformation. When the temperature reaches above the glass transition temperature (T_{trans}), SMP/SMPC is in a rubbery state with low stiffness and high-limit deformation. Generally, the elastic modulus at low temperatures is two orders of magnitude higher than that at high temperatures. To better understand the thermodynamic mechanism, a large number of constitutive theories for SMP and SMPC have been reported to predict the thermodynamic properties. Utilizing the variable stiffness, self-sensing, and self-recovery of SMP/SMPC, deployable structures for different purposes have been proposed. SMP/SMPC has great prospects in many fields, including aerospace, biomedicine, intelligent mold, intelligent release devices, etc., as shown in Fig. 1.

In this paper, we reviewed the development of SMP/SMPC. First, we review the underlying mechanism of SME, SMP with multiple and triple SME, two-way SMP, and SMPC with different actuation methods. To better describe the mechanical behavior of SMP/SMPC, a detailed review of the experimental and theoretical research of SMP and SMPC is presented in Sec. III. Subsequently, in Sec. IV, we give a summarization of the applications of SMP/SMPC, ranging from the aerospace field, biomedical medicine, and smart mold field to release devices. Finally, in Sec. V, we discuss the future directions and challenges of SMP/SMPC.

II. SHAPE MEMORY POLYMER AND SHAPE MEMORY POLYMER COMPOSITES

A. Shape memory polymer

1. Shape memory mechanism

SMP can recover from the temporary shape to the initial shape under the appropriate stimulus. The complete SME process is shown in Figs. 2(a) and 2(b), including four steps: heating and programming, cooling and unloading, and heating and recovery. First, SMP is heated to a high temperature above T_{trans} and applied to an external load. Second, SMP is gradually cooled down to a temperature lower than T_{trans}. Third, the residual stress is unloaded. Finally, reheating it to a temperature higher than T_{trans}, SMP gradually recovers to the initial shape.

Generally, it is assumed that the molecular structure of SMP mainly composes fixed and reversible phases to maintain the initial shape and enabled SMP to deform. The synergistic effect of the fixed phase and reversible phase endows SMP with SME. With the deepening of research, researchers[24] have given a further explanation of the shape memory mechanism as shown in Fig. 2(c). It is considered that the fixed phase should be the stable polymer networks represented by the red cube, existing in the form of chemical cross-linking, molecular entanglement, interpenetrating networks, or crystalline phases. The fixed phase can remember and recover the initial shape, preventing flow deformation. The transition process can be the rubbery–glassy phase transition, the anisotropic–isotropic transition of liquid crystal, the crystallization-melting transition, or the dissociation–association of reversible molecular and supramolecular. The "lock" represents the reversible phase, and when the external environment changes, the reversible phase will change between the softening and the hardening state, endowing the material with deformation ability.

2. SMP with triple and multiple SME

Generally, according to the number of temporary shapes, the SME can be divided into double SMEs and multiple SMEs. In the recovery process, only one transformation can occur, that is, the recovery from one temporary shape to a permanent shape is called double SME. SMP with multiple SMEs has multiple temporary shapes that can be fixed at a time, and the recovery process is carried out step by step.[25,26] For this kind of SMP, two strategies can obtain multiple SMEs. The first strategy is to design an SMP with a wide thermal transition temperature,[27,28] and the other is to design an SMP with multi phases, where each phase can transform individually with the recovery of a temporary shape.[29,30] In particular, the realization of the second strategy is more complex, because it requires a comprehensive design for the polymer molecular structure, especially strict interval requirements for the transition temperature of each phase.

In 2006, Lendlein *et al.*[29] reported a kind of SMP with triple SMEs, which was realized by constructing a two-phase polymer network. The polymer system consisted of two separate domains, the PCL domain, and the polyethylene glycol (PEG) domain, respectively. The melting temperature of the PCL domain was between 50 and 60 °C, while the melting temperature of the PEG domain was 38 °C. Different melting temperatures provided two separate transition temperatures for the realization of the triple SMEs. As shown in Fig. 3(a), the temporary shape was transformed from A to B at 40 °C, and with the temperature rising to 60 °C, the temporary shape B recovered to
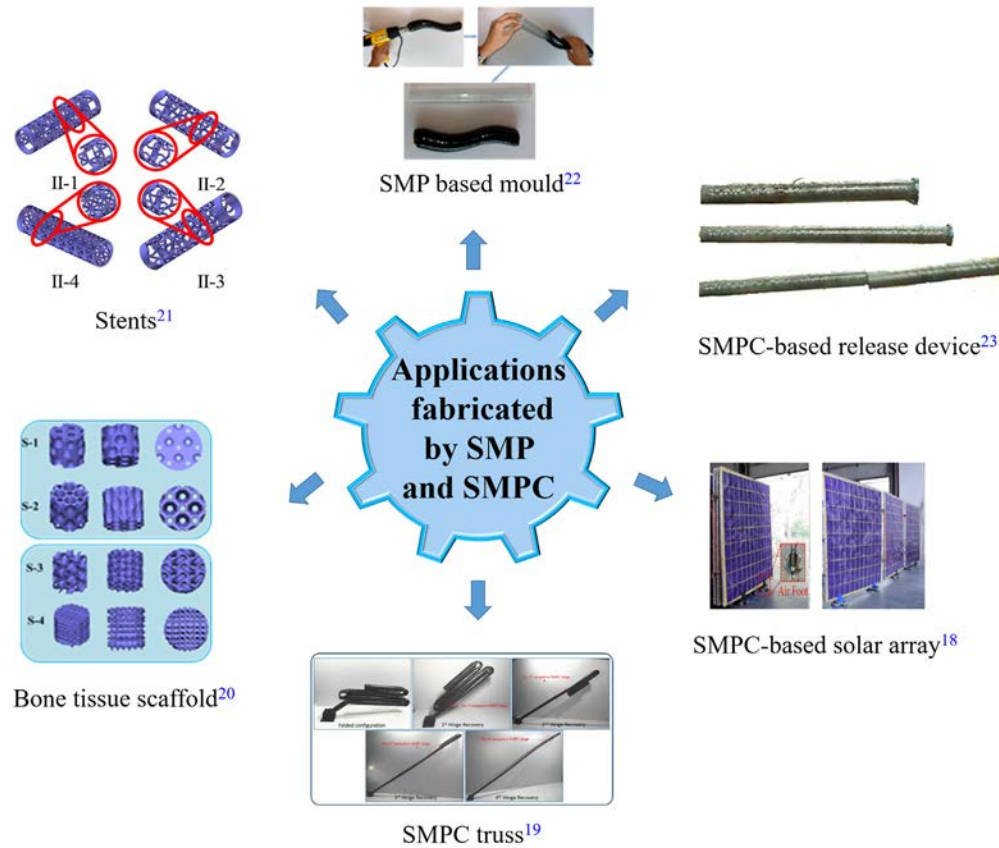
FIG. 1. Typical applications of SMP and SMPC. Reproduced with permission from Liu *et al.*, Compos. Part B **193**, 108056 (2020). Copyright 2020 Elsevier.[18] Reproduced with permission from Liu *et al.*, Compos. Struct. **206**(15), 164–176 (2018). Copyright 2018 Elsevier.[19] Reproduced with permission from Zhao *et al.*, Compos. Sci. Technol. **205**, 108563 (2021). Copyright 2021 Elsevier.[20] Reproduced with permission from Zhao *et al.*, Compos. Sci. Technol. **229**, 109671 (2022). Copyright 2022 Elsevier.[21] Reproduced with permission from Du *et al.*, Compos. Struct. **133**, 930–938 (2015). Copyright 2015 Elsevier.[22] Reproduced with permission from Zhao *et al.*, J. Harbin Inst. Technol. **48**(05), 1–17 (2016). Copyright 2016 Harbin Gongye Daxue/Harbin Institute of Technology.[23]

the initial state C. The sample experienced two recovery processes, realizing the triple SMEs.

Zhou *et al.*[31] fabricated a star-shaped shape memory polyurethane (SMPU) with a wide range of melting temperatures, which exhibited excellent triple SMEs. Star-shaped PCL was the soft segment, diphenylmethane diisocyanate was a chain extender, and butanediol was the hard segment. As shown in Fig. 3(b), the temporary state B was obtained from the original state A at 65 °C and fixed at 40 °C. Subsequently, temporary state C was obtained at 40 °C and fixed at 0 °C. When heated to 40 °C again, the temporary shape C began to recover to the temporary shape B in 10 s. Finally, temporary shape B recovered to its original state A when the temperature was heated to 65 °C. During the programming and recovery process, two temporary shapes were fixed and recovered, achieving triple SMEs.

Li *et al.*[32] fabricated a kind of SMPC with triple SMEs, which had two distinct T_{trans} of 50 and 110 °C. As shown in Fig. 3(c), the test sample was given a temporary state II at 130 °C and fixed at 75 °C for 60 s. Subsequently, the spiral-like temporary shape III was obtained at 75 °C and fixed at 20 °C for 60 s. After the programming process, the specimen was heated to 75 °C for 6 s, and it recovered from temporary

shape III to temporary shape II. Finally, temporary shape II recovered to initial shape I after being heated at 130 °C for 20 s. Maimaitiming *et al.*[33] fabricated a kind of SMP with triple SMEs by mixing polyolefin elastomer (POE) and polypropylene (PP). The triple SMEs were realized utilizing the layered crystallization of polypropylene and bundle crystallization of polyolefin elastomer. The programming process of the triple SMEs is shown in Fig. 3(d).

Lai *et al.*[34] fabricated a kind of SMP with triple SMEs as shown in Fig. 3(e). The triple SMEs were realized by using the crystallization and melting temperature of phase separation of olefin block copolymer (OBC) and PCL. Utilizing different T_{trans} of PU and PMMA, Zhang *et al.*[35] synthesized a microscopic island-separated polyurethane/polymethyl methacrylate (PU/PMMA) with triple SMEs as shown in Fig. 3(f). The shape-fixed ratio of the first shape was 76% at 50 °C, and the shape-fixed ratio of the second shape was 89% at 0 °C. The shape recovery ratio from the second shape to the first shape was 79% at 50 °C, and the shape-fixed ratio from the first shape to the original shape was 93% at 80 °C.

By the chemical method, mixing SMP with different T_{trans} is a common method of preparing SMP with multiple SMEs.[36,37] The key
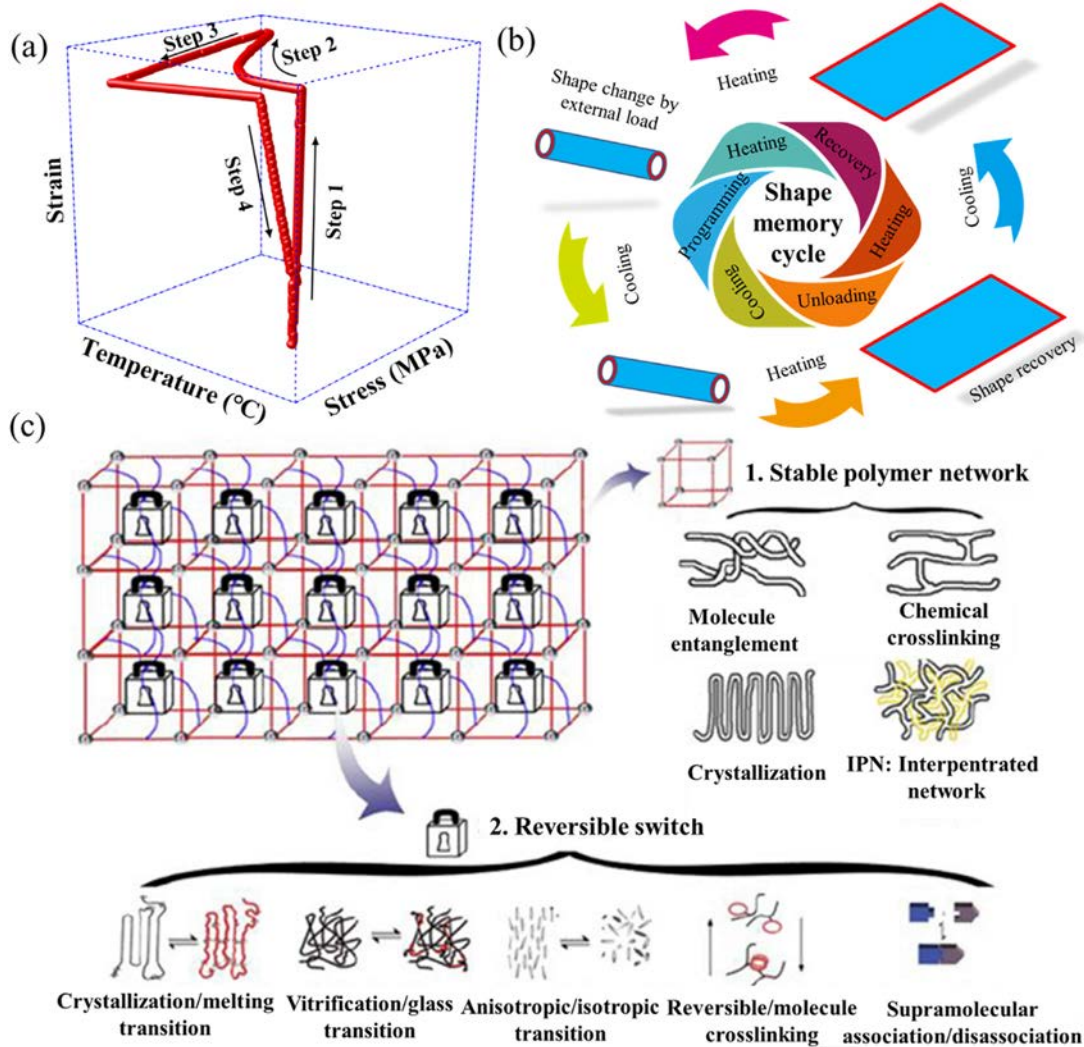
FIG. 2. Shape memory cycle (a) thermal–mechanical cycle experimental curve (b) schematic of the typical thermal–mechanical cycle (c) illustration of shape memory mechanism. Reproduced with permission from Meng *et al.*, Polymer **54**(9), 2199 (2013). Copyright 2013 Elsevier.[24]

is to obtain an SMP with multiple separated T_{trans}. Furthermore, Xie proposed a relatively simple method to achieve multi-SMEs.[27] Utilizing the wide phase transition temperature range (55–130 °C) of the perfluorinated sulfonic acid membrane (PSAM), they programmed and obtained three temporary shapes at different temperatures. When the specimen is heated to the corresponding programming temperatures, two obvious recovery processes can be observed in sequence. Consequently, it can be inferred that multiple SMEs can be achieved as long as the phase transition temperature range is wide enough. Figure 4(a) exhibits the quadruple SMEs of PSAM. The sample with the initial shape S0 is deformed at 140, 107, and 68 °C to obtain the temporary shapes S1, S2, and S3, respectively. Subsequently, when the sample is heated to the corresponding temperature, the temporary shapes are recovered step by step (S2rec, S1rec, S0rec).

By blending the polyolefin elastomer (POE) and olefin block copolymer (OBC), Gao *et al.*[38] fabricated a kind of SMP with four SMEs based on three crystallization-melt transition processes. As shown in Fig. 4(b), in the programming process, the stresses applied were 0.15, 0.3, and 0.5 MPa, the fixed temperatures were 50, 30, and 5 °C, and the recovery temperatures were 30, 50, and 85 °C, respectively. Using poly (methyl methacrylate)/polyethylene glycol (PMMA/PEG), Li *et al.*[39] prepared a kind of SMP with a semi-interpenetrating network structure and quadruple SMEs. The polymer network had a wider range of T_{trans} (45–125 °C), and 35, 50, 70, and 110 °C were the node temperatures to obtain the three temporary shapes. As shown in Fig. 4(c), the structure gradually recovered to the original shape through the quintuple SMEs when heated above the corresponding transition temperature. Moreover, Wu *et al.*[40] fabricated a kind of 3D printed heat-driven multilayer composite material with quadruple SMEs utilizing three
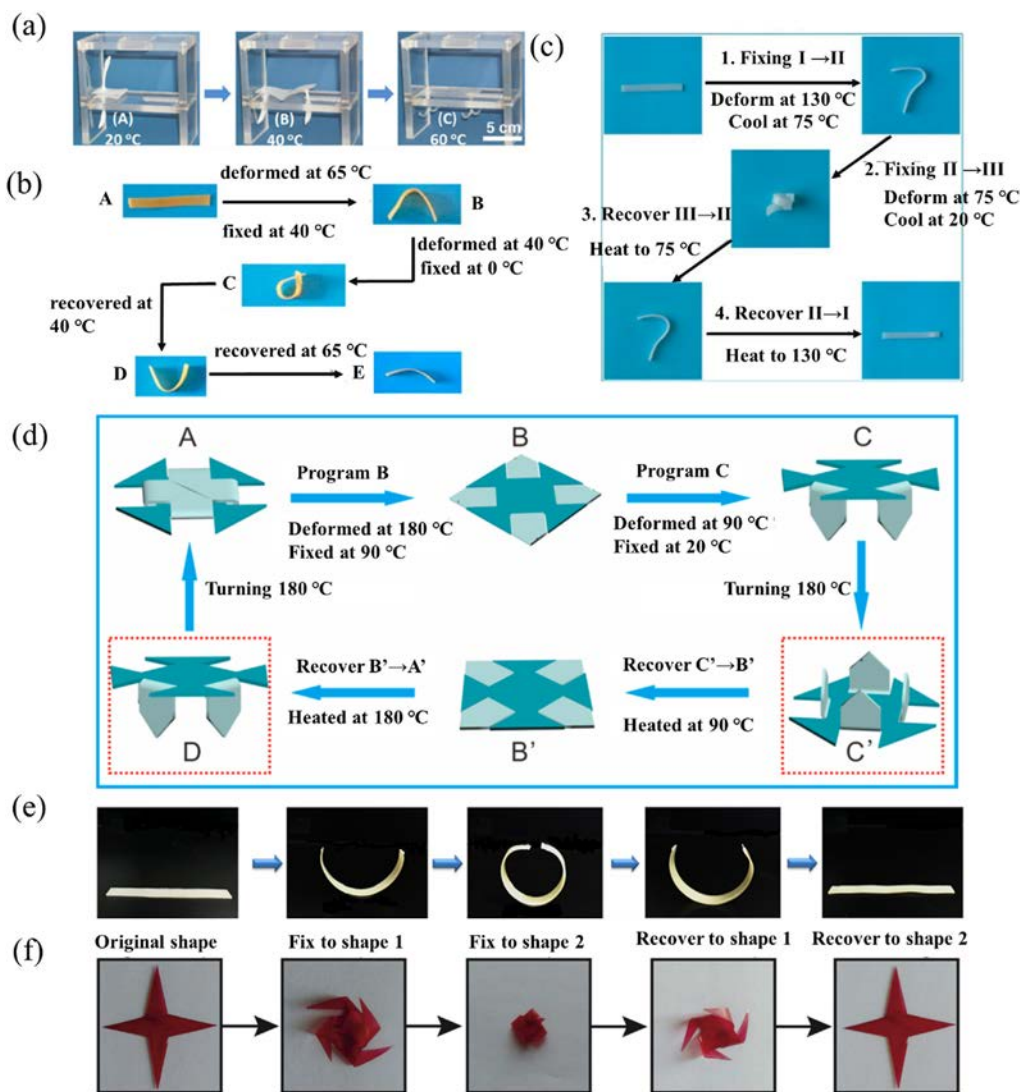
FIG. 3. Shape memory polymer with triple SMEs. (a) Demonstration of triple SMEs stimulated by heat flow with 40 and 60 °C. Reproduced with permission from Bellin et al., Proc. Natl. Acad. Sci. **103**(48), 18043–18047 (2006). Copyright 2006 National Academy of Sciences.[29] (b) Triple SMEs of polyurethane-based SMP with wide melting transition temperature. Reproduced with permission from Yang et al., ACS Appl. Mater. Interfaces **6**, 6545 (2014). Copyright 2014 American Chemical Society.[31] (c) Triple SMEs of SMP with two distinct glass transition temperatures of 50 and 110 °C. Reproduced with permission from Li et al., J. Mater. Chem. A **3**(48), 24532 (2015). Copyright 2015 Royal Society of Chemistry. (d) Schematic diagram of the triple SMEs of shape memory flower model of POE/PP[33] (e) Triple SMEs of TPU/OBC/PCL blend.[34] Reproduced with permission from Lai et al., J. Polym. Res. **24**(10), 161(2017). Copyright 2017 Springer Nature. (f) Triple SMEs of PU/PMMA.[35] Reproduced from Zhang et al., RSC Adv. **7**(54), 33701–33707 (2017). Copyright 2017 Royal Society of Chemistry.

kinds of SMP of Tango Blackplus, DM8530, and DM9895. During the heating process, the bending, spiral, and wavy deformation behaviors of the composite materials with different configurations was shown in Fig. 4(d).

3. Two-way SMP

Generally, SME is a one-way process and an irreversible behavior. After recovering to the initial shape, SMP should be programmed again before repeating the SME. However, SMP with reversible two-way SME can arbitrary switch between two different shapes by applying external stimuli and without an additional programming process.[41,42] The transitional process between the anisotropic and isotropic phases will cause the shrinking of the liquid crystal elastomers (LCE).[43] When the ambient temperature is below T_{trans}, LCE expands again, resulting in reversible contraction/extension behavior.

Behl et al.[42] synthesized a kind of crosslinked ethylene–vinyl acetate copolymer possessing a wide crystallization and melting temperature range. It spontaneously shortens when heated up, while elongates when cooled down to an appropriate temperature. As shown in Fig. 5(a),
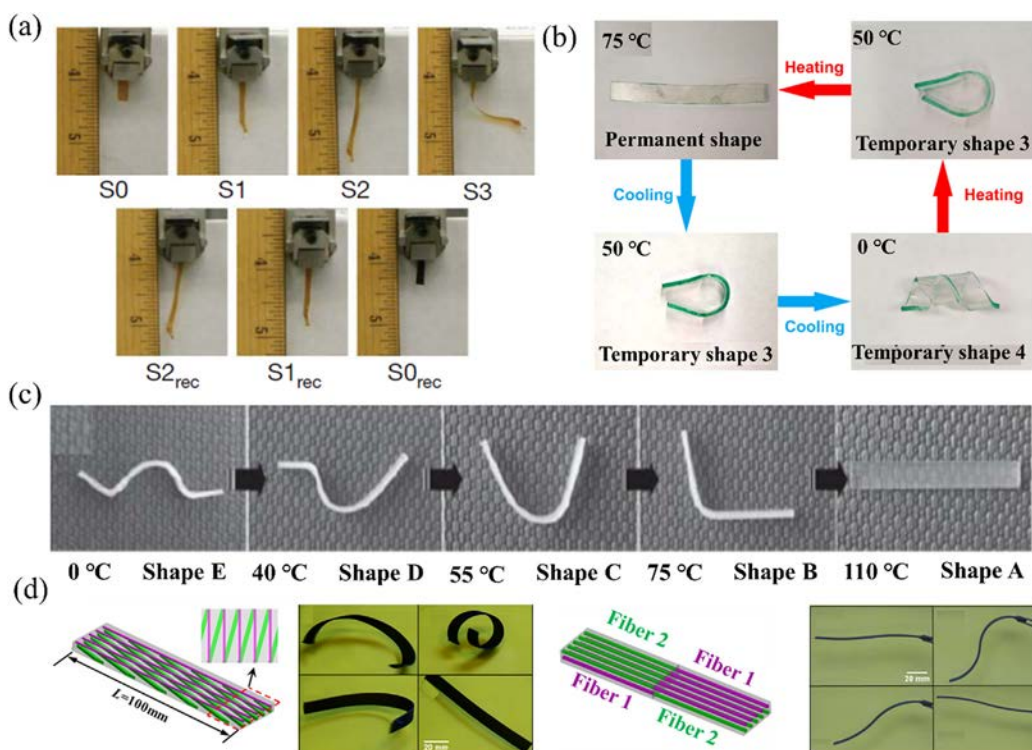
FIG. 4. Multiple shape memory deformations processes. (a) Quadruple SMEs.[27] Reproduced with permission from Xie *et al.*, Nature **464**, 267–170 (2010). Copyright 2010 Springer Nature. (b) Quadruple shape memory test of POE/OBC. Reproduced with permission from Gao *et al.*, Ind. Eng. Chem. Res. **58**(42), 19495–19502 (2019).[38] Copyright 2019 American Chemical Society. (c) Quadruple SMEs of PMMA/PEG with semi-interpenetrating polymer network.[39] Reproduced with permission from Li *et al.*, J. Mater. Chem. **21**(33), 12213 (2011). Copyright 2011 Springer Nature. (d) Multi-shape memory recovery process of curved and spiral-shaped structures.[40] Reproduced with permission from Wu *et al.*, Sci. Rep. **6**, 24224 (2016). Copyright 2016 Springer Nature.

when the temperature is above T_{prog}, all the crystallization regions of the polymer are melted, and it can reset the original shape. When the temperature T_{sep} is between T_{prog} and the lowest point (T_{low}) in the crystallization-melting temperature range, the polymer is in a semi-crystalline state. The crystallization region near T_{sep} corresponds to the reversible phase, and the region higher than T_{sep} corresponds to the fixed phase. When the temperature rises, T_{sep} moves toward a higher temperature, and conversely, T_{sep} moves to a lower temperature. In a certain temperature range, no matter whether the temperature increases or decreases, the material exhibits a two-way SME.

Furthermore, another kind of SMP with a two-way SME can be obtained by introducing crystalline liquid crystal monomers into the polymer network.[44] For example, Pei *et al.*[45] developed a kind of SMP with a two-way SME utilizing LCE that contained exchangeable covalent bonds, as shown in Fig. 5(b). After simple processing, the exchangeable covalent bond aligned directionally. Based on glass transition and liquid crystal transition, this system also exhibited triple SMEs. Generally, LCE-based polymers are just limited to changes in volume, and complex shape memory deformation cannot occur. However, the combination of LCE and polystyrene-based SMP can realize complex shape memory deformation behavior.[46] As shown in Fig. 5(c), when the material was heated to a certain temperature, the sample started to fold and wrinkle. When the temperature was above the T_{trans} of styrene, the

fold and wrinkle deformation was recovered. When the sample was cooled to 30 °C again, the sample bent and folded in the opposite direction, and the deformed shape was fixed again.

In addition to the LCE, a similar two-way SME can be achieved by other polymer systems.[47] For example, Behl *et al.*[41] synthesized a multiphase copolyester carbamate network with two different crystalline segments based on polycaprolactone and polypentagenolone (PPD), as shown in Fig. 6(a). These different chain segments formed the actuator domains (AD) and shifting-geometry determining domains (SGDD). The AD expanded during cooling and the SGDD contracted during heating. Therefore, the copolymer network can be activated repeatedly between two different shapes without stress, realizing a two-way SME. Sheiko *et al.*[48] proposed another polymer system with a two-way SME, which was realized by the partial melting and crystallization of the semi-crystalline elastomer. Through the heating (38 °C) and cooling (5 °C) cycle, the grab and release actions of the gripper triggered by temperature are illustrated in Fig. 6(b). Moreover, Li *et al.*[49] fabricated a kind of light-actuated SMPC with a two-way SME using polyvinyl alcohol–vinyl acetate. Stimulated by UV, the gripper opened to a certain extent to form shape II, while when the UV was closed, shape II recovered to the original shape I as shown in Fig. 6(c). Under cyclic opening and closing of UV irradiation, the sample realized the two-way SME.
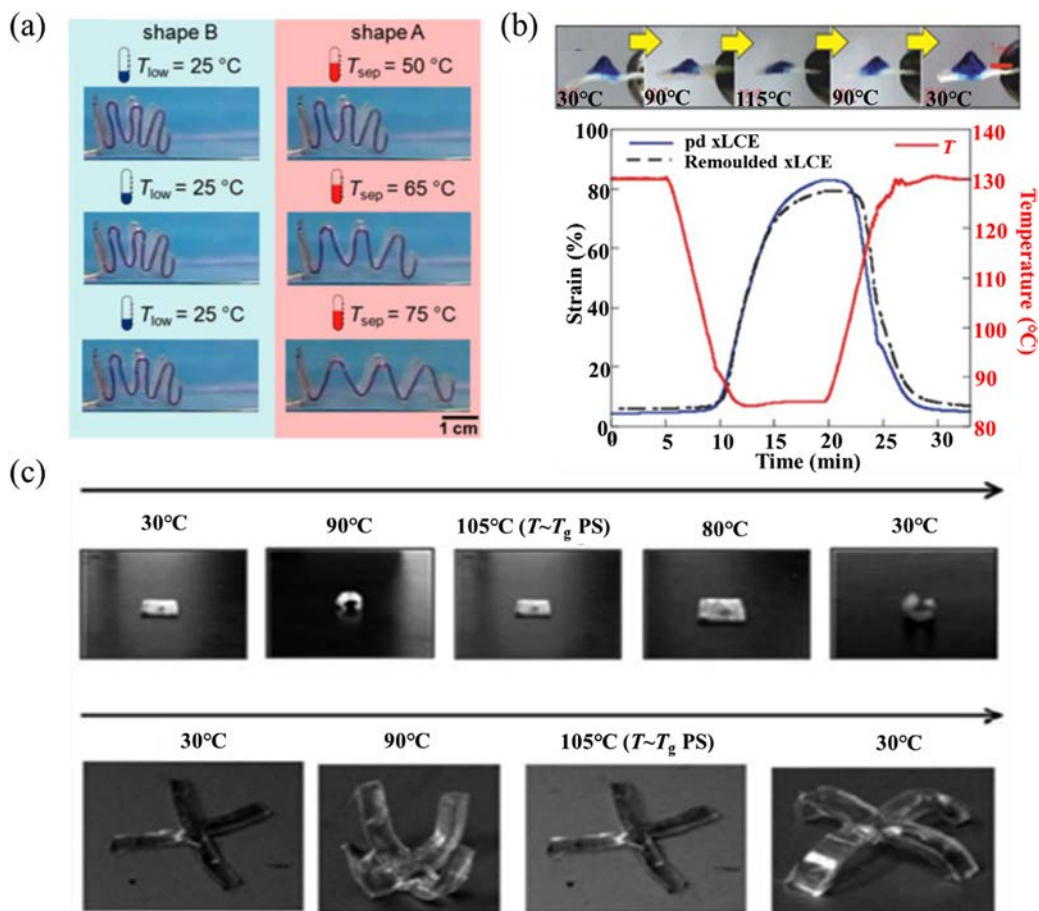
FIG. 5. Two-way LCE-based polymers (a) Two-way SME of ethylene–vinyl acetate copolymer.[42] Reproduced with permission from Behl et al., Proc. Natl. Acad. Sci. **110**(31), 12555–12559 (2013). Copyright 2013 National Academy of Sciences. (b) Two-way SME of liquid crystal elastomer. Reproduced with permission from Pei et al., Nat. Mater. **13**, 36–41 (2014). Copyright 2014 Springer Nature.[45] (c) Two-way SME of LCE/polystyrene.[46] Reproduced with permission from Agrawal et al., Soft Matter **10**, 1411–1415 (2014). Copyright 2014 Royal Society of Chemistry.

Ze et al.[50] developed a kind of magnetic actuation SMPC that integrated programmable, unconstrained, fast, and reversible shape conversion properties as shown in Fig. 6(d). The composite material was made of polyacrylate, micron-grade ferric tetroxide, and NdFeB particles. Utilizing the adjustable stiffness of polyacrylate matrix, it realized shape memory at a low temperature and fast drive at a high temperature. Under the action of the magnetic field, the oscillation of NdFeB particles actuated the material to produce reconfigurable rapid reversible deformation.

Gao et al.[51] developed a kind of thermoplastic ethylene/1-octene diblock copolymer with chain microstructure as shown in Fig. 6(e). The crystal size of the soft chain segment was smaller, and the melting temperature was lower, which acted as an actuator and fixed the temporary shape. Moreover, the SME properties were controlled by adjusting the chain microstructure and changing the proportion and length of the hard and soft chain segments. The copolymer exhibited not only the traditional unidirectional multi SMEs but also the two-way SME.

Wang et al.[13] fabricated a kind of bidirectional deformation soft actuator consisting of star-shaped oligomeric ε-caprolactone, star-shaped oligomeric ω-pentenolactone, and magnetic nanoparticles. The crystal deformation domain in the star oligomeric ε-caprolactone can realize the reversible drive of deformation. The geometric stability domain in the star oligomeric ω-pentenolactone was thermodynamically more stable, which can guarantee the overall stability in the deformation process. The two-way SME is shown in Fig. 6(f).

In recent years, the representative research work of SMP is shown in Table I.

B. Shape memory polymer composite

Although SMP has unique advantages, poor mechanical properties, low modulus and strength, and serious creep/relaxation phenomena of SMP greatly limit its application. By adding reinforcing phases to the polymer, all the properties are improved dramatically as shown in Table II. According to the inclusions, SMPC can be classified as
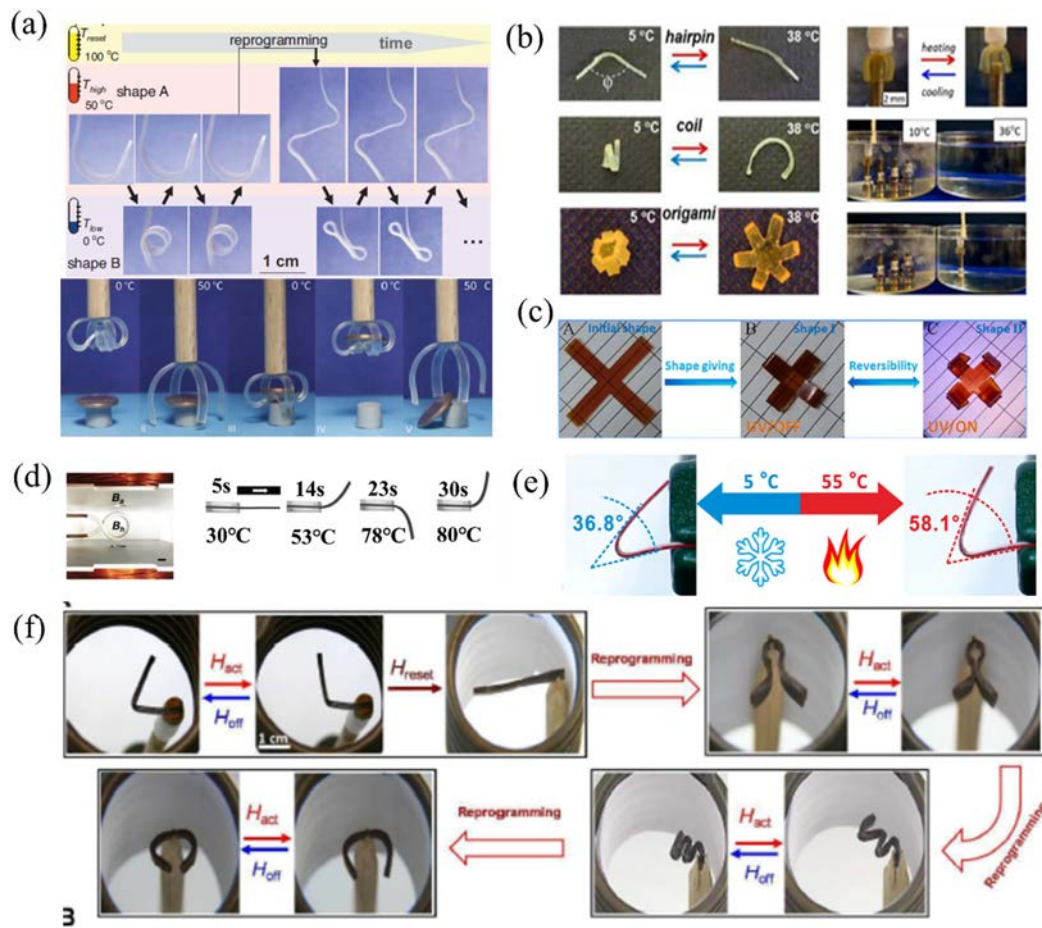
FIG. 6. SMP with two-way SME. (a) Two-way SME of the ribbon-like sample.[41] Reproduced with permission from Behl et al., Adv. Mater. **25**(32), 4466–4469 (2013). Copyright 2013 John Wiley and Sons.[41] (b) Two-way SME of semi-crystalline elastomer. Reproduced with permission from Zhou et al., Macromolecules **47**, 1768–1776 (2014). Copyright 2014 American Chemical Society.[48] (c) Two-way SME stimulated by UV irradiation. Reproduced with permission from Li et al., Compos. Part A **110**, 70–75 (2018). Copyright 2018 Elsevier.[49] (d) The working mechanism of magnetic actuation SMP and cantilever bending and gripper using a superimposed magnetic field to achieve reversible deformation.[50] Reproduced with permission from Hiraoka et al., Chem. Phys. **209**, 298–307 (2008). Copyright 2019 John Wiley and Sons.[44] (e) Schematic diagram of reversible shape memory mechanism. Reproduced with permission from Gao et al., ACS Appl. Mater. Interfaces **9**(5), 4882–4889 (2017). Copyright 2017 American Chemical Society.[51] (f) Reprogrammability under different drive geometry and reversible shape change actuated by a magnetic field.[13] Reproduced with permission from Wang et al., Mater. Horizons **5**(5), 861–867 (2018). Copyright 2018 Royal Society of Chemistry.[13]

particle reinforced SMPC, short fiber reinforced SMPC, and continuous fiber-reinforced SMPC, etc. (Fig. 7).

Heat actuation is one of the most commonly used methods to realize the shape recovery process. It requires an additional external heat source but is limited by heat transfer efficiency and energy dissipation. However, it is an effective means to achieve electric, magnetic or optical actuation functions by adding functional particles to the SMP matrix. At present, the actuation methods have developed from the initial heat actuation to a variety of indirect actuation. The electric actuation, optical actuation, magnetic actuation, and microwave actuation are indirect thermal actuation in essence. These new actuation methods, as well as multiple-stimulus response and selective actuation, provide the possibility for the comprehensive application of SMPC. According to different stimuli methods, SMPC can

be classified as heat, light, electric, magnetic, and microwave-actuated SMPC, etc.

1. Optical actuation SMPC

Introducing appropriate photosensitive groups into the SMP matrix can produce a reversible photo-covalent cross-linking reaction with the reversible conformational change of the molecular chain stimulated by light. The other method to achieve optical actuation property is to introduce photothermal functional material into the SMPC matrix.[99] By embedding the optical fiber into the SMPC matrix, the light energy with a specific wavelength can be absorbed and transformed into heat.[100] Biyani et al.[101] fabricated a kind of SMPC with an optical actuation function by utilizing the benzophenone-derivatized cellulose

TABLE I. Representative research work of SMP. Polyaminobismaleimide (PABM), shape fixed ratio (R_f), shape recovery ratio (R_r), Room temperature (T_r), High temperature (T_h), and Ultimate deformation (ε_{lim}).

Research group	SMP matrix	T_{trans} (°C)	R_f/R_r (%)	ε_{lim}(%)
Harbin Institute of Technology (Leng *et al.*)	Epoxy[52,53]	37–162.8	≥98 (R_f) ≥80 (R_r)	1.2–2.2 (T_r)
Cornerstone Research Group (Everhart *et al.*)	Epoxy[54]	100–110	≥95 (R_f) ≥97 (R_r)	3.3 (T_r) 107 (T_h)
Zhejiang University (Xie *et al.*)	Epoxy[55]	40–80	≥99 (R_f) ≥97 (R_r)	212 (T_h)
General Motors Company (Rousseau *et al.*)	Epoxy[56,57]	6–89	≥91.3 (R_f) ≥98.2 (R_r)	60 (T_h)
University of Mar Del Plata (Williams *et al.*)	Epoxy[58]	37.6–41.2	≥98 (R_f) ≥95 (R_r)	≈28 (T_r) ≈90 (T_h)
Vikram Sarabhai Space Center (Biju *et al.*)	Epoxy[59]	30–82	≥95 (R_f) ≥94 (R_r)	
3 M Company	Epoxy[60]	106		
Composite Technology Development, Inc.	Epoxy[61,62]	79.3/71		
Harbin Institute of Technology (Leng *et al.*)	Styrene[63,64]	50–90	≥95 (R_f) ≥95 (R_r)	19.1 (T_r) 204 (T_h)
Cornerstone Research Group (Everhart *et al.*)	Styrene[65–67]	47–106	≥97 (R_f) ≥98 (R_r)	3.9 (T_r) 236.4 (T_h)
Iowa State University (Larock *et al.*)	Styrene[67]	30–109	≥97 (R_f) 100 (R_r)	2–160 (T_r)
University of Mar Del Plata (Mosiewicki *et al.*)	Styrene[68]	22.4–91.2	≥84 (R_f) ≥94 (R_r)	1.05–8.32 (T_r) 4.17–32.8 (T_h)
Harbin Institute of Technology (Leng *et al.*)	cyanate ester[69,70]	156.9–259.6	≥97 (R_f) ≥95 (R_r)	2.2–8.9 (T_r)
Cornerstone Research Group (Everhart *et al.*)	Cyanate ester[71]	135–230		40 (T_h)
Vikram Sarabhai Space Center (Biju *et al.*)	Cyanate ester[72,73]	55–157	≥85 (R_f) ≥85 (R_r)	
Northwestern Polytechnical University (Wang *et al.*)	Cyanate ester[74]	101–119	≥98 (R_r)	
Xi'an Polytechnic University (Zhao *et al.*)	Cyanate ester[75]	138–165	100 (R_f) 100 (R_r)	
Harbin Institute of Technology (Leng *et al.*)	Polyimide[76–78]	321–323	≥98 (R_f) ≥98 (R_r)	
Air Force Research Laboratory (Koerner *et al.*)	Polyimide[79]	220	≥98 (R_f) ≥98 (R_r)	
Lanzhou Institute of Chemical Physics (Wang *et al.*)	Polyimide[80]	243.3–275.5	≥97 (R_f) ≥93 (R_r)	
Harbin Institute of Technology (Leng *et al.*)	PABM[81]	95–105	≥95 (R_f) ≥95 (R_r)	6.7–17.8 (T_r)
Vikram Sarabhai Space Center (Biju *et al.*)	PABM[82]	140.5–221.7	≥94 (R_f) ≥88 (R_r)	
Air Force Research Laboratory (McClung *et al.*)	PABM[83]	110–144	≥85 (R_f) ≥99.8 (R_r)	
SMP Technologies Inc.	Polyurethane[84]	−40–90		

nanocrystals as the photosensitive functional phase and ethylene oxide/epichlorohydrin copolymer as the matrix. Lendlein *et al.*[102] proposed a type of UV-actuated SMPC by introducing the cinnamic group into the SMP matrix. When the wavelength of light was greater than 260 nm, the temporary shape can be frozen by the newly formed covalent bonds. However, when the wavelength of light was less than 260 nm, the covalent bond formed in the polymer network disappeared, and SMP recovered to its initial shape.

TABLE II. Mechanical properties of SMPC. Multiwalled carbon nanotube (MWCNT).

Filling phase		wt.%	R_f (%)	R_r (%)	Moduli (MPa)	Recovery force	References
Carbon material	CNT + TPU	1–5	70	∼100		Increase by 50%	85
	Nanocarbon powder + styrene	10		75–80	2091 (20 °C) 6.4 (100 °C)	· · ·	86
	Carbon black + PLA + TPU	0–8	90	59–85.9	Increased more than one times	· · ·	87
	MWCNT + TPU	3.3	95	∼95	Increased more than one times	2 as much as polymer	88 and 89
	Carbon fiber + polyimide	5	81.3	86.1	1.81 times that of polymer (7480)	SMP is difficult to detect, and SMPC is 40.1	90
Metal	Nickel zinc iron particles + TPU	1–20			$T < T_{trans}$, increase 56 $T > T_{trans}$, increase 24	· · ·	91
Clay nanoparticle	TPU + Clay nanoparticle	1–5	93	∼85	5.2–12.2 MPa	Increase by 20% (3.8–4.8)	92
Glass fiber	TPU	10–30		∼80	$T < T_{trans}$:∼1000–2000 $T > T_{trans}$: ∼1–20	· · ·	93
	Short glass fiber + Styrene	< 2.0		∼100	Increase by 100% at 2 wt.%;	· · ·	94
	Glass fiber cloth + Epoxy	38	∼100%	99	Bending modulus increase by two orders		95
Ceramic	Epoxy + SiC particles	20	∼100%	100	Increase by 70% at 20 wt.%		96–98

Infrared light has an obvious photothermal effect, which can be used as a non-contact indirect heat source to actuate SME. Yu and Yu[103] developed a kind of graphene oxide (GO)/polymer-based material with photosensitive properties by solution casting method. The photothermal effect of GO and the programmable SME of polymer enables the nanocomposite film to exhibit fast, stable, and reversible photo-mechanical behavior. Zhang and Zhao[104] fabricated a type of SMPC with both optical actuation and self-repairing capacity utilizing surface plasmon resonance of gold nanoparticles effect. The self-repair capability triggered by light enabled it to repair the damage by itself, which was beneficial to prolong its service life. Zheng et al.[105] proposed a kind of optical actuated SMP-based microcolumn array

containing 0.1–0.2 mol. % gold nanorods. The light transmittance and the water contact angle can be adjusted by the bending degree of the microcolumn array stimulated by infrared light.

2. Electrical actuation SMPC

Most SMP is an electrically insulating material, and SMPC with conductive properties is generally fabricated by mixing with graphene oxide (GO), CNT, carbon black, and carbon nanofibers. When the voltage is applied to SMPC, SME can be triggered by the joule heat.

Valentini et al.[106] fabricated a kind of SMPC by transferring the GO sheet to the surface of the SMP, and the stiffness and hardness were
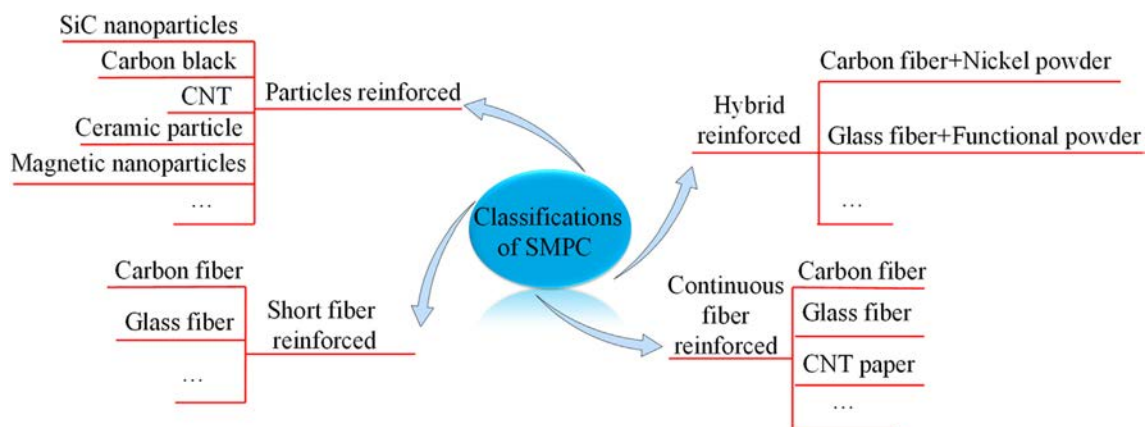

FIG. 7. Classification of SMPC.

significantly increased. Stimulated by voltage with 10 V, the specimen recovered to its original shape in 20 s. Utilizing polycyclooctene and polyethylene as the matrix, Wang et al.[107] proposed a kind of MWCNT-reinforced SMPC. The sample recovery process is stimulated by 150 V voltage and lasts for 2 min. Alam et al.[108] fabricated another electro-driven SMPC with MWCNT. When the weight fraction of MWCNT was 3%, the shape recovery ratio reached 95% within 45 s under the stimulation of 40 V voltage. Sahoo et al.[109] fabricated another polyurethane-based SMPC with electrical actuation properties by adding MWCNT. SMPC exhibited superb mechanical, and electrical properties and thermodynamics with a weight fraction of 2.5% of MWCNT. The shape recovery ratio reached 90%–96% within 20 s under 25 V voltage.

Carbon nanotube paper (CNTP) is a new functional material formed by CNT on the large-scale macroscopic surface, which is fabricated by physical vapor deposition and exhibits excellent electrical conductivity and mechanical strength.[110] The conductive properties of SMPC can be further improved by using CNTP as the conductive phase. Lu et al.[111] fabricated a kind of epoxy-based electric actuated SMPC by adding CNTP with the functional gradient property. Stimulated by the voltage of 4.8 V, the maximum temperature of SMPC mixing with 0.16 g CNTP reached 167.49 °C, and the shape recovery ratio reached 96.7% in 80 s. Utilizing nickel particles as a function phase, Leng et al.[112] fabricated a kind of electric-actuated SMPC. During the curing process, the nickel particles were induced to form a parallel conductive chain in the external uniform magnetic field, which greatly increased its conductivity efficiency. Experiments indicated that SMPC with nickel particles arranged in chains had better thermodynamic properties, electrical conductivity, and electric actuation properties. The sample with 10 wt. % nickel recovered to its initial shape stimulated by 20 V voltage in 90 s.

3. Solution actuation SMPC

With the solution permeating into the SMP matrix, the absorbed solvent molecules produce a plasticizing effect on the polymer network, which will reduce the interaction force of molecular chains and lower the transition temperature. When the T_{trans} drops to room temperature, the elastic strain energy fixed in the molecular chain will be released, and SME is triggered.[113] Generally, research on the solution or humidity-actuated SMP focuses on polyurethane-based SMP or gel-based SMP. However, the strength and stiffness of the solution-actuated SMP are relatively low, which limits the application of certain aspects.

Polyurethane-based SMP exhibits significant water actuation SME, and with the number of water molecules in the polymer increasing, T_{trans} decreases gradually until reaching diffusion equilibrium. Nanocellulose is the most abundant natural biopolymer in nature with biodegradable, renewable, and hydrophilic properties, which can be used as the hydrophilic phase to fabricate water-actuated SMPC. Zhu et al.[114] developed cellulose nano-whisker/thermoplastic polyurethane (CNW/TPU)-SMPC with water actuation properties. The reversible hydrogen bonds of the cellulose nanocrystals existing in 3D networks were the key to realizing the water actuation. When CNW/TPU-SMPC were wetting, water molecules broke the hydrogen bonds, making SMPC soft and easy to transform between the original and temporary shapes. After the CNW/TPU-SMPC was dried at 75 °C, the hydrogen bonds formed again enabling the temporary shape to be fixed. Dagnon et al.[110] developed cellulose nanocrystalline/vinyl acetate SMPC and verified that the charge on the surface of cellulose nanocrystals enhanced the molecular diffusion capacity of water in the composite system. By this method, the water actuation efficiency was improved without affecting the modulus of SMPC.

4. Magnetic actuation SMPC

By mixing magnetic nanoparticles with the SMP matrix, the obtained SMPC can be stimulated by the alternating magnetic field. Nanoparticles will undergo high-frequency reciprocating motion in the alternating magnetic field. The collision or friction between magnetic particles and polymer matrix will generate heat and actuate the shape recovery process. Therefore, each of the magnetic nanoparticles can be regarded as a microheat source. When a large number of magnetic particles interact together, a lot of heat will generate to heat SMPC. Magnetic-actuated SMPC can realize non-contact remote drives. For example, Gu et al.[115] proposed a kind of SMPU/Fe$_3$O$_4$-based self-expanding stent that recovered to its initial shape near body temperature.

5. Microwave actuation SMPC

Stimulated by microwave, the functional phase acting as an indirect heat source can absorb microwave energy and convert it into thermal energy. The induction heat generated at the molecular level can trigger the SME and realize the uniform, fast, and remote control. Generally, some particles, such as CNT and inorganic nanoparticles, are usually added to SMP to strengthen microwave absorption capacity. For example, Kalita and Karak[113] fabricated SMPU/Fe$_3$O$_4$ composite by mixing Fe$_3$O$_4$ nanoparticles into the SMPU matrix, which exhibited excellent shape recovery properties stimulated by microwave with 2.45 GHz and 350 W. Subsequently, Kalita and Karak[116] fabricated Fe$_3$O$_4$ at MWCNTS/SMPU by mixing with Fe$_3$O$_4$ nanoparticles modified MWCNTs, which exhibited more excellent shape recovery properties, and the recovery rate increased with the content of nanoparticles. By adding MWCNTs nanoparticles into styrene-based SMP, Yu et al.[117] fabricated SMPC, in which the shape recovery rate was enhanced with the increase of MWCNTs content. Du et al.[118] added SiC nanoparticles to polyvinyl alcohol (PVA), and the obtained SMPC not only showed good SME actuated by microwave (2.45 GHz, 300–600 W) but also greatly improved the mechanical properties.

6. Multiple-stimulus response and selective actuation SMPC

In addition to the single-stimulus response SMP and SMPC, multiple-stimulus response and selective actuation SMPC and SMPC have been developed. Kumpfer and Rowan[119] reported a kind of covalently crosslinked metal coordination SMP with heat, light, and solvent response functions. In this network system, the covalent optical crosslinking network determined the initial shape, while the metal coordination segments acted as reversible phases to obtain the temporary shape. The softening and the discoordination effect responding to the external stimulation result in the multi-stimulus response. Wang et al.[120] fabricated an SMPC containing TPU and polymethacrylic acid by inducing phase separation. By adjusting the weight fraction of TPU and polymethacrylic acid, SMPC exhibited excellent heat, water, and pH-induced SMEs.
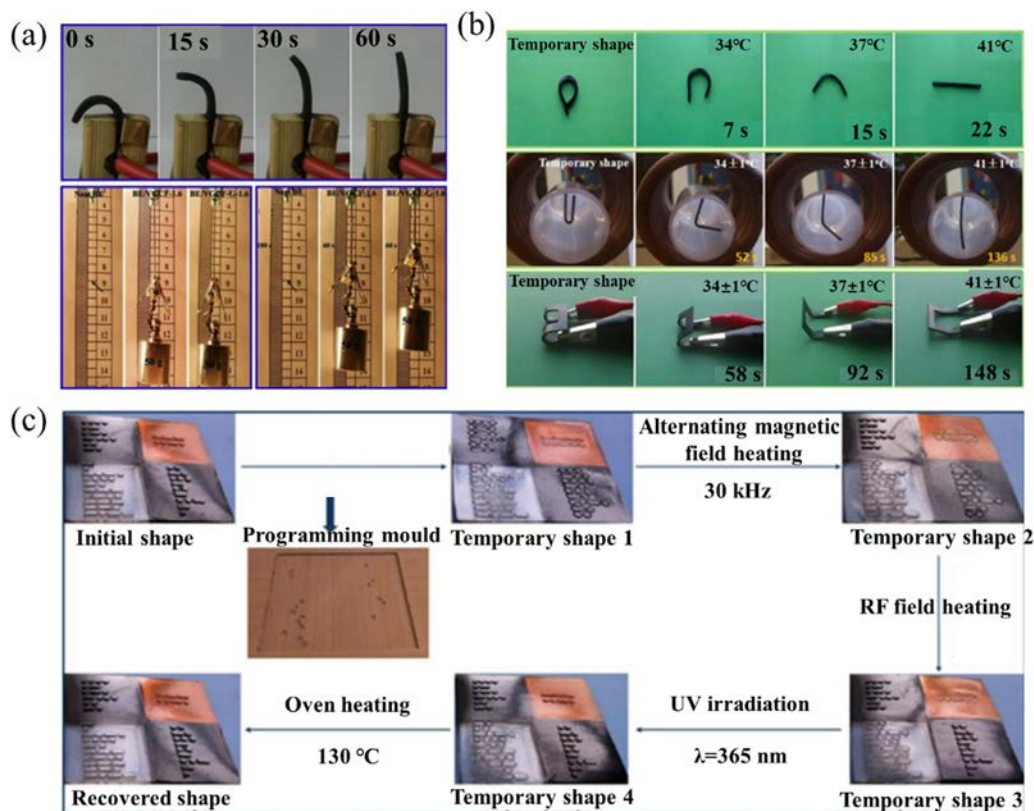
FIG. 8. Multiple-stimulus response and selective actuation. (a) SME of polyester/carbon nanofiber-GO actuated by electricity and infrared light. Reproduced with permission from Tang *et al.*, Carbon **64**, 487–498 (2013). Copyright 2013 Elsevier.[121] (b) SME stimulated by hot water, alternative magnetic field, and electric field.[122] Reproduced with permission from Li *et al.*, RSC Adv. **4**(106), 61847–61854 (2014). Copyright 2014 Royal Society of Chemistry. (c) The program and recovery of the Morse code pattern with the stimulation sequence of 30 kHz alternating magnetic field, 13.56 MHz radio frequency field, 365 nm U,V and heat in the oven at 130 °C. Reproduced with permission from Li *et al.*, ACS Appl. Mater. Interfaces **9**(51), 44792–44798 (2017). Copyright 2017 American Chemical Society.[123]

Guo *et al.*[121] fabricated a kind of SMPC with thermal, electrical, and optical response properties by mixing polyester with carbon nanofibers modified by GO. Figure 8(a) illustrated the SME of SMPC actuated by electric fields with 30 V, pure polyester stimulated by infrared light, and SMPC stimulated by infrared light. Moreover, Li *et al.*[122] fabricated a kind of SMPC with an excellent SME under the stimulation of the alternating magnetic, electric, and thermal fields as illustrated in Fig. 8(b). Leng *et al.*[123] achieved the programmable recovery of language code patterns by combining four functional modules, which were SMP, Fe_3O_4/SMPC, MWNT/SMPC, and SMPC-p-aminodiphenylimide, respectively. With imprint lithography technology, the four modules were programmed in different patterns. Subsequently, the initial code patterns were reprogrammed into temporary flat patterns. Finally, the delivered messages were obtained stimulated by the alternating magnetic field, radio frequency field, 365 nm UV, and heat in a certain order as shown in Fig. 8(c). The correct information that the carriers delivered can only be obtained with valid preset programming stimuli.

Xie *et al.*[124] proposed a kind of SMPC that can realize selective actuation stimulated by radio frequency (RF), which was fabricated using SMP-Fe_3O_4, SMP-MWCNTs, and epoxy-based SMP. As shown in Fig. 9(a), stimulated by the RF with 296 kHz and 13.56 MHz,

SMPC-Fe_3O_4 and SMPC-MWCNTs were recovered to the initial shape, respectively. Finally, when the sample was placed in the oven, the temporary shape of the pure epoxy SMP in the middle segment was recovered. Yang *et al.*[125] fabricated a kind of epoxy-based multi-response SMPC that can realize local control stimulated by light with different wavelengths as shown in Fig. 9(b). The three segments of the multi-response SMPC samples recovered to the initial shape step by step stimulated by light with wavelengths of 365 and 808 nm, and heat, respectively. Leng *et al.*[32] developed a kind of multi-stimulus response SMPC, which was fabricated by styrene-based SMP, SMP/Fe_3O_4, and SMP/MWCNTs. As shown in Fig. 9(c), the segments of the specimen filled with Fe_3O_4 nanoparticles and MWCNTs can be actuated by the alternating magnetic field and RF field. When the sample is exposed to different fields, only the corresponding part can respond to the change in the environment.

III. EXPERIMENTAL AND THEORETICAL RESEARCH OF SMP AND SMPC
A. Experimental research

To better describe the mechanical behavior of SMP and SMPC, a large number of theoretical and experimental studies of SMP and SMPC have been conducted.[126] Liu *et al.*[96] fabricated a kind of particle
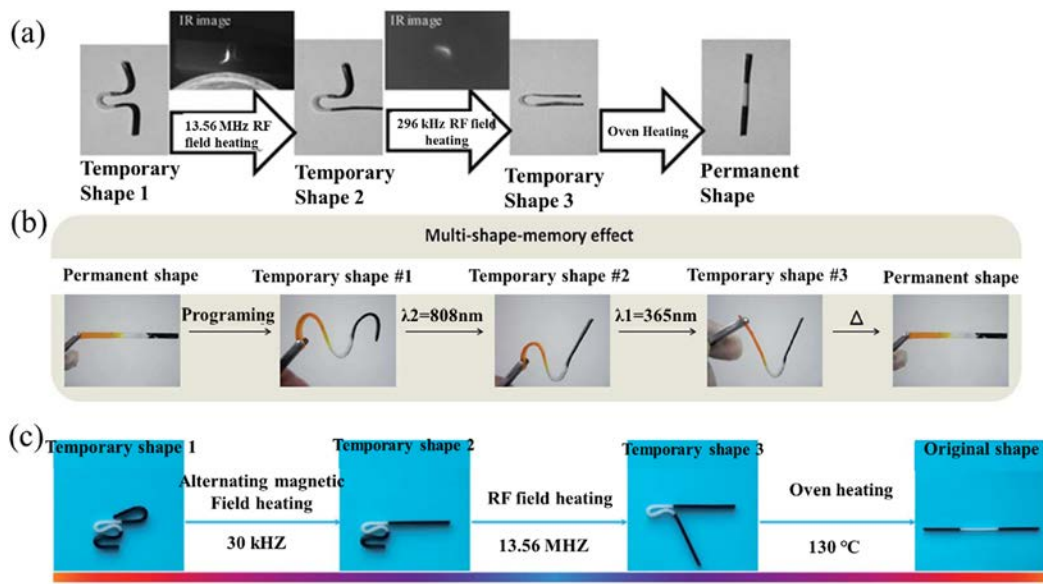
FIG. 9. Multi-stimulus response SMPC. (a) Selective actuation actuated by RF with different frequencies.[124] Reproduced with permission from He *et al.*, Adv. Mater. **23**, 3192–3196 (2011). Copyright 2013 John Wiley and Sons.[124] (b) Multi-stimulus response SMPC actuated by light with different wavelengths.[125] Reproduced with permission from Yu *et al.*, J. Mater. Chem. A **3**, 13953–13961 (2015). Copyright 2015 Royal Society of Chemistry. (c) Selective actuation with the magnetic field, RF, and heat.[32] Reproduced with permission from Li *et al.*, J. Mater. Chem. A **3**(48), 24532 (2015). Copyright 2015 Royal Society of Chemistry.

reinforced SMPC by adding SiC particles into the SMP matrix. The results of the three-point bending test indicated that the recovery force was significantly increased. Sahoo *et al.*[127] fabricated TPU-based SMPC with different mechanical and electrical properties by adding a double-walled carbon nanotube (DWCNT), polypyrrole (Ppy), and DWCNT wrapped by Ppy into the SMP matrix. The results indicated that DWCNT-reinforced SMPC had the maximum elastic modulus and strength, while SMPC reinforced by DWCNT/PPy had the best electrical conductivity.

Zhang and Ni[128] conducted three-point bending experiments on the carbon-fiber-reinforced SMPC laminated plates. The results indicated that the ply angles of fiber had a certain influence on the shape recovery property of SMPC, and when the ply angle was 90°, the shape recovery ratio reached the maximum value. Lee *et al.*[129] fabricated a series of TPU-based SMP foams and investigated the dynamic mechanical property and shape recovery properties. The results indicated that the R_f can be effectively improved by increasing the catalyst content and decreasing the molecular weight. Liu *et al.*[130] fabricated epoxy-based SMP with a high R_f (99.5%) and high R_r (100%). By controlling the curing degree of SMP, the T_{trans} can be adjustable between 44.7 and 145.3 °C.

Leng *et al.*[131] investigated the influence caused by the contents of linear monomers on the properties of SMP. DMA and DSC results indicated that the increase of linear monomers reduced the T_{trans}, breaking elongation, and elastic modulus. Westbrook *et al.*[132] designed a kind of new compression test device. The temperature difference between the specimen and the environment was effectively reduced by placing ceramic materials with low thermal conductivity at the joints of the extension rod and the compression platform. Xiao *et al.*[133] investigated the effect of scanning frequency on the storage modulus of SMP and summarized the evolution rule of relaxation time with

temperature, which was of great significance for analyzing the viscoelastic behavior of SMP. Yu *et al.*[134] fabricated a kind of SMPC by adding cup-stack CNT into the SMP matrix. With the same volume fraction of the SMP matrix, the newly fabricated SMPC exhibited stronger mechanical properties than short carbon fiber-reinforced SMPC.

The vacuum environment can cause problems, such as vacuum venting, mass loss, vacuum discharge, and vacuum cold welding, resulting in reduced sealing surface pollution of optical instruments, short circuits, breakdown of instruments, or obstruction of moving parts. Xie *et al.*[135] and Gao *et al.*[136] conducted a series of radiation experiments to investigate the resistance to space radiation properties of cyanate ester-based SMP and polyimide-based SMP. After ultraviolet radiation exposure tests, vacuum thermal cycling, and atomic oxygen, the results indicated that space irradiation did not make a significant effect on shape memory properties. Tan *et al.*[137] conducted a series of radiation experiments for epoxy-based SMP. The results indicated that it had excellent resistance capacity to space radiation. Moreover, the T_{trans}, mechanical properties, and SME were not greatly affected by space irradiation.

The traditional experimental methods are difficult to thoroughly investigate the mechanical response of SMPC and its structures because of the anisotropy and viscoelastic properties. However, the study of the mechanical properties of SMPC is the key to designing composite structures. Zhao *et al.*[138] systemically investigated the mechanical properties of SMPC structure utilizing the digital speckle correlation method (DSCM), which was of great significance for the comprehensive study of the mechanical behavior and preparation of SMPC. The DSCM can not only observe the macro-deformation of structure but also reflect the change of microstructure, which is important for understanding the internal structure of SMPC. Furthermore, Li *et al.*[139] investigated

the mechanical properties of unidirectional carbon fiber-reinforced epoxy-based SMPC through a series of experiments. The mechanical behavior of SMPC changing with temperature was summarized.

B. Constitutive theory of SMP

There are two main types of thermodynamic constitutive models for SMP: one is the macroscopic mechanical model based on the rheological theory, and the other is the microscopic mechanical model based on the phase transition theory.

1. Rheological theoretical model

Generally, the schematic of the viscoelastic rheological model usually consists of the spring element, damping element, and shape memory element. These models can qualitatively describe the shape memory and the viscoelastic and rate-dependent behavior of SMP. Tobushi et al.[140] first established a four-element thermodynamical constitutive equation by introducing a slip friction element to describe the freezing strain of SMPU. The stress–strain relationship is as follows:

$$\dot{\varepsilon} = \frac{\dot{\sigma}}{E} + \frac{\sigma}{\mu} - \frac{\varepsilon - \varepsilon_s}{\lambda} + \alpha\dot{T}, \quad \varepsilon_s = S\varepsilon_c, \tag{1}$$

where σ is the stress, ε is the strain, T is the temperature, E is the elastic modulus, α is the thermal expansion coefficient, and λ is the relaxation time. E, μ, and λ are temperature-dependent parameters. ε_c is the creep strain, ε_s is the residual strain, and S is the scale coefficient. The equations of exponential form are established to describe the change with temperature,

$$\mu = \mu_g \exp\left[\alpha_\mu\left(\frac{T_g}{T} - 1\right)\right], \quad \lambda = \lambda_g \exp\left[\alpha_\mu\left(\frac{\lambda_g}{\lambda} - 1\right)\right],$$
$$E = E_g \exp\left[\alpha_\mu\left(\frac{T_g}{T} - 1\right)\right]. \tag{2}$$

Subsequently, Tobushi et al.[141] amended the liner relationship by introducing nonlinear elastic and viscous stress. The constitutive relation of SMP under large strain is as follows:

$$\dot{\varepsilon} = \frac{\dot{\sigma}}{E} + m\left(\frac{\sigma - \sigma_y}{K}\right)^{m-1}\frac{\dot{\sigma}}{K} + \frac{\varepsilon}{\mu} + \frac{1}{b}\left(\frac{\sigma}{\sigma_c} - 1\right)^n - \frac{\varepsilon - \varepsilon_s}{\lambda} + \alpha\dot{T}. \tag{3}$$

The parameters in Eq. (3) have the same physical meaning as the relevant parameters in Eq. (1). σ_y and σ_c represent the yield stress and the ultimate creep stress. ε_s is residual strain and can be expressed as

$$\varepsilon_s = S(\varepsilon_c + \varepsilon_p). \tag{4}$$

Zhou et al.[142,143] developed a three-dimensional SMP constitutive model by introducing a solid mechanics model. An interpolation function was proposed to characterize the variation law of elastic modulus, viscosity coefficient, delay time, and thermal expansion coefficient with temperature. The model was inserted into ABAQUS utilizing the UMAT subroutine, and the mechanical properties of styrene-based SMP were simulated and predicted. Compared with the previous work, the model proved to be more effective and accurate.

Morshedian et al.[144] established a model of SMP by combining the spring unit and the dashpot unit. The viscosity coefficient η_1 was small at high temperatures, and SMP was easy to be stretched.

The shape memory properties depend on the spring element E and dashpot element η_1, and the dashpot element η_2 was mainly used to characterize the viscoelasticity. The constitutive model is as follows:

$$\sigma = \frac{E\varepsilon + \eta_1\frac{d\varepsilon}{dt}}{1 + \frac{\eta_1}{\eta_2} + \frac{t}{\tau}}, \tag{5}$$

where E is the elastic modulus and τ is the relaxation time.

Based on the thermodynamic theory, Diani et al.[145] proposed a model, which was developed on account of the assumption of deformation energy-entropy change-cohesion energy. The constitutive relation is as follows:

$$\boldsymbol{\sigma} = \frac{E^r}{3}\frac{T}{T_h}\mathbf{B} - p\mathbf{I} + \mathbf{L}^e[\ln(\mathbf{V}^e)], \tag{6}$$

where $\boldsymbol{\sigma}$, E^r, $\mathbf{B}$, p, $\mathbf{I}$, $\mathbf{L}^e$, and $\mathbf{V}^e$ represent the Cauchy stress, the elastic modulus at T_h, the left Cauchy–Green tensor, the Lagrange operator, the unit tensor, the fourth-order elastic constant tensor, and the left elongation tensor.

Based on the linear viscoelastic theory, Seok et al.[146] developed an integral type of constitutive relation by introducing the relaxation modulus, which can be expressed as

$$\sigma(t) = \int_{-\infty}^{t} E(\xi - \xi')\frac{d\varepsilon}{ds}\,ds, \tag{7}$$

where ξ denotes the intrinsic time and σ, ε and E represents stress, strain, and relaxation modulus, respectively.

Chen et al.[147] developed a rheological model to describe the mechanical properties of epoxy-based SMP. The results are highly consistent with the experiment results and can effectively predict mechanical behavior under different loading conditions and temperatures. The constitutive relation can be expressed as

$$\boldsymbol{\sigma} = \bar{\boldsymbol{\sigma}}_A + \bar{\boldsymbol{\sigma}}_B + p\mathbf{I}, \quad p = 3k\frac{\ln J}{J}, \tag{8}$$

$$\bar{\boldsymbol{\sigma}}_A = \frac{2}{J}(C_{10} + I_1 C_{01})\bar{\mathbf{B}}_M - \frac{2}{J}C_{01}\bar{\mathbf{B}}_M^2, \quad J = \det(\mathbf{F}_M), \tag{9}$$

$$\bar{\boldsymbol{\sigma}}_B = \frac{2\mu_B}{J}\mathbf{R}_B^e(\ln\mathbf{U}_B^e)\mathbf{R}_B^{et}, \tag{10}$$

where $\bar{\boldsymbol{\sigma}}_A$ is the deviator stress of the hyperelastic network, $\bar{\boldsymbol{\sigma}}_B$ is the deviator stress of the viscoelastic network, and C_{10} and C_{01} are Mooney–Rivlin material constants.

Nguyen et al.[148] established a model for amorphous-based SMP combined with the modified Eyring model. To describe the mechanical deformation, the nonlinear viscoelastic theory proposed by Reese and Govindjee[149] was introduced. In this work, the structural relaxation and viscoplastic flows below T_{trans} are linked and taken into consideration. The stress response can be expressed as

$$s = \frac{1}{J}\mu_N\frac{\lambda_L}{\lambda_{eff}}\varphi^{-1}\left(\frac{\bar{\lambda}_{eff}}{\lambda_L}\right)\left(\bar{\mathbf{b}}_M - \frac{1}{3}\bar{I}_{M1}\mathbf{1}\right) + \frac{1}{J}\mu^{neq}\left(\bar{\mathbf{b}}_M^e - \frac{1}{3}\bar{I}_{M1}^e\mathbf{1}\right), \tag{11}$$

$$p = \frac{1}{J}\kappa(\Theta_M - 1), \tag{12}$$

where κ is the bulk modulus.

Similar to Nguyen's model, Westbrook et al.[150] proposed another three-dimensional finite strain thermoviscoelastic theory. The schematic of this model consists of one balanced branch and two non-balanced branches. The balanced branch represented the mechanical behavior of SMP below T_{trans}, the nonequilibrium branches represented the mechanical behavior of SMP above T_{trans}. The Arruda–Boyce model was utilized in describing the mechanical properties represented by the equilibrium branch, and the viscous flow equation was used in describing the mechanical behavior represented by the nonequilibrium branches. The stress response for the equilibrium branch and the nonequilibrium branches can be expressed as

$$\sigma_{eq} = \frac{n\kappa_B T}{3J_M} \frac{\sqrt{N}}{\lambda_{chain}} \varphi^{-1}\left(\frac{\lambda_{chain}}{\sqrt{N}}\right) \bar{\mathbf{B}}' + K(J_M - 1)\mathbf{I}, \tag{13}$$

$$\sigma_{neq}^i = \frac{1}{J_e^i}\left[\mathbf{L}_e^i(T){:}\mathbf{E}_e^i\right], \tag{14}$$

with $J_e^i = \det(\mathbf{F}_e^i)$, $\mathbf{E}_e^i = \ln V_e^i$, $V_e^i = \mathbf{F}_e^i \mathbf{R}_e^{iT}$.

Yu et al.[151] developed a multi-branches model to characterize the glass transition process and SME of SMP. The transformation factor involved in this model depended on the temperature. When below T_{trans}, Williams–Landel–Ferry (WLF) was used to identify the transformation factor, otherwise, the Arrhenius equation was adopted to determine the value of the transformation factor.

By considering structural relaxation behavior, Castro et al.[152] proposed another viscoelastic model by introducing an enthalpy parameter. Both structural relaxation and temperature-dependent viscoelasticity were considered. The model can effectively predict the influence caused by the rate of heating on the SME circle of amorphous SMP. However, only the 1D stress recovery within a small deformation range was studied. The model is as follows:

$$\sigma(T, t) = E_1 e_m(T) + E_2 \int_0^t \frac{\partial e_m(T, s)}{\partial s} \exp\left[-\left(\int_s^t \frac{dt'}{\tau_M(T, t')}\right)^\beta\right] ds,$$

$$e_m = \ln \lambda_m, \tag{15}$$

where E_1 and E_2 represents the elastic moduli for the equilibrium and nonequilibrium network, τ_M represents the stress relaxation time, and β is the material parameter.

Srivastava et al.[153,154] proposed a model under large deformation to predict the strain–stress response of the heat-actuated SMP based on the nonlinear viscoplastic model. The model contained 45 material parameters that related to the plastic deformation and strain rate. Gu et al.[155,156] established a finite thermoviscoelastic–thermoplastic constitutive model for thermal-sensitive amorphous SMP. Fang et al.[157] proposed a fractional multi-branch thermoelastic model to better understand the free recovery behavior of SMP. Compared with the integer-order multi-branch models, the parameters were significantly reduced. The model can be utilized to predict the triple and multiple SMEs and the recovery behavior of SMP foam. Subsequently, Zeng et al.[158] proposed a multi-branch fractional derivative thermoelastic model by introducing a rate-dependent yield factor into it to describe the temperature dependence. Subsequently, Zeng et al.[159] proposed

another thermoelastic constitutive model with a clearer physical description by introducing internal variables and an uncoupled relaxation mechanism.

The rheological method based on viscoelastic theory can clearly describe aging characteristics such as creep and relaxation. However, the storage and release mechanism of shape memory strain cannot be explained reasonably, which limits the prediction ability of this kind of model.

2. Theoretical model based on phase transition approach and rheological theoretical model

Compared with the rheological theoretical model, the parameters in the phase transition model have clearer physical meanings. The constitutive model can reasonably describe the glass transformation process and SME. However, viscosity and time dependence are not considered in this model, and the creep and stress relaxation behavior cannot be described. These kinds of models are limited within the thermoelastic theory framework, and the time-dependent properties cannot be described. Consequently, by combining the rheological theoretical model and phase transition concept, more reasonable and accurate constitutive models can be established.

Relatively little research has been done on models only involving the theory of phase transitions concept. The first phase transition theory was established by Liu et al.[160] The concept of stored strain was introduced into the model to better describe the storage and release process of strain. The model can effectively describe the small deformation behavior of SMP under uniaxial tensile load. The total strain can be divided into three parts,

$$\varepsilon = \varepsilon_s + \varepsilon_m + \varepsilon_T, \tag{16}$$

where ε_s, ε_m, and ε_T are the stored strain, the elastic strain, and the thermal expansion strain, respectively. The constitutive model can be written as

$$\sigma = (\phi_f \mathbf{S}_i + (1 - \phi_f)\mathbf{S}_a) : (\varepsilon - \varepsilon_T - \varepsilon_S), \tag{17}$$

where ϕ_f, $\mathbf{S}_f$, and $\mathbf{S}_a$ are the volume fraction of the frozen phase, the flexibility tensor of the frozen phase, and the flexibility tensor of the active phase, respectively.

Chen and Lagoudas[161,162] proposed a nonlinear theory for SMP. In this model, two internal state parameters were defined: the glassy phase and the rubbery phase. According to the kinematics theory, SMP completed the phase transition process through a series of crystal nucleus molding, and the transformation between the glassy phase and the rubbery phase can be realized. The deformation gradient of a point X is as follows:

$$\mathbf{F} = \mathbf{F}_e^g(P(X, t), \theta(X, t))\mathbf{F}_{nat}, \quad \mathbf{F}_e^g = (P(X, t), \theta(X, t)), \tag{18}$$

where P is the First–Piola–Kirchhoff stress, θ is the temperature, and $\mathbf{F}_{nat}$ is the intermediate variable from the rubbery phase to the glassy phase. $\mathbf{F}_e^g$ is the elastic response and deformation of point X in the glassy phase. Furthermore, the average deformation gradient $\bar{\mathbf{F}}(t)$ is expressed as

$$\bar{\mathbf{F}}(t) = [1 - \varphi(\theta)]\mathbf{F}_e^r(P, \theta) + \int_0^t \mathbf{F}_e^g(P, \theta)\mathbf{F}_{nat}(P(\tau), \theta(\tau))\varphi'(\theta'(\tau))d\tau, \tag{19}$$

where $\mathbf{F}_e^r(P(X,t), \theta(X,t))$ is the elastic response of point X in the rubbery state and $\varphi(\theta)$ is the fraction of the glassy phase. The constitutive model is as follows:

$$P^r = -P^r \mathbf{F}_e^{r-T} + \mu^r F_e^r, P^g = -P^g \mathbf{F}_e^{g-T} + \mu^g F_e^g, \quad (20)$$

where μ is the shear modulus. The results indicated that the model prediction was in great agreement with the experiments.

Qi et al.[163] developed a three-dimensional finite deformation constitutive model. It was assumed that SMP was composed of three phases: the rubbery phase, the initial glassy phase, and the frozen glassy phase. The mechanical behavior of the glassy phase was described by the rheological model combined with the gradient decomposition, and the rubbery phase was described by Arruda–Boyce eight-chain model, and it can be expressed as

$$H_{total} = f_r H_r + f_{g0} H_{g0} + f_T H_T \quad (21)$$

with $f_r = \frac{1}{\exp(-(T-T_g)/A)}$ and $f_g = 1 - \frac{1}{\exp(-(T-T_g)/A)}$. H represents the Helmholtz free energy, and f_r, f_{g0}, and f_T represents the volume fraction of the rubbery phase, the volume fraction of the initial glassy fraction, and the volume fraction of the frozen glassy phase, respectively.

Barot and Rao[164] established a thermodynamic constitutive equation for crystallized SMP based on the assumption that the crystals increased gradually with the decrease in temperature. The constitutive model can be written as

$$\mathbf{T} = -p\mathbf{I} + (1-\alpha(t))\mu_\alpha \mathbf{B}_{k_\alpha} + \int_{t_1}^{t_2} \mu_1 \mathbf{B}_{k_{\alpha(t)}} \frac{d\alpha}{dt}$$
$$+ \int_{t_1}^{t_2} \left(\mathbf{F}_{k_{\alpha(t)}} \left(\mu_2 (J_1 - 1) \eta_{k_{\alpha(t)}} \otimes \eta_{k_{\alpha(t)}} \right.\right.$$
$$\left.\left. + \mu_3 (K_1 - 1) m_{k_{\alpha(t)}} \otimes m_{k_{\alpha(t)}} \right) \right) \frac{d\alpha}{d\tau} d\tau, \quad (22)$$

where p, $\alpha(t)$ represents the operator and the crystal weight fraction at time t. μ_1, μ_2, and μ_3 are material constants, $\mathbf{B}_{k_\alpha}$ and $\mathbf{B}_{k_{\alpha(t)}}$ represents the left Cauchy–Green tensor, $\mathbf{F}_{k_{\alpha(t)}}$ is the deformation tensor, J_1 and K_1 is the strain invariant, and $n_{ka(t)}$ and $m_{ka(t)}$ is a unit vector.

Zhao et al.[165] reported a constitutive model, which can clearly describe the viscoelastic and shape memory behavior. Combined with the phase transition concept, SMP was considered a kind of composite composed of glassy and rubbery phases. According to different mechanical responses, two different constitutive relations were used in describing the mechanical properties of glassy and rubbery phases. The modified equilibrium path concept was introduced into the model to characterize the glassy phase, and the Mooney–Rivlin model was introduced to describe the rubbery phase. The constitutive relation is as follows:

$$\sigma_R = \left(2c_3^{R_1} + \frac{2c_4^{R_1}}{\lambda_{R_1}} \right) \left(\lambda_{R_1}^2 - \frac{1}{\lambda_{R_1}} \right) = \left(2c_3^{R_2} + \frac{2c_4^{R_2}}{\lambda_{R_2}} \right) \left(\lambda_{R_2}^2 - \frac{1}{\lambda_{R_2}} \right), \quad (23)$$

$$\sigma_{G_1} = \frac{3\mu_{G_1}}{J} \ln\lambda_{G_1}, \quad \sigma_{G_2} = \frac{3\mu_{G_2}}{J} \ln\lambda_{G_2}, \quad (24)$$

where σ_R represents the stress of the rubbery phase and σ_{G_1} and σ_{G_2} are the stress of the two networks representing the glassy phase. $c_3^{R_1}$, $c_4^{R_1}$, $c_3^{R_2}$, and $c_4^{R_2}$ are material parameters, which can be obtained by

experiments. λ_{R_1} and λ_{R_2} are elongation ratios. μ_{G_1} and μ_{G_2} are shear moduli.

Gilormini and Diani[166] developed another constitutive model. Based on the inclusion theory, the constitutive relation was defined as

$$d\sigma = \mathbf{L} : (d\varepsilon - d\varepsilon^{th} - dd\varepsilon^s) + \left(\frac{\partial \mathbf{L}}{\partial \varphi} \bigg|_T \varphi' + \frac{\partial \mathbf{L}}{\partial T} \bigg|_\varphi \right) : \mathbf{L}^{-1} : \sigma dT. \quad (25)$$

The stored strain ε^s can be expressed as

$$d\varepsilon^s = \left(\frac{1}{9k^2} \frac{\partial k}{\partial \phi} \bigg|_T + \frac{1}{3u^2} \frac{\partial u}{\partial \phi} \bigg|_T \right) \sigma \phi' dT, \quad (26)$$

where $\mathbf{L}$, ε^{th}, φ, k, and u represent the stiffness tensor, the thermal expansion strain, the volume fraction of the glassy phase, the volume modulus, and the shear modulus.

Combined with the phase transition concept and viscoelastic theory, Guo et al.[167] proposed a three-dimensional constitutive model to describe the mechanical behavior of SMP. The total strain can be expressed as

$$\varepsilon = \varphi_f \left(\varepsilon^S + \varepsilon_f^m \right) + \sum_1^n \varphi_i \varepsilon_i^m + \varepsilon^T$$
$$= \sigma \left(\varphi_f(T) J_f(T,t) \right) + \sum_1^n \varphi_i(T) J_i(T,t) + \varphi_f \varepsilon^S + \varepsilon^T, \quad (27)$$

where φ_f, ε^S, ε^T, ε_f^m, and $J_i(T,t)$ represent the volume fraction of the glassy phase, the stored strain, the thermal expansion strain, the strain of the glassy phase, and the creep compliance in time t, respectively.

Combined with Clausius–Duhem energy inequality and the Maxwell model, Bodaghi et al.[168] constructed a model to describe the SME and mechanical behavior. In this work, SMP was divided into three parts: hard segment, glassy phase, and rubbery phase. The strain can be obtained by Helmholtz free energy and can be expressed as

$$\dot{\varepsilon}^{ir} = \frac{1}{\eta_r} \frac{\partial \Psi_r^{neq}}{\partial \varepsilon^{er}}; \quad \dot{\varepsilon}^{ig} = \frac{1}{\eta_g} \frac{\partial \Psi_g^{neq}}{\partial \varepsilon^{eg}}; \quad \dot{\varepsilon}^{ih} = \frac{1}{\eta_h} \frac{\partial \Psi_h^{neq}}{\partial \varepsilon^{eh}}; \quad \dot{\varepsilon}^i = \frac{1}{\eta_i} \sigma, \quad (28)$$

where η_r, η_g, and η_h are the viscosity coefficients of the rubbery state, glassy state, and fixed state. Ψ_r^{neq}, Ψ_g^{neq}, and Ψ_h^{neq} are the Helmholtz free energy density functions. The change rule of stored strain ε^s with temperature is thoroughly discussed and can be expressed as

$$\varepsilon^s = k_{s1} \int \varepsilon_r d\varphi_g + k_{s2} \int \frac{\varepsilon^s}{\varphi_g} d\varphi_g; \quad \begin{cases} k_{s1} = 1, k_{s2} = 0, \dot{T} < 0, \\ k_{s1} = 0, k_{s2} = 1, \dot{T} > 0, \\ k_{s1} = 0, k_{s2} = 0, \dot{T} = 0. \end{cases} \quad (29)$$

where s_1 and s_2 are parameters to distinguish the heating and the cooling process.

According to the phase transition concept and rheological theory, Liu et al.[169] proposed a viscoelastic model with a more specific physical meaning. To describe the phase transition process, two constitutive relations were defined, respectively. For the rubbery phased, the Mooney–Rivlin model was adopted, and the Cauchy stresses of the two hyperelastic elements can be expressed as

$$\sigma_{R1} = -p_{R1}\mathbf{I} + 2C_{10}^{R_1} \mathbf{B}_{R1} - 2C_{01}^{R_1} \mathbf{B}_{R_1}^{-1}, \quad (30)$$

$$\sigma_{R2} = -p_{R2}\mathbf{I} + 2C_{10}^{R_2}\mathbf{B}_{R2} - 2C_{01}^{R_2}\mathbf{B}_{R_2}^{-1}. \tag{31}$$

For the glassy phase, the Hencky model was utilized to describe the mechanical behavior. The stress–strain relation is as follows:

$$J_i\sigma_x^i = \frac{E_i}{(1-2\nu_i)(1+\nu_i)}\left[(1-\nu_i)\ln\lambda_x^i + \nu_i\left(\ln\lambda_y^i + \ln\lambda_z^i\right)\right], \tag{32}$$

$$J_i\sigma_y^i = \frac{E_i}{(1-2\nu_i)(1+\nu_i)}\left[(1-\nu_i)\ln\lambda_y^i + \nu_i\left(\ln\lambda_x^i + \ln\lambda_z^i\right)\right], \tag{33}$$

$$J_i\sigma_z^i = \frac{E_i}{(1-2\nu_i)(1+\nu_i)}\left[(1-\nu_i)\ln\lambda_z^i + \nu_i\left(\ln\lambda_y^i + \ln\lambda_x^i\right)\right]. \tag{34}$$

The expression for the volume fraction of the frozen phase is summarized in Table III. The schematics of the viscoelastic constitutive model mentioned above are summarized in Table IV.

3. Theoretical research of SMPC

Generally, the mechanical properties of particle-reinforced SMPC were investigated by meso-mechanics models such as Mori–Tanaka and Eshelby. Yang et al.[184] established a micromechanical model to predict the thermodynamics behavior and microstructure inhomogeneity of CNT-reinforced SMPC. The constitutive relation of CNT was elastic, and SMP obeyed the thermodynamic constitutive law. The degree of polymerization was described by the polymerization coefficient, and the effective properties of SMPC were analyzed by a step-by-step method. By extending Escheby's single equivalent inclusion to the matrix with two inclusions, Jarali et al.[185] calculated the effective properties of SMPC reinforced by the carbon fiber and CNT. Through a two-step homogenization process, the relationship between the effective modulus and the inelastic strain tensor was derived. Zhao et al.[186] established another constitutive model for particle-reinforced SMPC combined with Mori–Tanaka micromechanical theory and generalized Maxwell model. By this method, the SME of SMPC can be predicted by only determining the materials parameters of the SMP matrix and inclusion

$$\bar{\boldsymbol{\sigma}}_{kk}(t) = 3k\left(\frac{a_2-a_1}{a_2(\mathbf{T}-a_2)}e^{-a_2 t} + \frac{a_1-\mathbf{T}}{\mathbf{T}(\mathbf{T}-a_2)}e^{-Tt} + \frac{a_1}{\mathbf{T}a_2}\right)\dot{\bar{\boldsymbol{\varepsilon}}}_{kk}, \tag{35}$$

$$\bar{\boldsymbol{\sigma}}_{ij}(t) = 2\mu\left(\frac{b_2-b_1}{b_2(\mathbf{T}-b_2)}e^{-b_2 t} + \frac{b_1-\mathbf{T}}{\mathbf{T}(\mathbf{T}-b_2)}e^{-Tt} + \frac{b_1}{\mathbf{T}b_2}\right)\dot{\bar{\boldsymbol{\varepsilon}}}_{ij} \tag{36}$$

with $a_1 = \frac{(c_p\alpha_p+c_g)k_gT}{(c_p\alpha_p+c_g)(k_g-k_p)+k_p}$, $a_2 = \frac{c_p\alpha_p k_g T}{c_g a_g(k_p-k_g)+k_g}$, $b_1 = \frac{(c_p\alpha_p+c_g)\mu_g T}{(c_g\beta_g+c_p)(\mu_p-\mu_g)+\mu_g}$ and $b_2 = \frac{c_p\beta_p\mu_g T}{c_p\beta_p(\mu_g-\mu_p)+\mu_p}$.

Compared with particle-reinforced SMPC, fiber-reinforced SMPC exhibit higher stiffness and recovery force. Generally, the maximum longitudinal deformation ratio is determined by the fiber. However, in practical application, the unfolding dynamics under large deflection and buckling deformation characteristics are a major concern. Dow and Rosen[187] developed a micro-buckling instability model for unidirectional fiber-reinforced SMPC based on Timoshenko's theory.[188] In this work, SMPC was simplified to a two-dimensional unidirectional plate in which the fiber layer and the matrix layer were distributed alternately. The minimum critical stress in shear and tensile buckling deformation can be expressed as

$$\sigma_{cr}^S = \frac{G_m}{(1-\nu_f)} + \frac{\pi^2 E_f h^2 \nu_f}{12\lambda^2}, \tag{37}$$

$$\sigma_{cr}^T = \frac{\pi^2 E_f h^2 \nu_f}{12}\left[\frac{1}{\lambda^2} + \frac{24 E_m \lambda^2}{\pi^4 ch^3 E_f}\right], \tag{38}$$

where λ and V_f represent the micro-buckling half-wavelength and the volume fraction of the fiber, E_f and E_m are the elastic modulus of fiber and matrix, h is the fiber diameter, G_m is the shear modulus of the matrix, and $2c$ is the distance between two adjacent fiber layers. According to Eq. (37), the minimum critical stress of shear buckling corresponded to the maximum buckling wavelength, and half-wave buckling was most likely to occur. However, for tensile buckling, the critical buckling wavelength corresponding to the minimum buckling stress was found to be significantly different from the experimental results, which greatly limited the prediction capacity of this model.

By considering the micro-buckling problem of a single fiber in the elastic matrix, Campbell et al.[189] developed a pure shear micro-buckling model for continuous fiber-reinforced SMPC plates. According to the hypothesis that the shear deformation energy of the matrix was equal to the deformation energy of fiber, the theoretical solution of the critical half wavelength of buckling is given by

$$\lambda_{cr} = \frac{\pi h}{4}\sqrt{\frac{E_f V_f}{G_m(1-V_f)}}. \tag{39}$$

The theoretical solutions for critical stress σ_c and critical strain ε_c are as follows:

$$\sigma_c = \frac{2G_m(1-V_f)}{V_f}, \tag{40}$$

$$\varepsilon_c = \frac{2G_m(1-V_f)}{E_f V_f}. \tag{41}$$

Subsequently, Campbell and Maji[190,191] considered the micro-buckling deformation of multiple fibers in the elastic matrix and obtained the buckling half-wavelength according to the deformation energy formula of the flexion rod. The buckling half-wavelength is as follows:

$$\lambda_{cr} = \sqrt{\frac{\pi E_f I_f}{G_m\left(\dfrac{d}{t}\right)}}, \tag{42}$$

where t is the plate thickness.

The theoretical buckling models mentioned above were proposed based on pure tensile or pure shear modes. However, the fiber will experience shear/tensile hybrid buckling mode during the bending deformation. For the bending deformation of unidirectional laminates, Wang et al.[192] proposed a simplified tension-shear coupled buckling model, and the critical buckling wavelength can be expressed as

$$\lambda_c = 2\pi^4\sqrt{\frac{2E_f I_f c}{E_m h}\cdot\frac{\displaystyle\sum_1^n\left(2i-1-2\sqrt{i(i-1)}\right)}{n(n+1)}}, \tag{43}$$

where n is the number of fiber layers in laminated plates. The critical buckling wavelength calculated by the formula was in good agreement
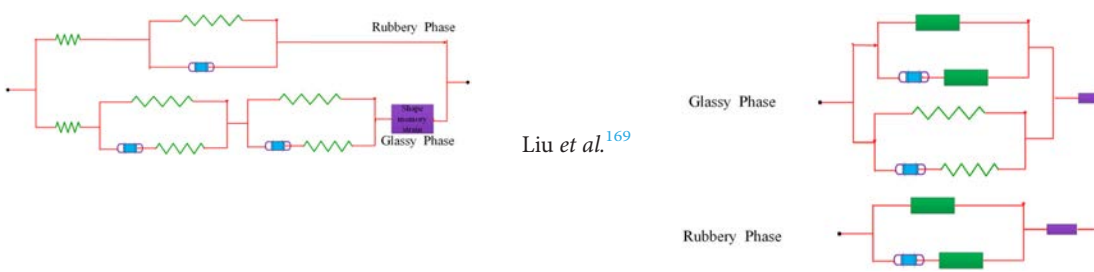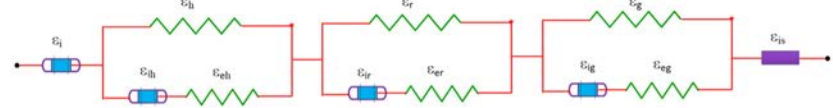
TABLE III. The expression for the volume fraction of the frozen phase.

References	Expressions	References	
Liu et al.[160]	$\varphi(\mathrm{T}) = 1 - \dfrac{1}{1 + c_f(T_h - T)^n}$	Chen and Lagoudas[161]	$\varphi(\theta) = \dfrac{1}{V}\displaystyle\int_{\Omega_f(\theta)} dV$
Qi et al.[163]	$\varphi(T) = \dfrac{1}{1 + \exp\left(-\dfrac{T - T_t}{a}\right)}$	Wang et al.[170]	$\varphi(\mathrm{T}) = \alpha \exp\left[-\left(\dfrac{T_t}{T}\right)^m \beta^n\right]$
Reese et al.[171]	$\varphi(T) = \dfrac{1}{1 + \exp\left(\dfrac{2w}{T - T_t}\right)}$	Volk et al.[172–174]	$\varphi(T) = \dfrac{\tanh\left(\dfrac{T_{\max} - A}{B}\right) - \tanh\left(\dfrac{T - A}{B}\right)}{\tanh\left(\dfrac{T_{\max} - A}{B}\right) - \tanh\left(\dfrac{T_{\min} - A}{B}\right)}$
Gilormini and Diani[166]	$\varphi(\mathrm{T}) = \left[1 - \left(\dfrac{T - T_{\min}}{T_{\max} - T_{\min}}\right)^m\right]^n$	Kim et al.[176]	$\xi_{sf_0} = \xi_{sf} - \displaystyle\int_t \dfrac{d\xi_{sa}}{dt} dt$
Yang and Li[175]	$\varphi(T, \dot{T}) = 1 - \displaystyle\int_{r_c(T)}^{\infty} p(r)\,dr \times \left\{1 - \left[1 - \exp\left(-\dfrac{\Delta H_a(T)}{k_B T}\right)\right]\dfrac{\Delta t}{\tau_0}\right\}$		
Guo et al.[167]	$\varphi(\mathrm{T}) = \displaystyle\int_{T_s}^{T} \dfrac{1}{s\sqrt{2\pi}} \exp\left(-\dfrac{T - T_g}{2s^2}\right) dT$	Park et al.[177]	$\varphi_g = \begin{cases} 1 \\ \varphi_g^0 \ 0 \le \varphi_g^0 \le 1 \ , \\ 0 \end{cases} \quad \varphi_g^0 = \dfrac{b}{1 + \exp\left(c(T - T_{tr})\right)} - d$
Guo et al.[178]	$1 - \varphi_f = \varphi \exp\left(-(k T_{tran})/(T - \tau\beta)^m / \beta^n\right)$	Pan and Liu[181]	$\varphi(T, \dot{T}) = 1 - \dfrac{1}{1 + \exp\left\{-\left[T - T_{tr}(\dot{T})/b\right]\right\}}$
Lu et al.[179]	$\varphi_f = 1 - \gamma = 1 - AT \exp\left(-\dfrac{\Delta G(T_h) 10^{-\frac{c_1(T - T_h)}{c_2 + T - T_h}}}{kT} + \dfrac{T_h - T}{bT - T}\right)$	Arvanitakis[183]	$\varphi = \dfrac{1}{\mathrm{v}} \displaystyle\int_{\Omega} \dfrac{1}{2}(1 + \tanh(\psi/s))\,dv$
Bouaziz et al.[180]	$\varphi_f = 1 - \dfrac{1 - b}{1 + \exp\left(-a_1(T - T_r)\right)} - \dfrac{b}{1 + \exp\left(-a_2(T - T_c)\right)}$		
Scalet et al.[182]	$\xi^c = \begin{cases} \dfrac{1}{1 + \exp\left[\beta_{cool}(T - T_{c,eff})\right]} & \text{if } \dot{T} \le 0 \\ \dfrac{1}{1 + \exp\left[\beta_{cool}(T_{END} - T_{c,eff})\right]} \dfrac{1}{1 + \exp\left[\beta_{heat}(T - T_{m,eff})\right]} & \text{if } \dot{T} \ge 0 \end{cases}$		
Bodaghi et al.[168]	$\varphi = 1 + \dfrac{\tanh(\gamma_1 T_g - \gamma_2 T) - \tanh(\gamma_1 T_g - \gamma_2 T_h)}{\tanh(\gamma_1 T_g - \gamma_2 T_h) - \tanh(\gamma_1 T_g - \gamma_2 T_1)}$		

TABLE IV. Schematics of the viscoelastic constitutive model.

References	Rheological schematic		
Tobushi et al.[140]		Morshedian et al.[144]	
Diani et al.[145]		Nguyen et al.[148]	
Srivastava et al.[153,154]		Gu et al.[155,156]	
Fang et al.[157]		Zeng et al.[158]	
Chen and Lagoudas[161,162]		Qi et al.[163]	
Zhao et al.[165]		Kim[176]	
Guo et al.[167]			

TABLE IV. (*Continued.*)

References	Rheological schematic

Park *et al.*[177]

Liu *et al.*[169]

Bodaghi *et al.*[168]

---

with the experiments, but the model was established by assuming plates as a two-dimensional structure.

Ignoring the fracture of carbon fiber and the viscoelastic effect of the matrix, Lan *et al.*[193] studied the post-buckling behavior of carbon fiber-reinforced SMPC by assuming that both the fiber and the matrix were elastomer materials. SMPC was divided into three parts in the section direction: the unbuckling tensile part, the unbuckling compression part, and the buckling compression part. The critical buckling strain of the structure is given as follows:

$$k_c = \frac{4}{t} \frac{v_m G_m}{v_m E_m + v_f E_f}. \tag{44}$$

Tan *et al.*[194] studied the buckling behavior of SMPC with a metal film attached to its surface. The total energy was given by analyzing the main energy forms of SMPC during the deformation process, and the critical buckling strain can be expressed as

$$\varepsilon_{cr} = 4 \frac{h}{f E_{xx}} \left(z - \left(1 + \frac{E_m t}{E_{xx}} - \frac{f}{h}(g + G_s v_s) \right) \right) \tag{45}$$

with $h = v_s G_s(E_m t + E_{xx} z_m)$ and $f = E_{xx} z_m^2 + E_m t^2 + 2 E_m t z_m$.

Based on the assumption that the material has a bilinear constitutive relation, Campbell *et al.*[195] investigated the post-buckling behavior of long fiber reinforced SMPC plate by dividing the section into buckling region and non-buckling region. According to that the resultant force of the cross section along the longitudinal direction is zero under the pure bending condition, and the position coefficient of the neutral layer α was deduced. Furthermore, the nonlinear relation between bending moment and curvature was derived. The numerical analysis model was established based on the fact that the bending moment on the cross section was equal to the external couple moment.

Francis and Lake[196] investigated the local post-buckling behavior of the fiber in the bending deformation process of SMPC. The expressions of key parameters, such as the offset distance of the neutral plane and the fiber buckling wavelength, were obtained. Researchers from Composite Technology Development, Inc. (CTD), have tested and theorized various cases of buckling behavior and verified the recovery performance of epoxy-based SMP by the viscoelastic constitutive

relation. The failure mode of fiber-reinforced SMPC was verified by testing and preliminary theory.[197–199]

IV. APPLICATIONS OF SMP AND SMPC
A. Applications in the aerospace field
1. Space deployable truss structures

In 1986, Miura and Miyazaki[200] proposed the concept of the tension truss antenna and applied it to the flexible self-spring back antenna to meet the requirements of large space deployable reflectors. The truss surface is divided by many small triangular elements, and the truss frame is composed of a highly resilient flexible material. Therefore, it can be easily coiled into the effective enveloping space of the spacecraft. When the satellite is put into orbit, the external driving force is used to deploy the structure. However, these kinds of trusses are fabricated by casting technology, the profile accuracy is relatively low, and the aperture is limited. With the development of intelligent materials and structures technology, SMPC is gradually applied in the deployable truss realizing the integration of unfolding and locking. Compared with traditional structures, the trusses based on SMPC have the advantages of lightweight, no vibration during deployment, and small space occupancy.

CTD designed a type of SMPC-based deployable truss, which consisted of three longitudinal foldable laminates with an interval of 120°.[201] In the folded state, the longitudinal SMPC-based laminates shrink in an S-type. After reaching the working orbit, the truss gradually unfolds with the recovery of SMPC-based laminates stimulated by the electric field. Furthermore, CTD[202] proposed another spiral compression beam with a large contraction ratio. Traditional beam structures will store large strain energy during the helically wrapped process. When the deformation exceeds the critical state of the material, the structure will damage. However, replacing the traditional materials with SMPC can effectively eliminate the storage strain energy. Utilizing the variable stiffness property, SMPC based beam exhibits excellent toughness. Cornerstone Research Group (CRG) fabricated a truss with an expanded diameter of 6.3 cm and a height of 72 cm using cyanate-based SMPC.[203] The folded truss is only 6.5 cm in length and can deploy smoothly in the rigid plastic pipe. However,

it is worth noting that the truss cannot be fully expanded due to the influence of gravity.

Lan *et al.* proposed a kind of SMPC hinge with high specific strength and specific stiffness,[204] which mainly consisted of aluminum end devices, two SMPC composite laminates, and electrothermal films as shown in Fig. 10(a). Utilizing the SMPC hinges, the principle prototype of a solar panel was developed. Heated by the electrothermal film, the structure deployed smoothly within 120 s without vibration. Zhang *et al.*[205] proposed a deployable truss system utilizing SMPC, and the truss was deployed in 100 s stimulated by heat as shown in Fig. 10(b). The optimal torque-deformation angle and the stress–strain relationship of the SMPC beam in the deployment process were thoroughly investigated with finite element analysis (FEA). Furthermore, the deployable properties and the support capacity of the truss with different geometric configurations, material components, and laminate thickness were investigated, which provided a theoretical basis for the design.

Leng *et al.*[206] proposed a kind of SMPC-based deployable cantilever truss system with a tension base and an auxiliary support frame. The folded state and the unfolded state of the truss structure are shown in Fig. 11(a). The hinges were fabricated by carbon fiber-reinforced cyanate-based SMPC, and the structural reliability was verified by FEA and mechanical experiments. For the truss system with a 1.3 kg top load on it, the modal experiments, including sine sweep frequency vibration and shock tests, were carried out. The structure completes all ground tests, and the strength and stability are enough. However, for a variety of reasons, the structure is not launched into space. Furthermore, Leng *et al.*[18] made a further improvement on the SMPC hinge and determined the optimal design parameters. The debonding problem existing in the bending process was solved by adjusting the thickness and the bending path of the hinge. The SMPC hinges were assembled into a solar array principle prototype and successfully deployed as shown in Fig. 11(b).

Different from the hinges mentioned above, Liu *et al.*[19] proposed an integrated hinge; by this hinge, a truss used for multi-angle imaging systems was developed and folded in a Z-shape as shown in Fig. 11(c). The truss system deployed along the predetermined path was stimulated by the heat of the electrothermal film. The integrated design significantly improved the structure stiffness.

Utilizing SMPC and composite spring strip, Chen *et al.*[207] developed a deployable antenna reflector, and the deployment process was driven by eight symmetrically distributed hinges. The multi-curvature design of the SMPC hinge section is expected to improve its overall mechanical properties. Furthermore, the SMPC hinge played the role of the damper to prevent damage caused by the shock during the deployment process. The composite spring strip greatly enhanced the recovery force and deployment precision of the hinge. Rakow *et al.*[208] proposed a kind of lightweight solar array for micro–nanosatellites and small spacecraft utilizing SMPC hinges. The solar array can be folded to a "Z" type and deploy smoothly and control driven by the SMPC hinges. The deployed dimension was 1 m in length and 0.36 m in width.

Lan *et al.*[209] designed a deployable flexible solar cell array system (SMPC-FSAS) without the conventional electric explosive device and motor control and launched it on December 27, 2019, aboard the SJ20 synchronous satellite. During the launching process, the locking release mechanism functioned normally. The deployment of the system was heated and triggered in the geosynchronous orbit on January 5, 2020. The SMPC variable stiffness tube drove the flexible solar array to unfold slowly and finally achieved a nearly 100% R_f in 60 s as shown in Fig. 11(d). The in-orbit flight of the SMPC deployable flexible solar array system will accelerate research and products of release mechanisms and space deployable structures for the next generation.

2. Space deployable antenna structure

An effective method to enhance the coverage area and improve the detection accuracy is to increase the aperture of the satellite antenna. However, it faces limitations in the effective space and carrying capacity of the rocket. Consequently, the design of the deployable structure is essential for the large-aperture space satellite antenna. The deployable antennas currently in service can be divided into petal-type antennas, umbrella-type antennas, and inflatable deployable antennas.

The rigid-rib umbrellas-like antenna developed by Harris Corporation[205] for NASA's TDRS satellite consists of 16 parabolic ribs and connects to the central axis by hinges. The unfolding and folding processes of the rigid-rib antenna are controlled by the hinges. It is carried into space by Galileo spacecraft but failed to unfold due to excessive friction force. NASA's Jet Propulsion Laboratory (JPL) collaborated with Lockheed corporation on the development of the twisted rib antenna and developed a 48-rib umbrella concept structure.
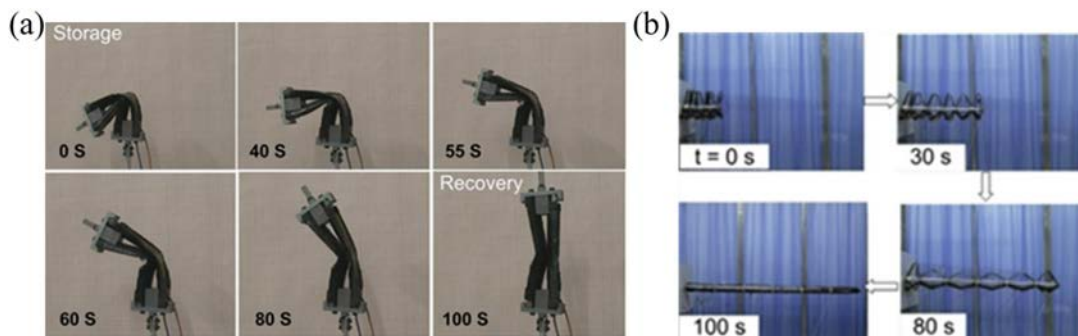

FIG. 10. Space deployable truss structures. (a) Deployment process of the solar panel driven by SMPC hinges. Reproduced with permission from Lan *et al.*, Smart Mater. Struct. **18**(2), 024002 (2009). Copyright 2009 Elsevier.[204] (b) Deploy process of the SMPC truss. Reproduced with permission from Zhang *et al.*, Compos. Struct. **112**, 226–230 (2014). Copyright 2014 Elsevier.[205]
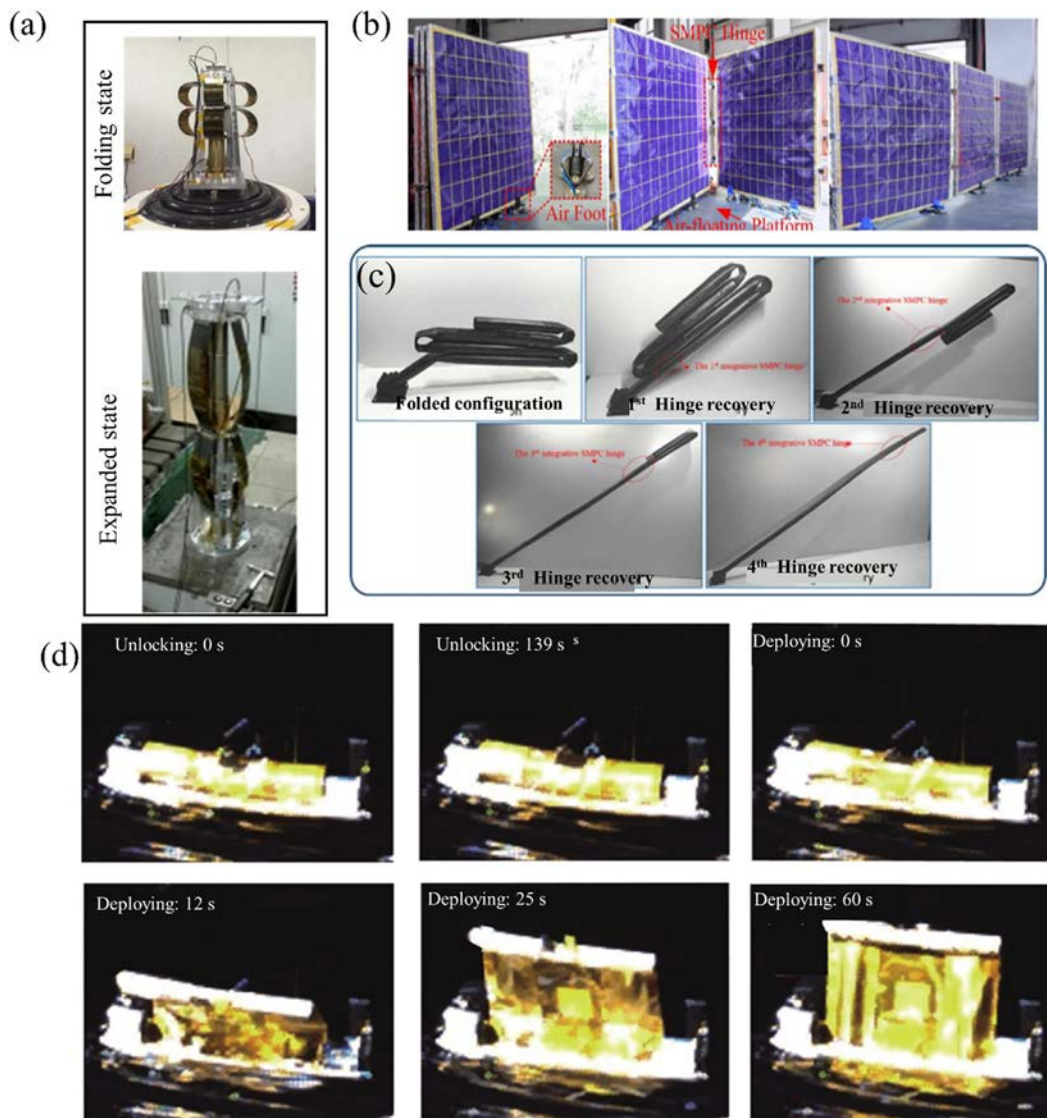
FIG. 11. Space deployable structures. (a) The compressed state and the deployment state of the SMPC-based truss structure. Reproduced with permission from Li *et al.*, Compos. Struct. **242**, 112196 (2020). Copyright 2020 Elsevier.[206] (b) The deployment process of SMPC-based solar array prototype on air floating platform. Reproduced with permission from Liu *et al.*, Compos. Part B **193**, 108056 (2020). Copyright 2020 Elsevier.[18] (c) Deployment process of the truss structure fabricated with the integrated hinge, Reproduced with permission from Liu *et al.*, Compos. Struct. **206**(15), 164–176 (2018). Copyright 2018 Elsevier.[19] (d) Deployable process of SMPC-FSAS in the geosynchronous orbit.[209] Reproduced with permission from Lan *et al.*, Sci. China-Technol. Sci. **63**, 1436–1451 (2020). Copyright 2020 Springer Nature.[209]

The torsion of the hinge on the top of the rib enables the structure to wrap tangentially around the edge of the central hub. When the constraint line is cut, the energy stored in the rib will be released, and the antenna will recover to its initial shape.[210] However, the surface precision and size of the structure are limited, and the rapid expansion is bound to be accompanied by huge vibrations. Furthermore, JPL[211] developed a series of inflatable space deployable structures. Generally, the spring strip reinforced aluminum laminated booms are used as the main inflatable frame. However, the leakage may lead to the failure of the entire structure. The antenna based on SMPC will not produce vibration and shock during the deployment process. The solar panels

of the U.S. Intelligent Micro Controllable Satellite and RoadRunning satellites were deployed driven by SMPC hinge.[201] Arzberger *et al.*[212] developed a kind of lightweight deployable mirror, which was fabricated by novel SMPC with appropriate reinforcements. The surface of the mirror was composed of electroplated nickel to ensure an excellent reflection effect. The experimental results indicated that the deployable mirror exhibits excellent deployable and optical properties. Varlese and Hardaway[213] developed a type of optical reflector that used cyanate-based SMPC coated with nickel powder film as the framework. The reflector can be curled up to reduce the occupancy space and recover to its initial shape at high temperatures. By replacing the traditional metal
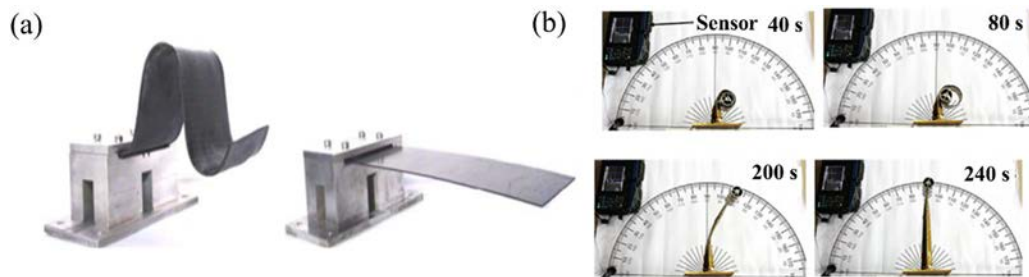
FIG. 12. Space deployable structure based on SMPC, (a) Prototype of solar array substrates at folded and unfolded states. Reproduced with permission from Li *et al.*, Smart Mater. Struct. **28**(7), 075023 (2019). Copyright 2019 IOP Publishing.[217] (b) The deployment process of the SMPC-based lenticular tube structure. Reproduced with permission from Liu *et al.*, Compos. Struct. **223**, 110936 (2019). Copyright 2019 Elsevier.[218]

hinge with SMPC hinges, Francis *et al.*[214] proposed the reflector concept with a solid surface. The reflector composes of six sub-reflectors, and it can deploy driven by SMPC hinges. Combined with an inflatable structure and SMPC, Keller *et al.*[215] fabricated a large-diameter space deployable antenna. The antenna disk and support rod are made of SMPC, which can be folded into an umbrella-shaped corrugated structure to reduce the occupied space. Combined with SMPC, ILC[216] developed another inflatable rigid deployable reflector with a solid surface. The supporting frame at the edge and the bottom of the reflector is made of SMPC, and the surface is made of a thin film.

Leng *et al.*[217] reported a kind of solar array substrate utilizing carbon fiber cloth-reinforced SMPC as shown in Fig. 12(a). The solar array substrate was tested on an experimental satellite for orbital deployment and anti-irradiation verification. Stimulated by the sunlight, the substrate deploys from the initial "Ω" shape to the flat plate in orbit and exhibits good long-term radiation resistance. Liu *et al.*[218] proposed an SMPC-based lenticular tube structure [Fig. 12(b)] and thoroughly investigated its mechanical and deformation properties. Compared with the traditional lenticular tube, the structure exhibits excellent controllability and stability during the deployment process.

B. Applications in biomedical medicine

SMP has attracted a great deal of attention in biomedical fields, such as tissue engineering, stents, and biological sutures, as shown in Fig. 13. Its potential for minimally invasive surgery, in which SMP
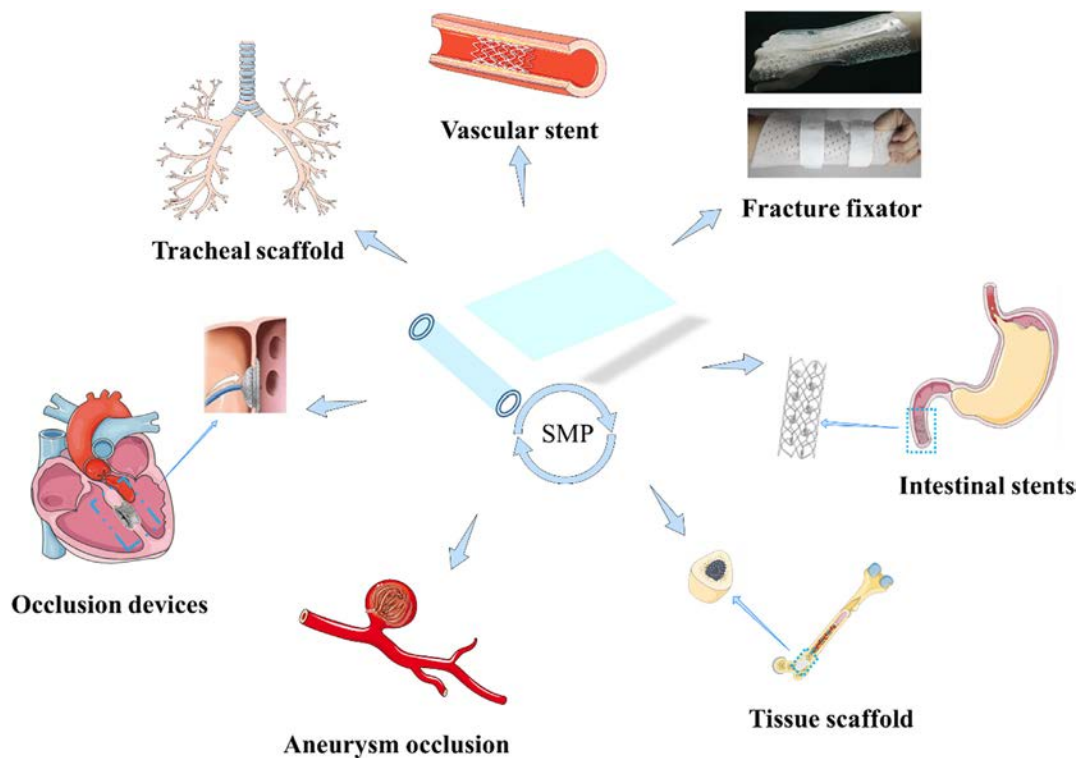

FIG. 13. Biomedical applications of SMP and SMPC.

expands from a temporary compact structure to its original incompact shape in response to external stimulation, has also been well studied. In addition to the potential of minimally invasive implantation, SMP-based scaffolds can provide excellent self-adaptation ability, while smaller SMP scaffolds can fully match the defect boundary after shape restoration. Shape memory polyurethane, polylactic acid, and polycaprolactone exhibit excellent chemical stability, good biocompatibility, and biodegradation.

1. Applications in bone tissue repair

The bone defect is the destruction of structure integrity, which is a common disease in clinical. For many bone defects, self-healing is difficult to realize due to the dimensional limit. Bone tissue scaffolds are a commonly used method for the treatment of bone defects. However, the conventional bone tissue scaffolds are brittleness and poor induction. Most importantly, it is difficult to implant into the body through minimally invasive surgery (MIS) and contact with the edge of the bone defects perfectly.

The SMP bone tissue scaffolds can adapt to various irregular defects taking advantage of the SME. Grunla et al.[219] fabricated a kind of biological scaffold using photo across-linked polycaprolactone. As shown in Fig. 14(a), the scaffolds have a porous structure and can adapt to various irregular bone defects. Zhou et al.[220] proposed a kind of porous nanocomposite scaffold based on shape memory polycaprolactone as shown in Fig. 14(b). The scaffolds are implanted into the body in the compressed state and recover to the porous shape stimulated by heat. Meanwhile, the scaffold can release the growth factors to promote the formation of new bone. Furthermore, Rychter et al.[221] developed a type of scaffold based on shape memory lactide/ethyl ester/cyclopropane, which can rapidly fill the bone defects stimulated by body temperature as shown in Fig. 14(c). Animal experiments showed that the scaffolds can induce the adhesion and proliferation of bone cells.

Senatov et al.[222] fabricated a kind of SMPC-based porous bone tissue scaffold utilizing PLA mixed with hydroxyapatite as shown in Fig. 14(d). The thermal–mechanical properties of the scaffolds were thoroughly researched. The addition of hydroxyapatite, as the results
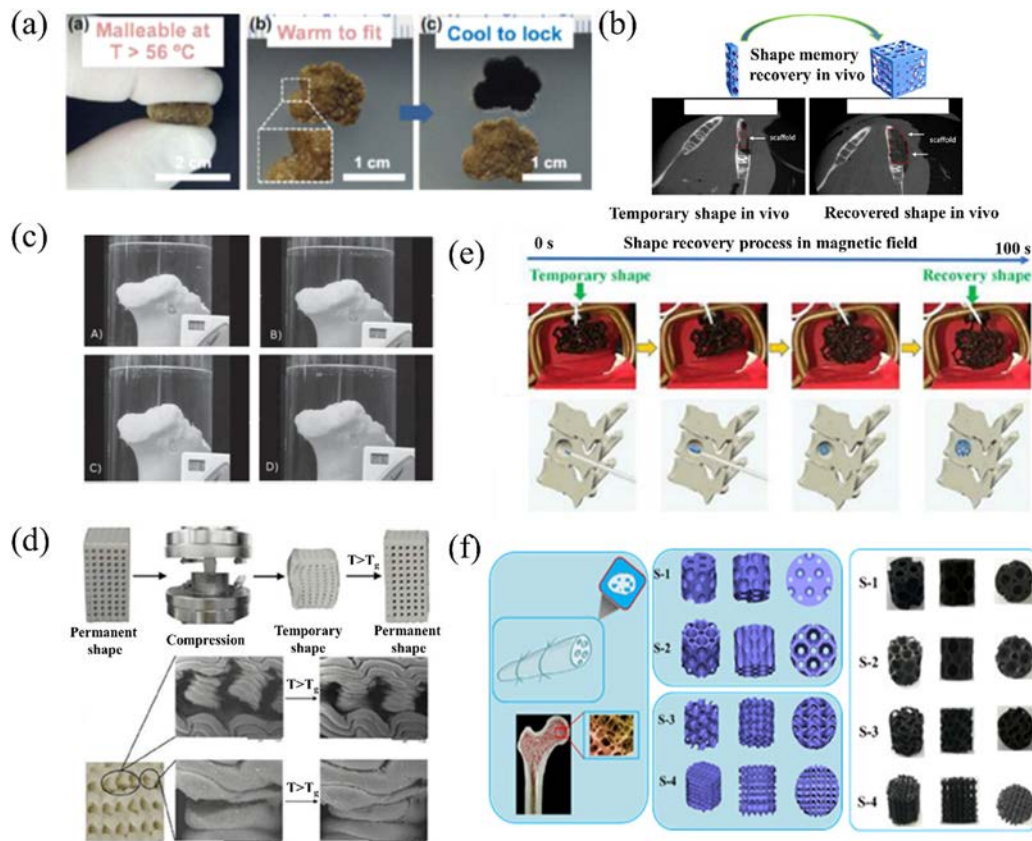

FIG. 14. SMP-based bone tissue scaffolds. (a) Recovery process of polydopamine-coated SMP-based bone tissue scaffolds. Reproduced with permission from Zhang et al., Acta Biomater. **10**(11), 4597–4605 (2014). Copyright 2014 Elsevier.[219] (b) Porous nanocomposite bone tissue scaffold. Reproduced with permission from Liu et al., Biomacromolecules **15**(3), 1019–1030 (2014). Copyright 2014 American Chemical Society.[220] (c) Deployment process of SMP-based scaffold.[221] Reproduced with permission from Rychter et al., J. Biomed. Mater. Res. Part A **103**, 3503 (2015). Copyright 2015 John Wiley and Sons.[221] (d) Self-healing and self-healing processes of porous scaffolds. Reproduced with permission from Senatov et al., J. Mech. Behav. Biomed. Mater. **57**, 139–148 (2016). Copyright 2016 Elsevier.[222] (e) Shape recovery behavior of scaffold in the magnetic field. Reproduced with permission from Zhang et al., Compos. Part A **125**, 105571 (2019). Copyright 2019 Elsevier.[223] (f) Bionic bone tissue scaffold. Reproduced with permission from Zhao et al., Compos. Sci. Technol. **205**, 108563 (2021). Copyright 2021 Elsevier.[20]

indicated, resulted in the transition temperature increasing from 53 to 57.1 °C. Furthermore, the recovery force of SMPC was significantly increased. Utilizing the shape memory PLA-based filament, Zhang et al.[223] fabricated a kind of bone tissue scaffold as shown in Fig. 14(e). The scaffolds can be implanted through MIS in a compressed state and recovered to their initial shape in a magnetic field.

Zhao et al.[20] developed a series of scaffolds by investigating the multi-channel structure of biomimetic lotus roots and the trabecular structure of porous cancellous bone as shown in Fig. 14(f). The scaffolds were fabricated by 4D printing technology using the self-manufacturing SMPC filament, and the mechanical properties were analyzed from the perspectives of theory, simulation, and experiment. When the porosity is 60%, the strength of the structure is about 27 MPa, which can provide sufficient support for the bone defect. The toughness of the scaffold is far more than that of the clinical artificial bone. Similarly, the scaffolds can be implanted by MIS in the compaction state, and the remote non-contact actuation mode such as a magnetic field can be used to expand the scaffolds to the working state.

2. Applications in stents

Similarly, biodegradable SMP and SMPC-based stents may be an ideal choice for the treatment of cardiovascular and tracheal diseases. The first biodegradable SMP-based stent used in humans is named as Igaki-Tamai, developed by Tamai et al.[224] The stent is fabricated by shape memory PLA, and when the temperature of the stent is heated to 70 °C, it can recover to the permanent shape. Eventually, the stent was implanted into the body and deployed at 80 °C with the aid of a balloon. Utilizing shape memory PCL, Morrison et al.[225] developed a stent for tracheal softening to prevent airway collapse during normal breathing. The personalized stent was fabricated by 3D printing as shown in Fig. 15(a), and it can expand as the airway grow to accommodate changes in airway size. Three years later, the stent was completely removed from the body, and the trachea was able to work independently.[226,227] Zarek et al.[228] developed a kind of shape memory PCL ink used for 4D printing and fabricated a tracheal stent utilizing stereolithography technology as shown in Fig. 15(b). Utilizing SME, the stent can be implanted into the lesion site through MIS, and when the shape recovery is triggered again, the structure matches the trachea perfectly.

Wei et al.[229] developed a kind of UV cross-linked shape memory PLA ink and fabricated a stent by direct writing printing technology as shown in Fig. 15(c). Once the material is squeezed out of the nozzle, the material solidifies rapidly. By mixing Fe_3O_4 nanoparticles into the matrix, the stents can be triggered to recover to the working state stimulated by the magnetic field, which can realize remote non-contact actuation. Kim and Lee[230] fabricated a novel SMP-based bifurcated vascular stent combined with kirigami technology as shown in Fig. 15(d). The stent can be folded into a compact cylindrical shape, allowing it to move in the blood vessels without being impeded or obstructed. Once the stent reaches the target location, it will be triggered to recover to the initial shape to dilate the blocked or narrowed blood vessels.

Liu et al.[231] developed an SMP-based vascular stent with a hierarchically adjustable micropatterned surface. As shown in Fig. 15(e), the vessel stent is a 3D multilayered tubular structure. Stimulated by the body temperature, the stent is curled up so that the square micropattern is in the lumen layer and the rectangular micropattern is in the outer layer. Zhao et al.[21,232,233] developed a series of SMP-based stents

utilizing 4D printing technology and SMPC. As shown in Fig. 15(f), by studying the structural characteristics of the glass sponge, the bioinspired stents were designed and customized according to different tracheal sizes. Mechanical experiments indicate that the stents exhibit high strength and stability, and the unique design enables it to adapt to the complex environment in the soft tissue.

3. Other biomedical applications

Furthermore, SMP has been used in other fields, including biological sutures, aneurysm occlusion devices, heart valve repair, etc. Suture nail is a simple and convenient suture method for the skin, which can avoid over-sparseness or over-tightness. Generally, the suture nails are made of medical stainless steel and titanium alloy, and the size and specification are relatively single. However, to match the wound perfectly, suture nails of different sizes are required for different wounds or tissues. SMP-based suture nails have a greater advantage than conventional nails, which can realize the most suitable locking state by applying suitable stimulation. Furthermore, SMP-based biological suture nails can meet the requirements of different tissues and provide a flexible restoring force to close the wound as shown in Fig. 16(a).[234]

In gastrointestinal surgery, gastrointestinal anastomosis is one of the important parts of the operation process. Seamless suture technology has a long history in the operation process. Figure 16(b) illustrated the shape memory PLA-based spring used for wireless sutures. The spring was first pre-inflated to a certain extent, then placed where the tubes intersect and heated to human body temperature. With the contraction of the spring, the two tubes are tight together, which can be used for bleeding control.[234]

Intracranial aneurysms, also known as cerebral aneurysms, are aneurysmal bulges in the brain, caused by local congenital defects in the cerebral artery wall or increased intracavity pressure. If ruptured, it can cause intracranial bleeding and further result in hemorrhagic strokes, brain damage, or death. The original treatment is to insert a metal coil into the aneurysm to seal it off. However, this technique requires a high level of clinical experience and technical operation, which will cause the burst of an aneurysm even with a slight mistake. The coil based on SMPU can provide a better sealing effect.[235] Hampikian et al.[236] designed an SMP coil, which can form stable support within the aneurysm and reduce the risk of recanalization of aneurysms. Figure 16(c) illustrated the deployment process in an intracranial aneurysm model. The coil is implanted in the aneurysm model as straight fibers, and it will quickly revert to its original spiral shape upon contact with hot water. Furthermore, SMP-based foam has a certain application prospect in aneurysm occlusion. Metcalfe et al.[237] reported the treatment of aneurysms in the neck using SMPU foam, which was verified to improve the angiography of aneurysms three weeks after implantation. The histological results indicated a thick film had grown on the surface of the foam and sealed off most of the aneurysm as shown in Fig. 16(d).

When the mitral valve fails to close completely, part of the blood in the left ventricle will return to the left atrium with the contract of the left ventricle. Since the prosthetic rings are proposed to reduce hole diameter and strengthen the contact between valve lobes, a series of implants have been proposed, roughly divided into rigid implants and flexible implants. However, the ideal therapies are to apply pressure gradually to avoid postoperative problems. Lantada et al.[238]
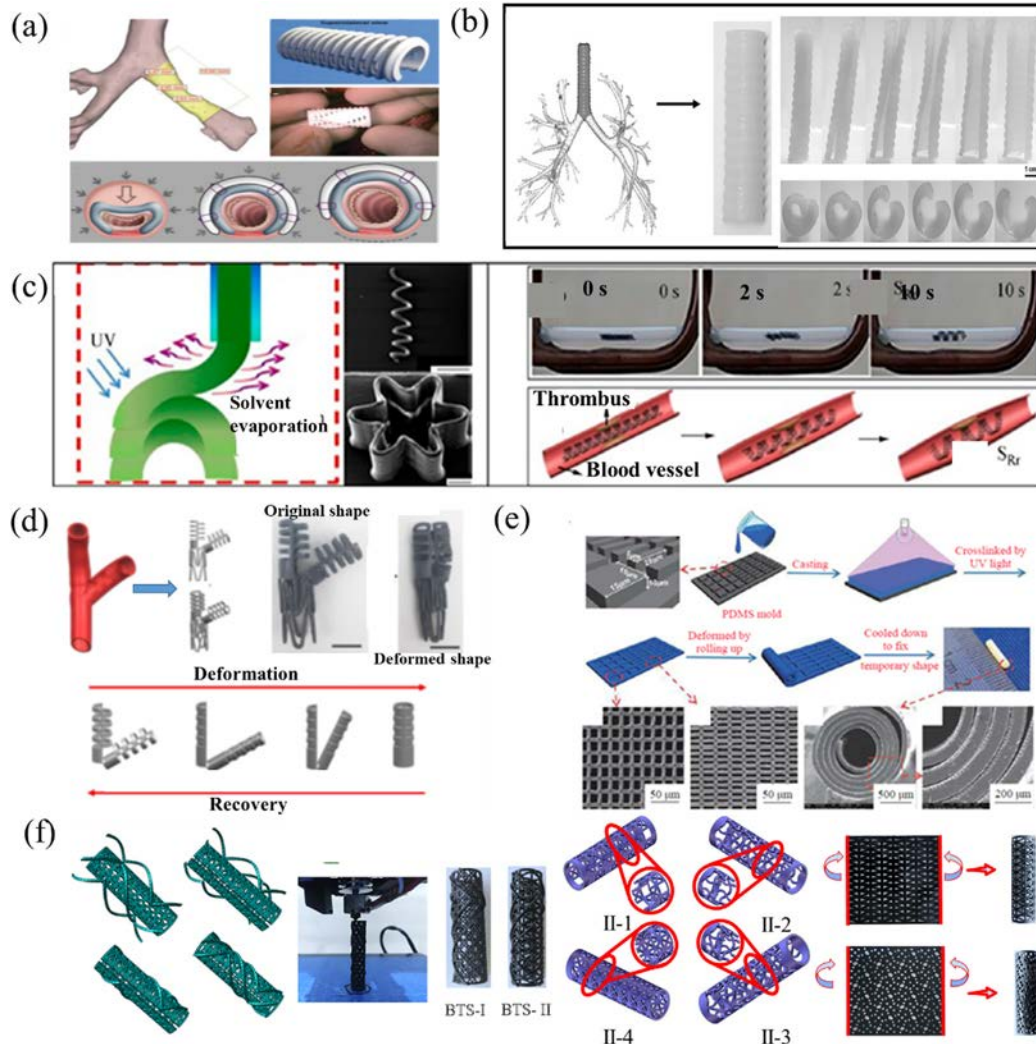
FIG. 15. Shape memory stent. (a) Stent used for the tracheal softening.[225] Reproduced with permission from Morrison et al., Sci. Transl. Med. **7**(285), 285ra64 (2015). Copyright 2015 The American Association for the Advancement of Science. (b) Fabrication and deployment process of SMP-based trachea stent. Reproduced with permission from Zarek et al., Macromol. Rapid Commun. **38**, 1600628 (2017). Copyright 2017 John Wiley and Sons.[228] (c) Vessel stent stimulated by the magnetic field. Reproduced with permission from Wei et al., ACS Appl. Mater. Interfaces **9**(1), 876–883 (2017). Copyright 2017 American Chemical Society.[229] (d) Design and the deployment process of the bifurcated vascular stent.[230] Copyright 2018 Authors, licensed under a Creative Commons Attribution (CC BY) license. (e) Vessel stent with a three-dimensional multi-layered tubular structure. Reproduced with permission from Liu et al., ACS Appl. Mater. Interfaces **9**(23), 19725–19735 (2017). Copyright 2017 American Chemical Society.[231] (f) Design and 4D printing of bionic trachea stents. Reproduced with permission from Zhao et al., Compos. Sci. Technol. **184**, 107866 (2019). Copyright 2019 Elsevier.[21] Reproduced with permission from Zhao et al., Compos. Sci. Technol. **229**, 109671 (2022). Copyright 2022 Elsevier.[232]

proposed a thermal-actuated SMP-based ring for the treatment of mitral valve imperfection, which can be controlled remotely to reduce the aperture. The spring can be implanted into the body by MIS, and the resistance element embedded in the SMP ring can be used to heat the ring and apply pressure on the heart valve as shown in Fig. 16(e).

Implantable occlude, as an effective method to treat structural heart disease, has aroused wide concern. Occlusion devices are self-expanding double-umbrella structures placed in the heart defect. By 4D printing, Lin et al.[239] fabricated a kind of SMPC-based occlusion

device with a double-disk structure. The diagram of the structures and the implanted process is shown in Fig. 16(f). By mixing Fe_3O_4 nanoparticles into SMPC, the deployment process can be remotely controlled and stimulated by the magnetic field. The SMPC-based occlusion device is expected to be an alternative to metal occluders. Zhao et al.[240] developed a kind of SMP-based adaptive fracture fixation device as shown in Fig. 16(g). Generally, the tightness of the fracture fixture is difficult to control, easily causing press on tissue, fracture displacement, or allergic symptom. When the fixator becomes loose due to the detumescence, the fracture fixator can readjust the
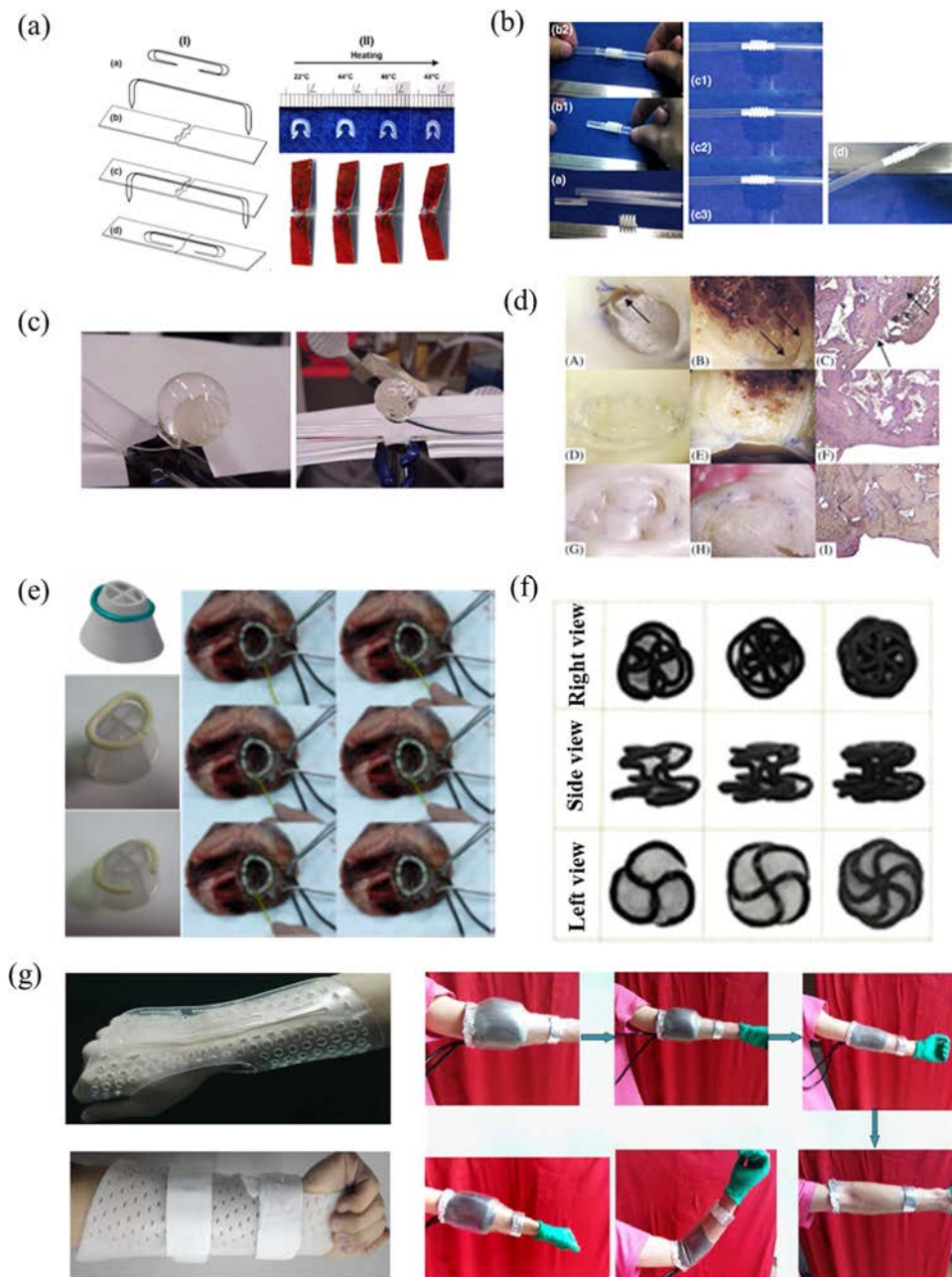
FIG. 16. Biological applications of SMP. (a) Biological suture nails based on SMP. Reproduced with permission from Huang *et al.*, Adv. Drug Delivery Rev. **65**(4), 515–535 (2013). Copyright 2013 Elsevier.[234] (b) Shape memory PLA-based spring used for wireless suture. Reproduced with permission from Huang *et al.*, Adv. Drug Delivery Rev. **65**(4), 515–535 (2013). Copyright 2013 Elsevier.[234] (c) Aneurysm embolization device based on SMP. Reproduced with permission from Hampikian *et al.*, Mater. Sci. Eng., C **26**(8), 1373–1379 (2006). Copyright 2006 Elsevier.[236] (d) Aneurysm embolization device based on SMP foam. Reproduced with permission from Metcalfe *et al.*, Biomaterials **24**, 491 (2003). Copyright 2003 Elsevier.[237] © Heart valve repair ring based on SMP.[238] Reproduced with permission from Lantada *et al.*, *Biostec, Biomedical Engineering Systems and Technologies* (Springer, Berlin, Heidelberg—, 2008), Vol. 25, pp. 59–72. Copyright 2008 Springer Nature. (f) Occlusion devices based on SMP.[239] Reproduced with permission from Lin *et al.*, Adv. Funct. Mater. **29**(51), 1906569 (2019). Copyright 2019 John Wiley and Sons.[239] (g) The adaptive fracture fixture based on SMP and its working mechanism. Reproduced with permission from Zhao *et al.*, Smart Mater. Struct. **26**(2), 025027 (2017). Copyright 2017 IOP Publishing.[240]

limb and maintain the optimal fixation state by applying thermal stimulation.

C. Applications in the intelligent mold

At present, the molds used for the fabrication of composites include multi-piece metal mandrels, water-soluble mandrels, and inflation mandrels. The multi-piece metal mandrel has the characteristics of large weight, a long cycle of production, and a complicated demolding process. The water-soluble mandrels are disposable products,

which need to cure the core mold, dry in the sun, and treat the surface twice. The core mandrels need to be dissolved after the component is formed, which will lead to a long production cycle. The surface stiffness of the inflation mandrel is low, and the internal pressure should always be maintained during the forming process. To overcome the defects of traditional mandrels, SMP-based intelligent mandrels are developed to prepare composite structures with complex shapes.

The intelligent mandrels based on SMP are a new concept in the design and manufacture of a deformable mold and have the potential to produce composites with complex curvature. The forming process

of the intelligent mold is simple, the manufacturing cycle is short, and the demolding process is easy.[241,242] First, an SMP-based tube needs to be fabricated according to the size of the structure to be prepared; Second, place the SMP tubes into a metal mold with the contour of the desired workpiece, and the mandrel is prepared by heating, and pressurizing the polymer tube; Subsequently, the required composite structures are fabricated on the intelligent mandrels by filament winding; Finally, the intelligent mandrels recover to the original tubular shape by heating it to a high temperature, and the composite structure can be obtained.

CRG[241] reported a kind of intelligent mandrel and fabricated composite structures by wrapping fibers on the mandrels. However, the SME of the mandrel has not been studied in depth. Leng et al. have done a lot of work on theoretical research, development, and function tests on the intelligent mandrel. Utilizing SMP, a series of intelligent mandrels with different cross section deformation ratios are fabricated. Subsequently, the composite structures are fabricated by fiber winding. Zhang et al.[242] designed an SMP-based mandrel, which would shrink back to its original shape at high temperatures to demould the composite structure wrapped on it. The shape recovery process of the smart mandrel is shown in Fig. 17(a).

Du et al.[22] developed a special-shaped structure mandrel for aircraft inlet, which is an S-shaped pipe with a circular section at one end and a rectangular section at the other end. The demoulding process is shown in Fig. 17(b). Furthermore, Du et al.[243] developed another intelligent mandrel with two cross sections expanded by 50% and 75% as shown in Fig. 17(c). The intelligent mandrel was fabricated using SMP with different transition temperatures, $T_{trans} = 60.08\,^{\circ}C$ (corresponding to cross section with 75% deformation) and $T_{trans} = 41.05\,^{\circ}C$ (corresponding to cross section with 50% deformation). During the demoulding process, the smart mandrel will recover to its initial shape in steps.

Microarrays have been widely used in ice resistance, cell manipulation, and antibiotic adherence, which are generally made using expensive and time-consuming lithography techniques. Du et al.[244] reported a new strategy to introduce SMP into microarray manufacturing and studied the deformation and recovery of SMP microarrays. It can be indicated that the SMP-based microarray exhibited good controllability, stable surface wettability, and a high shape recovery ratio. Using SMP films as intelligent tunable molds, a series of microarrays with continuously variable microscales were replicated as shown in Fig. 17(d).

D. Applications in release devices

For a long time, space release devices are mainly mechanical and pyrotechnic release devices, but there are many shortcomings. For example, during the release process, there will be violent vibrations, which will cause an impact on the spacecraft, leading to damage or misoperations on the surrounding parts.[245,246] Moreover, since the pyrotechnic release devices cannot be reused, the reliability of the devices cannot be verified on the ground in advance. With the rapid development of space technology, the applications of pyrotechnic nuts and explosive bolts are decreasing, while non-impact and non-pyrotechnic release devices attract much attention.

In 2003, GallMark et al.[247] developed an SMPC-based release nut called the Star Nut. The device is mainly composed of two SMPC cylinders, bolts, and nuts. The two SMPC cylinders have uniform dimensions in their initial state. When the devices need to be locked, the two

cylinders are heated above T_{trans} to reduce or increase part of their diameter, then lower the device to room temperature and lock them together utilizing the difference in diameter. The maximum carrying capacity of Star Nut is 13.6 kN, the release time is less than 30 s, the driving energy is less than 15 W, and the operating temperature is -30–$60\,^{\circ}C$.

Leng et al.[248] developed a series of intelligent release devices utilizing carbon fiber reinforced styrene-based SMPC, including the "Lotus" type [Fig. 18(a)], "Eight-claw" type [Fig. 18(b)] and the "Bamboo" type. The locking mechanisms of the three release devices rely on bending, torsion, and compression, respectively. The locking loads of the Lotus type and the Bamboo type release device were obtained through tensile tests. The maximum load of the Bamboo type device was 430 N, which was higher than the 284 N of the Lotus type device. However, the Eight-claw release device failed to complete the locking force test due to the disbonding during the test. The three intelligent-release devices can be fully released in less than 30 s.

Leng et al.[23] proposed a type of high load-bearing compression-type SMPC-based release device fabricated by fiber winding technology as shown in Fig. 18(c). The device can adjust its bearing capacity by the number and depth of indentation as required. Zhao et al.[249] developed another release device with high load capacity based on carbon fiber-reinforced epoxy-based SMPC as shown in Fig. 18(d). The structure is composed of an hourglass-like metal core inside and an SMPC sleeve. In the locked state, the external sleeve is pressed to fit the metal core and can withstand axial tension. When the outer sleeve is reheated, the sleeve returns to its original cylindrical shape and can be easily separated from the metal core. The locking force of the release device increases with the increase of the indentation number and depth. However, the more the indentation depth is, the more the surface damage to the sleeve is. The maximum locking force of the release device can reach 4 kN. However, its mass and volume are larger than the traditional pyrotechnic release device.

Zhang et al.[250] developed an ultralight release device based on SMPC for CubeSat solar array. The release device was an SMPC plate, which can be deformed into a U-shaped hook to realize the locking. The heating circuit was printed on the SMPC plate by screen printing technology; thus, the U-shaped hook can recover to its initial shape stimulated by electricity. Driven by 3 V voltage, the solar panel completed the deployment in 24 s as shown in Fig. 18(e). The SME cycle test and high–low temperature cycle tests prove that the release device has good reusability and reliable locking performance. The release device has the advantages of lightweight, small and simple structure, high integration, and low cost. However, the locking force is low, and its application is limited to small deployable structures.

V. CONCLUSIONS AND OUTLOOK

SMP and SMPC are characterized by lightweight, variable stiffness, large deformation, etc. This work retrospects the constitutive models of SMP and SMPC, the applications in aerospace, intelligent mold, release devices, and biomedical fields. The advantages of SMP and SMPC have shown potential values in many fields. However, the studies on the thermodynamic constitutive theory and the deformation mechanism are still being further explored because of the complexity of the intrinsic mechanism. With the deepening research, the mechanical properties and SME will be improved, and the scope and depth of applications in various fields will be broadened.
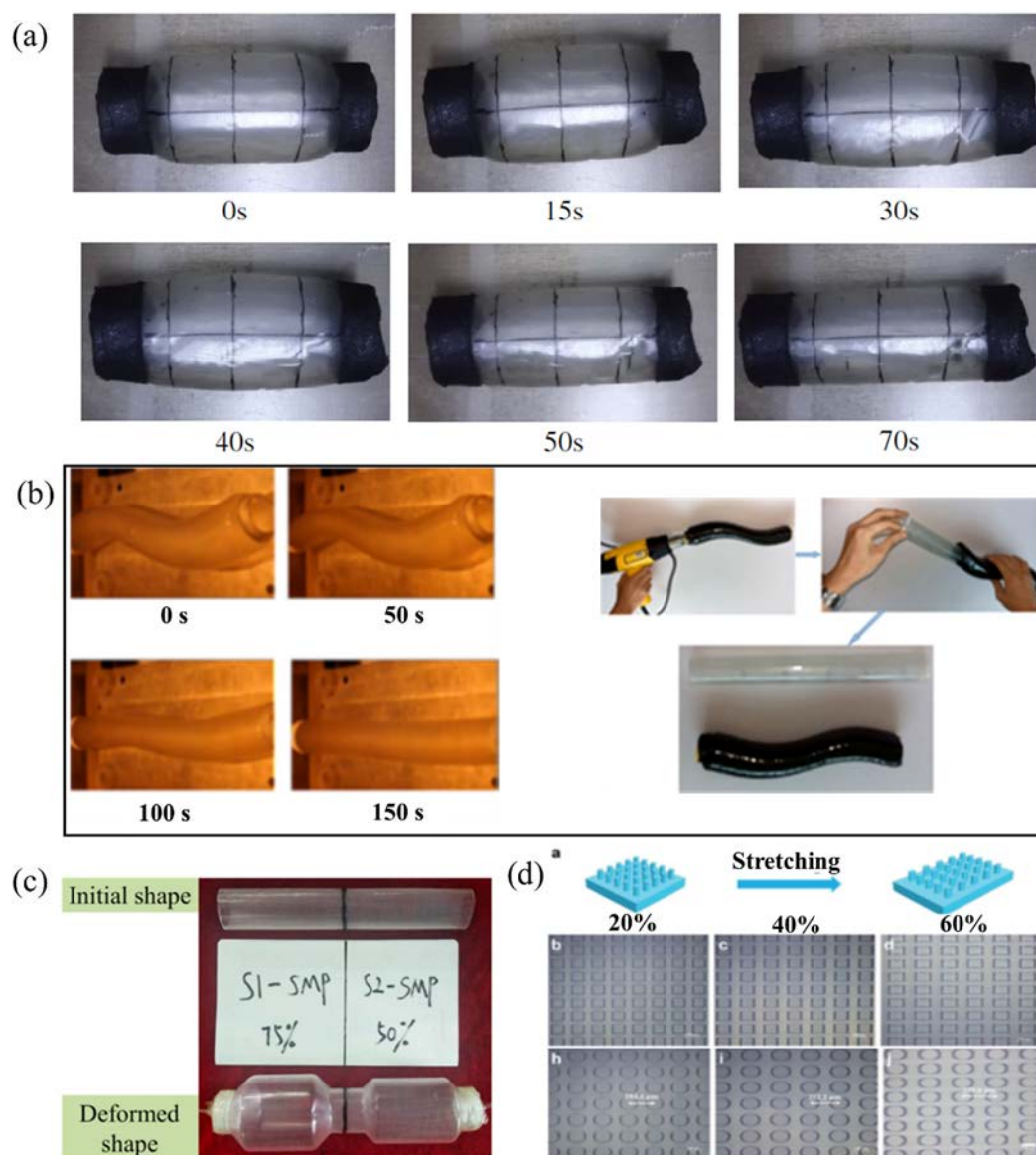
FIG. 17. Intelligent molds. (a) Shape recovery process of the smart mandrel. Reproduced with permission from Zhang *et al.*, Compos. Part B **59**, 230–237 (2014). Copyright 2014 Elsevier.[242] (b) Shape recovery process of S-shaped SMP and the demoulding process of SMP based mold. Reproduced with permission from Du *et al.*, Compos. Struct. **133**, 930–938 (2015). Copyright 2015 Elsevier.[22] (c) Initial shape and deformation shape of the two-bottle SMP mandrel. Reproduced with permission from Du *et al.*, Compos. Part B **173**, 106905 (2019). Copyright 2019 Elsevier.[243] (d) Microarrays mold with different sizes.[244] Reproduced with permission from Wang *et al.*, J. Mater. Chem. A **6**, 24748 (2018). Copyright 2018 Royal Society of Chemistry.

For SMP, although the research framework established by the main functional structure, memory mechanism, and related applications has been formed, however, broad research space and challenges still exist in molecular design, constitutive model prediction, precision control of shape recovery, and industrialization.

(1) Develop a wider variety of shape memory materials that can withstand harsh and special environments by regulating the molecular structure. SMP-based structures in aerospace need to be able to withstand extreme environmental conditions so that materials should have the corresponding environmental adaptability. In the biomedical applications field, materials require good biocompatibility and biodegradability. Presently, there is relatively little research on multifunctional SMP related to biomedical applications. From the perspective of technology development trends, this kind of SMP is an important development direction.

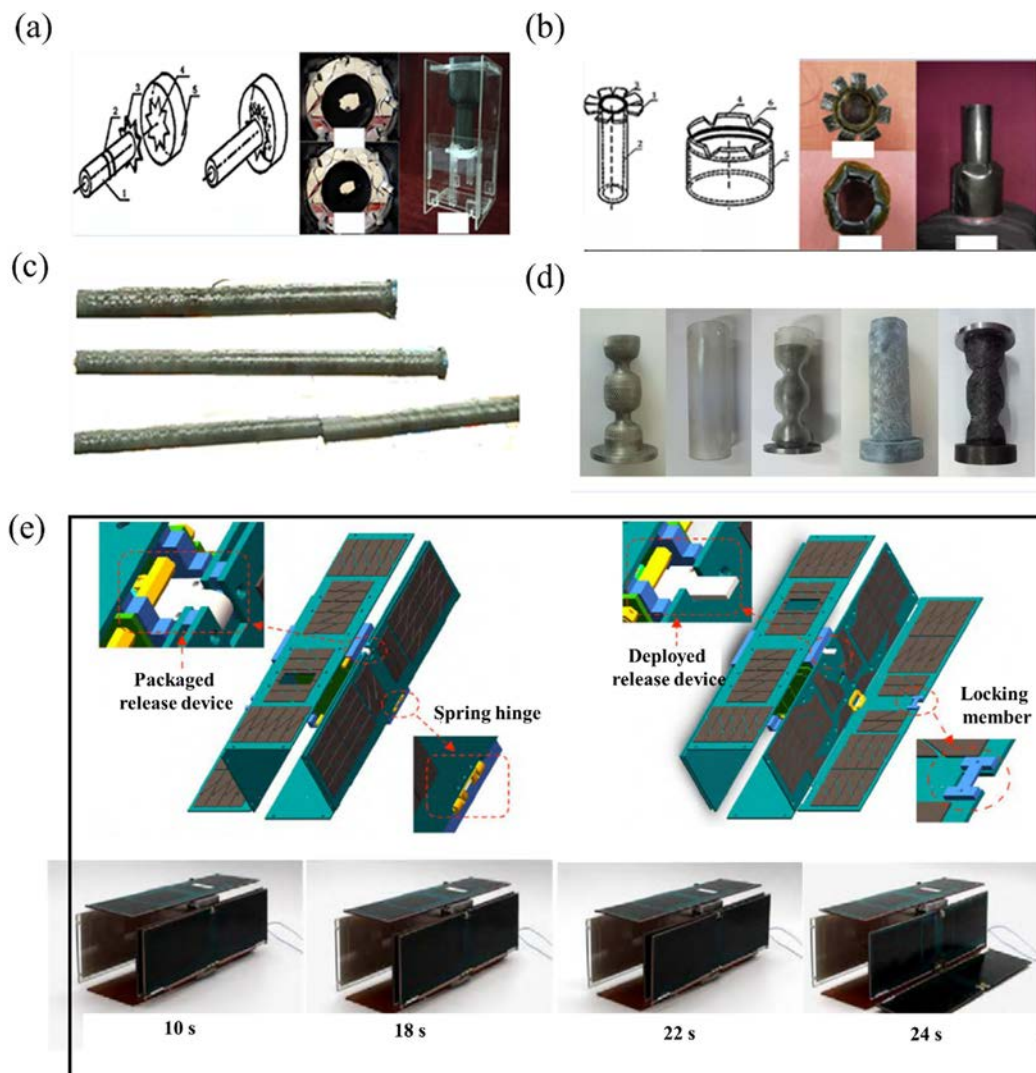(2) Due to the wide application of SMP and SMPC in many fields, the construction of mechanical constitutive models has

FIG. 18. SMPC-based release devices. (a) "Eight paws" release device. Reproduced with permission from Wei *et al.*, Compos. Struct. **133**, 642–651 (2015). Copyright 2015 Elsevier.[248] (b) Lotus release device. Reproduced with permission from Wei *et al.*, Compos. Struct. **133**, 642–651 (2015). Copyright 2015 Elsevier.[248] (c) Unlocking process of SMPC-based release device with large carrying capacity. Reproduced with permission from Zhao *et al.*, J. Harbin Inst. Technol. **48**(05), 1–17 (2016). Copyright 2016 Harbin Gongye Daxue/Harbin Institute of Technology.[23] (d) Sandglass-like smart release device. Reproduced with permission from Zhao *et al.*, Compos. Struct. **223**, 110958 (2019). Copyright 2019 Elsevier.[249] (e) Ultralight release device. Reproduced with permission from Zhang *et al.*, Compos. Struct. **232**, 111561 (2020). Copyright 2020 Elsevier.[250]

gradually become a research hotspot. However, these constitutive models still have some shortcomings. For example, the parameter acquisition process is complicated. Moreover, for constitutive models based on the phase transformation concept, some parameters are obtained by complex shape memory cycle tests. All these factors increase the difficulty of the practical application of the constitutive model. Furthermore, the current constitutive models are only suitable for SMP with the same loading conditions, which greatly limits its applicability. For SMPC, different moduli between fiber and matrix will lead to internal stress. However, most of the constitutive models do not consider this factor.

(3) Combining with other disciplines to realize the high precision control of SMEs is one of the most important research directions. SMP has emerged in the field of 3D printing and 4D printing, and with further development, they will integrate with frontiers in other fields. For example, the development of SMP and 4D printing technology has broken the constraints of traditional flexible optical/electronic machining and increased the designability of structure and function. This not only promotes the further development of SMP but also provides a new method for new flexible optical/electronic devices with multi-function, large areas, and low power consumption.

In conclusion, SMP has a good development prospect in many fields, especially in the high-tech field, but still, there are many key technologies to be overcome in its practical application.

AUTHOR DECLARATIONS
Conflict of Interest

The authors have no conflicts to disclose.

Author Contributions

Wei Zhao: Writing – original draft (equal); Writing – review & editing (equal). **Nan Li:** Writing – original draft (equal); Writing – review & editing (equal). **Liwu Liu:** Supervision (equal); Writing – review & editing (equal). **Jinsong Leng:** Supervision (equal); Writing – review & editing (equal). **Yanju Liu:** Funding acquisition (equal); Supervision (equal); Writing – review & editing (equal).

DATA AVAILABILITY

Data sharing is not applicable to this article as no new data were created or analyzed in this study.

NOMENCLATURE

AD	actuator domains
CNTP	carbon nanotubes paper
CNW	cellulose nano-whisker
CRG	Cornerstone Research Group
CTD	Composite Technology Development Inc.
DWCNT	double-walled carbon nanotube
DSCM	digital speckle correlation method
FEA	finite element analysis
GO	graphene oxide
JPL	Jet Propulsion Laboratory
LCE	liquid crystal elastomers
MIS	minimally invasive surgery
MWCNT	multiwalled carbon nanotube
OBC	olefin block copolymer
PABM	polyaminobismaleimide
PCL	polycaprolactone
PEG	polyethylene glycol
PEG	polyethylene glycol
PLA	polylactic acid
PMMA	polymethyl methacrylate
POE	polyolefin elastomer
PP	polypropylene
PPD	polypentagenolone
Ppy	polypyrrole
PSAM	perfluorinated sulfonic acid membrane
RF	radiofrequency
R_f	shape fixed ratio
R_r	shape recovery ratio
SGDD	shifting-geometry determining domains
SME	shape memory effect
SMP	shape memory polymer
SMPC	shape memory polymer composites
SMPU	shape memory polyurethane
TPU	polyurethane
T_h	high temperature
T_{low}	lowest point
T_{trans}	glass transition temperature
T_r	room temperature
WLF	Williams–Landel–Ferry
ε_{lim}	ultimate deformation

REFERENCES

[1] C. Laschi and R. J. Wood, "Smarter materials for smarter robots," Sci. Rob. **6**(53), eabh4443 (2021).

[2] Q. C. Zheng, C. X. Xu, Z. L. Jiang, M. Zhu, C. Chen, and F. F. Fu, "Smart actuators based on external stimulus response," Front. Chem. **9**, 650358 (2021).

[3] W. Zhao, L. W. Liu, F. H. Zhang, J. S. Leng, and Y. J. Liu, "Shape memory polymers and their composites in biomedical applications," Mat. Sci. Eng. C-Mat. **97**, 864–883 (2019).

[4] Y. Zhang, L. M. Huang, H. J. Song, C. J. Ni, J. J. Wu, Q. Zhao, and T. Xie, "4D printing of a digital shape memory polymer with tunable high performance," ACS Appl. Mater. Interfaces **11**, 32408–32413 (2019).

[5] W. Zhao, C. B. Yue, L. W. Liu, Y. J. Liu, and J. S. Leng, "Research progress of shape memory polymer and 4D printing in biomedical application," Adv. Healthc. Mater. (published online) (2022).

[6] Y. Mao, F. Chen, S. Hou, H. J. Qi, and K. Yu, "A viscoelastic model for hydrothermally activated malleable covalent network polymer and its application in shape memory analysis," J. Mech. Phys. Solids **127**, 239–265 (2019).

[7] W. S. Miao, W. K. Zou, B. J. Jin, C. J. Ni, N. Zheng, Q. Zhao, and T. Xie, "On demand shape memory polymer via light regulated topological defects in a dynamic covalent network," Nat. Commun. **11**, 4257 (2020).

[8] X. Wang, H. Lu, X. Shi, K. Yu, and Y. Q. Fu, "A thermomechanical model of multi-shape memory effect for amorphous polymer with tunable segment compositions," Compos. Part B **160**, 298–305 (2019).

[9] W. Zhao, C. B. Yue, L. W. Liu, J. S. Leng, and Y. J. Liu, "Mechanical behavior analyses of 4D printed metamaterials structures with excellent energy absorption ability," Compos. Struct. **304**, 116360 (2023).

[10] K. Dong, C. Zhao, M. Z. Yan, J. N. Wang, X. Cui, X. J. Yu, and X. L. Xiao, "Recent advances of two-way shape memory polymers and four-dimensional printing under stress-free conditions," Smart Mater. Struct. **29**(2), 023001 (2020).

[11] Q. Ze, X. Kuang, S. Wu, J. Wong, S. M. Montgomery, R. Zhang, and J. M. Kovitz, "Shape memory polymers: Magnetic shape memory polymers with integrated multifunctional shape manipulation," Adv. Mater. **32**(4), 2070025 (2020).

[12] T. W. Wong, M. Behl, N. I. S. M. Yusoff, T. F. Li, M. U. Wahit, A. F. Ismail, Q. Zhao, and A. Lendlein, "Bio-based composites from plant based precursors and hydroxyapatite with shape-memory capability," Compos. Sci. Technol. **194**, 108138 (2020).

[13] L. Wang, M. Y. Razzaq, A. Lendlein, T. Rudolph, M. Heuchel, U. Nochel, U. Mansfeld, Y. Jiang, O. E. C. Gould, M. Behl, K. Kratz, and A. Lendlein, "Reprogrammable, magnetically controlled polymeric nanocomposite actuators," Mater. Horiz. **5**(5), 861–867 (2018).

[14] W. Zhao, L. W. Liu, X. Lan, J. S. Leng, and Y. J. Liu, "Thermomechanical constitutive models of shape memory polymers and their composites," Appl. Mech. Rev. **75**(2), 020802 (2023).

[15] N. Roudbarian, M. Baniasadi, P. Nayyeri, M. Ansari, R. Hedayati, and M. Baghani, "Enhancing shape memory properties of multi-layered and multi-material polymer composites in 4D printing," Smart Mater. Struct. **30**(10), 105006 (2021).

[16]X. Z. Xin, L. W. Liu, Y. J. Liu, and J. S. Leng, "Prediction of effective thermomechanical behavior of shape memory polymer composite with microdamage interface," Compos. Commun. **25**, 100727 (2021).

[17]C. J. Zeng, L. W. Liu, J. S. Leng, and Y. J. Liu, "Compression behavior and energy absorption of 3D printed continuous fiber reinforced composite honeycomb structures with shape memory effects," Addit. Manuf. **38**, 101842 (2021).

[18]Z. X. Liu, X. Lan, W. F. Bian, L. W. Liu, Q. F. Li, Y. J. Liu, and J. S. Leng, "Design, material properties and performances of a smart hinge based on shape memory polymer composites," Compos. Part B **193**, 108056 (2020).

[19]T. Z. Liu, L. W. Liu, M. Yu, Q. F. Li, C. J. Zeng, X. Lan, Y. J. Liu, and J. S. Leng, "Integrative hinge based on shape memory polymer composites: Material, design, properties and application," Compos. Struct. **206**(15), 164–176 (2018).

[20]W. Zhao, Z. P. Huang, L. W. Liu, W. B. Wang, J. S. Leng, and Y. J. Liu, "Porous bone tissue scaffold concept based on shape memory PLA/Fe_3O_4," Compos. Sci. Technol. **203**, 108563 (2021).

[21]W. Zhao, Z. P. Huang, L. W. Liu, W. B. Wang, J. S. Leng, and Y. J. Liu, "Bionic design and performance research of tracheal stent based on shape memory polycaprolactone," Compos. Sci. Technol. **229**, 109671 (2022).

[22]H. Y. Du, L. W. Liu, J. S. Leng, H. X. Peng, F. Scarpa, and Y. J. Liu, "Shape memory polymer S-shaped mandrel for composite air duct manufacturing," Compos. Struct. **133**, 930–938 (2015).

[23]L. W. Liu, W. Zhao, X. Lan, Y. J. Liu, and J. S. Leng, "Soft intelligent material and its applications in aerospace," J. Harbin Inst. Technol. **48**(05), 1–17 (2016).

[24]H. Meng and G. Q. Li, "A review of stimuli-responsive shape memory polymer composites," Polymer **54**(9), 2199 (2013).

[25]J. G. Pang, G. Wang, M. Qu, and X. Y. Shi, "Progress on mechanism, characterization and multiple shape memory effect of shape memory polymer," Cailiao Gongcheng **46**(5), 64–71 (2018).

[26]H. Xiao, C. Ma, X. Le, L. Wang, W. Lu, P. Theato, T. Hu, J. Zhang, and T. A. Chen, "A multiple shape memory hydrogel induced by reversible physical interactions at ambient condition," Polymers **9**(4), 138 (2017).

[27]T. Xie, "Tunable polymer multi-shape memory effect," Nature **464**, 267–270 (2010).

[28]C. Zeng, H. Seino, J. Ren, and N. Yoshie, "Polymers with multishape memory controlled by local glass transition temperature," ACS Appl. Mater. Interfaces **6**, 2753 (2014).

[29]I. Bellin, S. Kelch, R. Langer, and A. Lendlein, "Polymeric triple-shape materials," Proc. Natl. Acad. Sci. U.S.A. **103**(48), 18043–18047 (2006).

[30]A. H. Torbati, H. B. Nejad, M. Ponce, J. P. Sutton, and P. T. Mather, "Properties of triple shape memory composites prepared via polymerization-induced phase separation," Soft Matter **10**, 3112 (2014).

[31]X. Yang, L. Wang, W. X. Wang, H. M. Chen, G. Yang, and S. Zhou, "Triple shape memory effect of star-shaped polyurethane," ACS Appl. Mater. Interfaces **6**, 6545 (2014).

[32]W. Li, Y. Liu, and J. Leng, "Selectively actuated multi-shape memory effect of a polymer multicomposite," J. Mater. Chem. A **3**(48), 24532 (2015).

[33]A. Maimaitiming, M. Zhang, H. Tan, M. Wang, and G. Z. Wu, "High-strength triple shape memory elastomers from radiation-vulcanized polyolefin elastomer/polypropylene blends," ACS Appl. Polym. Mater. **1**(7), 1735–1748 (2019).

[34]S. M. Lai, P. Y. You, Y. T. Chiu, and C. W. Kuo, "Triple-shape memory properties of thermoplastic polyurethane/olefin block copolymer/polycaprolactone blends," J. Polym. Res. **24**(10), 161 (2017).

[35]Y. Zhang, W. Li, R. Wu, and W. Wang, "PU/PMMA composites synthesized by reaction induced phase separation: A general approach to achieve a shape memory effect," RSC Adv. **7**(54), 33701–33707 (2017).

[36]I. S. Kolesov and H. J. Radusch, "Multiple shape-memory behavior and thermal-mechanical properties of peroxide cross-linked blends of linear and short-chain branched polyethylenes," Express Polym. Lett. **2**, 461 (2008).

[37]R. Hoeher, T. Raidt, C. Krumm, M. Meuris, F. Katzenberg, and J. C. Tiller, "Tunable multiple-shape memory polyethylene blends," Macromol. Chem. Phys. **214**, 2725 (2013).

[38]Y. Gao, W. Liu, and S. Zhu, "Thermoplastic polyolefin elastomer blends for multiple and reversible shape memory polymers," Ind. Eng. Chem. Res. **58**(42), 19495–19502 (2019).

[39]J. Li, T. Liu, S. Xia, Y. Pan, Z. Zheng, X. Ding, and Y. Peng, "A versatile approach to achieve quintuple-shape memory effect by semi-interpenetrating polymer networks containing broadened glass transition and crystalline segments," J. Mater. Chem. **21**(33), 12213 (2011).

[40]J. Wu, C. Yuan, Z. Ding, M. Isakov, Y. Q. Mao, T. J. Wang, M. L. Dunn, and H. J. Qi, "Multi-shape active composites by 3D printing of digital shape memory polymers," Sci. Rep. **6**, 24224 (2016).

[41]M. Behl, K. Kratz, and A. Lendlein, "Reversible bidirectional shape-memory polymers," Adv. Mater. **25**(32), 4466–4469 (2013).

[42]M. Behl, K. Kratz, U. Noechel, T. Sauter, and A. Lendlein, "Temperature-memory polymer actuators," Proc. Natl. Acad. Sci. U.S.A. **110**(31), 12555–12559 (2013).

[43]J. Hu, Y. Zhu, H. Huang, and H. H. Huang, "Recent advances in shape-memory polymers: Structure, mechanism, functionality, modeling and applications," Prog. Polym. Sci. **37**, 1720–1763 (2012).

[44]K. Hiraoka, N. Tagawa, and K. Baba, "Shape-memory effect controlled by the crosslinking topology in uniaxially-deformed smectic C* Elastomers," Macromol. Chem. Phys. **209**, 298–307 (2008).

[45]Z. Pei, E. M. Terentjev, Q. M. Chen, E. M. Terentjev, Y. Wei, and Y. Ji, "Mouldable liquid-crystalline elastomer actuators with exchangeable covalent bonds," Nat. Mater. **13**, 36–41 (2014).

[46]A. Agrawal, T. H. Yun, and R. Verduzco, "Shape-responsive liquid crystal elastomer bilayers," Soft Matter **10**, 1411–1415 (2014).

[47]T. Chung, A. Romo-Uribe, and P. T. Mather, "Two-way reversible shape memory in a semicrystalline network," Macromolecules **41**, 184–192 (2008).

[48]J. Zhou, S. A. Turner, and S. S. Sheiko, "Shapeshifting: Reversible shape memory in semicrystalline elastomers," Macromolecules **47**, 1768–1776 (2014).

[49]B. W. Li, Y. J. Liu, and J. S. Leng, "Light-actuated reversible shape memory effect of a polymer composite," Compos. Part A **110**, 70–75 (2018).

[50]Q. J. Ze, X. Kuang, S. Wu, J. Wong, S. M. Montgomery, R. D. Zhang, J. M. Kovitz, F. Y. Yang, H. J. Qi, and R. K. Zhao, "Magnetic shape memory polymers with integrated multifunctional shape manipulations," Adv. Mater. **32**(4), 1906657 (2019).

[51]Y. Gao, W. Liu, and S. Zhu, "Polyolefin thermoplastics for multiple shape and reversible shape memory," ACS Appl. Mater. Interfaces **9**(5), 4882–4889 (2017).

[52]X. L. Wu, H. Zheng, Y. J. Liu, and J. S. Leng, "Thermomechanical property of epoxy shape memory polymers," Int J Mod Phys B. **24**, 2386–2391 (2009).

[53]J. S. Leng, F. Xie, X. L. Wu, and Y. J. Liu, "Effect of γ-radiation on the properties of epoxy-based shape memory polymers," J. Intell. Mater. Syst. Struct. **25**(10), 1256–1263 (2014).

[54]J. Ivens, M. Urbanus, and C. D. Smet, "Shape recovery in a thermoset shape memory polymer and its fabric-reinforced composites," Express Polym. Lett. **5**(3), 254–261 (2011).

[55]N. Zheng, G. Q. Fang, Z. L. Cao, Q. Zhao, and T. Xie, "High strain epoxy shape memory polymer," Polym. Chem. **6**(16), 3046–3053 (2015).

[56]T. Xie and I. A. Rousseau, "Facile tailoring of thermal transition temperature of epoxy shape memory epoxy," Polymer **50**(8), 1852–1856 (2009).

[57]I. A. Rousseau and T. Xie, "Shape memory epoxy: Composition, structure, properties and shape memory performances," J. Mater. Chem. A **20**(17), 3431–3441 (2010).

[58]A. B. Leonardi, L. A. Fasce, I. A. Zucchi, C. E. Hoppe, and E. R. Soule, "Shape memory epoxies based on networks with chemical and physical crosslinks," Eur. Polym. J. **47**(3), 362–369 (2011).

[59]R. Biju and C. P. R. Nair, "Synthesis and characterization of shape memory epoxy-anhydride system," J. Polym. Res. **20**(2), 82 (2013).

[60]L. Santo, F. Quadrini, E. A. Squeo, F. Dolce, G. Mascetti, D. Bertolotto, W. Villadei, P. L. Ganga, and V. Zolesi, "Behavior of shape memory epoxy foams in microgravity: Experimental results of STS-134 mission," Microgravity Sci. Technol. **24**(4), 287–296 (2012).

[61]K. Gall, M. L. Dunn, Y. Liu, D. Finch, M. Lake, and N. A. Munshi, "Shape memory polymer nanocomposites," Acta Mater. **50**(20), 5115–5126 (2002).

[62]S. C. Arzberger, N. A. Munshi, M. S. Lake, J. Wintergerst, S. Varlese, and M. P. Ulmer, "Elastic memory composite technology for thin lightweight

space-and ground-based deployable mirrors," in *Proceedings of the Optical Materials and Structures Technologies Conference*, San Diego (M. P. Ulmer Composite Technology Development, 2003), pp. 143–154.

[63]F. Xie, L. N. Huang, J. S. Leng, and Y. J. Liu, "Thermoset shape memory polymers and their composites," J. Intell. Mater. Syst. Struct. **27**(18), 2433–2455 (2016).

[64]J. Sun, Y. J. Liu, and J. S. Leng, "Mechanical properties of shape memory polymer composites enhanced by elastic fibers and their application in variable stiffness morphing skins," J. Intell. Mater. Syst. Struct. **26**(15), 2020–2027 (2015).

[65]M. C. Everhart, J. B. Stahl, E. W. Traxler, and E. Havens, "Shape memory polymer configurative tooling," Proc. SPIE **5388**, 87–94 (2004).

[66]G. P. Tandon, K. Goecke, and K. Cable, "Durability assessment of styrene-and epoxy-based shape memory polymer resins," J. Intell. Mater. Syst. Struct. **20**(17), 2127–2143 (2009).

[67]F. K. Li, A. Perrenoud, and R. C. Larock, "Thermophysical and mechanical properties of novel polymers prepared by the cationic copolymerization of fish oils, styrene and divinylbenzene," Polymer **42**(26), 10133–10145 (2001).

[68]C. Meiorin, M. I. Aranguren, and M. A. Mosiewicki, "Smart structural thermosets from the cationic copolymerization of a vegetable oil," J. Intell. Mater. Syst. Struct. **124**(6), 5071–5078 (2012).

[69]F. Xie, L. N. Huang, Y. J. Liu, and J. S. Leng, "Synthesis and characterization of high temperature cyanate-based shape memory polymers with functional polybutadiene/acrylonitrile," Polymer **55**(23), 5873–5879 (2014).

[70]F. Xie, X. B. Gong, L. N. Huang, L. W. Liu, J. S. Leng, and Y. J. Liu, "Effects of accelerated aging on thermal, mechanical, and shape memory properties of a cyanate-based shape memory polymer: II Atomic oxygen," Polym. Degrad. Stab. **186**, 109515 (2021).

[71]M. C. Everhart, D. M. Nickerson, and R. D. Hreha, "High-temperature reusable shape memory polymer mandrel," Proc. SPIE **6171**, 61710K (2006).

[72]R. Biju and C. P. Reghunadhan Nair, "Effect phenol end functional switching segments on the shape memory properties of epoxy-cyanate ester system," J. Intell. Mater. Syst. Struct. **131**(23), 41196 (2014).

[73]R. Biju, C. Gouri, and C. P. Reghunadhan Nair, "Shape memory polymers based on cyanate ester-epoxy-poly (tetramethyleneoxide) co-reacted system," Eur. Polym. J. **48**(3), 499–511 (2012).

[74]K. Wang, G. M. Zhu, Y. K. Wang, and F. Ren, "Thermal and shape memory properties of cyanate/polybutadiene epoxy/polysebacic polyanhydride copolymer," J. Intell. Mater. Syst. Struct. **132**(23), 42045 (2015).

[75]Y. M. Zhao, D. D. Zhang, and L. Guo, "Shape memory behavior of bisphenol a-type cyanate ester/carboxyl-terminated liquid nitrile rubber coreacted system," Colloid Polym. Sci. **292**(10), 2707–2713 (2014).

[76]X. L. Xiao, D. Y. Kong, X. Y. Qiu, W. B. Zhang, F. H. Zhang, L. W. Liu, Y. J. Liu, S. Zhang, Y. Hu, and J. S. Leng, "Shape memory polymers with adjustable high glass transition temperatures," Macromolecules **48**(11), 3582–3589 (2015).

[77]X. L. Xiao, X. Y. Qiu, D. Y. Kong, W. B. Zhang, Y. J. Liu, and J. S. Leng, "Optically transparent high temperature shape memory polymers," Soft Matter **12**(11), 2894–2900 (2016).

[78]X. L. Xiao, D. Y. Kong, X. Y. Qiu, W. B. Zhang, Y. J. Liu, S. Zhang, F. H. Zhang, Y. Hu, and J. S. Leng, "Shape memory polymers with high and low temperature resistant properties," Sci. Rep. **5**, 14137 (2015).

[79]H. Koerner, R. J. Strong, M. L. Smith, D. H. Wang, L. S. Tan, K. M. Lee, T. J. White, and R. A. Vaia, "Polymer design for high temperature shape memory: Low crosslink density polyimides," Polymer **54**(1), 391–402 (2013).

[80]Q. H. Wang, Y. K. Bai, Y. Chen, J. P. Ju, F. Zheng, and T. M. Wang, "High performance shape memory polyimides based on π-π interactions," J. Mater. Chem. A **3**(1), 352–359 (2015).

[81]Q. W. Zhang, H. Q. Wei, Y. J. Liu, J. S. Leng, and S. Y. Du, "Triple shape memory effects of bismaleimide based thermosetting polymer networks prepared via heterogeneous crosslinking structures," RSC Adv. **6**(13), 10233–10241 (2016).

[82]R. Biju and C. P. Reghunadhan Nair, "High transition temperature shape memory polymer composites based on bismaleimide resin," High Perform. Polym. **25**(4), 464–474 (2013).

[83]A. J. W. McClung, J. A. Shumaker, J. W. Baur, S. D. Reed, and S. A. Matthys, "Bismaleimide based shape memory polymers: Correlation between chemical

composition and mechanical properties," AIAA Paper No. 2011-2112, 2011, pp. 4–11.

[84]W. Huang, B. Yang, Y. Zhao, and Z. Ding, "Thermomoisture responsive polyurethane shape-memory polymer and composites: A review," J. Mater. Chem. A **20**(17), 3367–3381 (2010).

[85]H. Koeren, G. Price, N. Pearce, M. Alexander, and R. A. Vaia, "Remotely actuated polymer nanocomposites-stress-recovery of carbon-nanotube-filled thermoplastic elastomers," Nat. Mater. **3**(2), 115–120 (2004).

[86]J. S. Leng, X. Lan, Y. J. Liu, and S. Y. Du, "Electroactive thermoset shape memory polymer nanocomposite filled with nanocarbon powders," Smart Mater. Struct. **18**(7), 074003–074008 (2009).

[87]X. Qi, H. Xiu, Y. Wei, Y. Zhou, Y. L. Guo, R. Huang, H. W. Bai, and Q. Fu, "Enhanced shape memory property of polylactide/thermoplastic poly(ether)-urethane composites via carbon black self-networking induced co-continuous structure," Compos. Sci. Technol. **139**, 8–16 (2017).

[88]Q. Q. Ni, C. S. Zhang, Y. Fu, G. Z. Dai, and T. Kimura, "Shape memory effect and mechanical properties of carbon nanotube/shape memory polymer nanocomposites," Compos. Struct. **81**(2), 176–184 (2007).

[89]F. P. Du, E. Z. Ye, and W. Yang, "Electroactive shape memory polymer based on optimized multiwalled carbon nanotubes/polyvinyl alcohol nanocomposites," Compos. Part B **68**(2), 170–175 (2015).

[90]X. Li, L. Wang, Z. Zhang, D. Y. Kong, X. L. Ao, and X. L. Xiao, "Electroactive high-temperature shape memory polymers with high recovery stress induced by ground carbon fibers," Macromol. Chem. Phys. **220**, 1900164 (2019).

[91]P. R. Buckley, G. H. Mckinley, T. S. Wilson, W. Small, W. J. Benett, J. P. Bearinger, M. W. McElfresh, and D. J. Maitland, "Inductively heated shape memory polymer for the magnetic actuation of medical devices," IEEE Trans. Biomed. Eng. **53**(10), 2075–2083 (2006).

[92]F. Cao and S. Jana, "Nanoclay-tethered shape memory polyurethane nanocomposites," Polymer **48**(13), 3790–3800 (2007).

[93]T. Ohki, Q. Q. Ni, and N. Ohsako, "Nanoclay-tethered shape memory polyurethancomposites with shape memory polymer," Compos. Part A **35**(9), 1065–1073 (2004).

[94]Y. K. Wang, G. M. Zhu, Y. S. Tang, T. T. Liu, J. Q. Xie, and F. Ren, "Short glass fiber reinforced radiation crosslinked shape memory SBS/LLDPE blends," J. Intell. Mater. Syst. Struct. **131**(17), 40691 (2014).

[95]M. Fejos, G. Romhany, J. Karger, and J. Reinf, "Shape memory characteristics of woven glass fiber fabric reinforced epoxy composite in flexure," Plast. Compos. **31**(22), 1532–1537 (2012).

[96]Y. Liu, K. Gall, M. L. Dunn, and P. McCluskey, "Thermomechanics of shape memory polymer nanocomposites," Mech. Mater. **36**(10), 929–940 (2004).

[97]K. Gall, M. L. Dunn, Y. Liu, G. Stefanic, and D. Balzar, "Internal stress storage in shape memory polymer nanocomposites," Appl. Phys. Lett. **85**(2), 290 (2004).

[98]C. Likitaporn, P. Mora, S. Tiptipakorn, and S. J. Rimdusit, "Recovery stress enhancement in shape memory composites from silicon carbide whisker–filled benzoxazine-epoxy polymer alloy," J. Intell. Mater. Syst. Struct. **29**(3), 388–396 (2017).

[99]H. B. Lu, Y. T. Yao, W. M. Huang, J. S. Leng, and D. Hui, "Significantly improving infrared light-induced shape recovery behavior of shape memory polymeric nanocomposite via a synergistic effect of carbon nanotube and boron nitride," Compos. Part B **62**, 256–261 (2014).

[100]M. J. Duncan, M. F. Metzeger, D. Schumann, A. Lee, and T. S. Wilson, "Photothermal properties of shape memory polymers micro-actuators for treating stroke," Lasers Surg. Med. **30**(1), 1–11 (2002).

[101]M. V. Biyani, M. Jorfi, and C. Weder, "Light-stimulated mechanically switchable, photopatternable cellulose nanocomposites," Polym. Chem. **5**(19), 5716–5724 (2014).

[102]A. Lendlein, H. Y. Jiang, O. Junger, and R. Langer, "Light-induced shape-memory polymers," Nature **434**, 879–882 (2005).

[103]L. Yu and H. F. Yu, "Light-powered tumbler movement of graphene oxide/polymer nanocomposites," ACS Appl. Mater. Interfaces **7**(6), 3834–3839 (2015).

[104]H. J. Zhang and Y. Zhao, "Polymers with dual light-triggered functions of shape memory and healing using gold nanoparticles," ACS Appl. Mater. Interfaces **5**(24), 13069–13075 (2013).

[105]Y. W. Zheng, J. Li, E. Lee, and S. Yang, "Light-induced shape recovery of deformed shape memory polymer micropillar arrays with gold nanorods," RSC Adv. **5**(39), 30495–30499 (2015).

[106]L. Valentini, M. Cardinali, and J. Kenny, "Hotpress transferring of graphene nanoplatelets on polyurethane block copolymers film for electroactive shape memory devices," J. Polym. Sci., Part B **52**(16), 1100–1106 (2014).

[107]Z. W. Wang, J. Zhao, M. Chen, M. H. Yang, L. Y. Tang, Z. M. Dang, F. H. Chen, M. M. Huang, and X. Dong, "Dually actuated triple shape memory polymers of cross-linked polycyclooctene-carbon nanotube/polyethylene nanocomposites," ACS Appl. Mater. Interfaces **6**(22), 20051–20059 (2014).

[108]J. Alam, M. Alam, M. Raja, Z. Abduljaleel, and L. A. Dass, "MWCNTs-reinforced epoxidized linseed oil plasticized polylactic acid nanocomposite and its electroactive shape memory behavior," Int. J. Mol. Sci. **15**(11), 19924–19937 (2014).

[109]N. G. Sahoo, Y. C. Jung, and J. W. Cho, "Electroactive shape memory effect of polyurethane composites filled with carbon nanotubes and conducting polymer," Mater. Manuf. Process. **22**(4), 419–423 (2007).

[110]K. L. Dagnon, A. E. Way, S. O. Carson, J. Silva, J. Maia, and S. J. Rowan, "Controlling the rate of water-induced switching in mechanically dynamic cellulose nanocrystal composites," Macromolecules **46**(20), 8203–8212 (2013).

[111]H. B. Lu, W. M. Huang, and J. S. Leng, "Functionally graded and self-assembled carbon nanofiber and boron nitride in nanopaper for electrical actuation of shape memory nanocomposites," Compos. Part B **62**(3), 1–4 (2014).

[112]J. S. Leng, X. Lan, Y. J. Liu, S. Y. Du, W. M. Huang, N. Liu, S. J. Phee, and Q. Yuan, "Electrical conductivity of thermoresponsive shape-memory polymer with embedded micron sized Ni powder chains," Appl. Phys. Lett. **92**(1), 014104 (2008).

[113]H. Kalita and N. Karak, "Hyperbranched polyurethane/Fe_3O_4 thermosetting nanocomposites as shape memory materials," Polym. Bull. **70**(11), 2953–2965 (2013).

[114]Y. Zhu, J. L. Hu, H. S. Luo, R. J. Young, L. B. Deng, S. Zhang, Y. Fan, and G. D. Ye, "Rapidly switchable water-sensitive shape-memory cellulose/elastomer nanocomposites," Soft Matter **8**(8), 2509–2517 (2012).

[115]S. Y. Gu, K. Chang, and S. P. Jin, "Dual-induced self-expandable stent based on biodegradable shape memory polyurethane nanocomposites (PCLAU/Fe_3O_4) triggered around body temperature," J. Appl. Polym. Sci. **135**, 45686 (2018).

[116]H. Kalita and N. Karak, "Hyperbranched polyurethane/Fe_3O_4 nanoparticles decorated multiwalled carbon nanotube thermosetting nanocomposites as microwave actuated shape memory materials," J. Mater. Res. **28**(16), 2132–2141 (2013).

[117]K. Yu, Y. Liu, and J. Leng, "Shape memory polymer/CNT composites and their microwave induced shape memory behaviors," RSC Adv. **4**(6), 2961–2968 (2014).

[118]H. Du, Z. Song, J. Wang, Z. H. Liang, Y. H. Shen, and F. You, "Microwave-induced shape-memory effect of silicon carbide/poly(vinyl alcohol) composite," Sens. Actuators, A **228**, 1–8 (2015).

[119]J. R. Kumpfer and S. J. Rowan, "Thermo-, photo-, and chemo-responsive shape-memory properties from photo-cross-linked metallo-supramolecular polymers," J. Am. Chem. Soc. **133**(32), 12866–12874 (2011).

[120]Y. Zhang, X. Jiang, R. L. Wu, and W. Wang, "Multi-stimuli responsive shape memory polymers synthesized by using reaction-induced phase separation," J. Intell. Mater. Syst. Struct. **133**(24), 43534 (2016).

[121]Z. Tang, H. L. Kang, Q. Y. Wei, B. C. Guo, L. Q. Zhang, and D. M. Jia, "Incorporation of graphene into polyester/carbon nanofibers composites or better multi-stimuli responsive shape memory performances," Carbon **64**, 487–498 (2013).

[122]W. B. Li, Y. J. Liu, and J. S. Leng, "Shape memory polymer nanocomposite with multi-stimuli response and two-way reversible shape memory behavior," RSC Adv. **4**(106), 61847–61854 (2014).

[123]W. B. Li, Y. J. Liu, and J. S. Leng, "Programmable and shape-memorizing information carriers," ACS Appl. Mater. Interfaces **9**(51), 44792–44798 (2017).

[124]Z. He, T. Xie, and J. Z. Hilt, "Remote controlled multishape polymer nanocomposites with selective radiofrequency actuations," Adv. Mater. **23**, 3192–3196 (2011).

[125]L. Yu, Q. Wang, H. Yang, J. Sun, C. Y. Li, C. Zou, Z. M. He, Z. D. Wang, L. Zhou, L. Y. Zhanga, and H. Yang, "Multi-shape-memory effects in a wavelength-selective multicomposite," J. Mater. Chem. A **3**, 13953–13961 (2015).

[126]E. A. Pieczyska, W. K. Nowacki, H. Tobushi, and S. Hayashi, "Thermomechanical properties of shape memory polymer subjected to tension in various conditions," QIRT J. **6**(2), 189–205 (2009).

[127]N. Sahoo, Y. Jung, H. Yoo, and J. W. Cho, "Influence of carbon nanotubes and polypyrrole on the thermal, mechanical and electroactive shape memory properties of polyurethane nanocomposites," Compos. Sci. Technol. **67**(9), 1920–1929 (2007).

[128]C. Zhang and Q. Q. Ni, "Bending behavior of shape memory polymer based laminates," Compos. Struct. **78**(2), 153–161 (2007).

[129]S. H. Lee, M. K. Jang, H. S. Kim, and B. M. Kim, "Shape memory effects of molded flexible polyurethane foam," Smart Mater. Struct. **16**(6), 2486–2491 (2007).

[130]Y. Y. Liu, C. M. Han, H. F. Tan, and X. W. Du, "Thermal, mechanical and shape memory properties of shape memory epoxy resin," Mater. Sci. Eng., A **527**(10–11), 2510–2514 (2010).

[131]J. S. Leng, X. L. Wu, and Y. J. Liu, "Effect of a linear monomer on the thermomechanical properties of epoxy shape-memory polymer," Smart Mater. Struct. **18**, 095031 (2009).

[132]K. K. Westbrook, F. Castro, K. N. Long, A. J. Slifka, and H. J. Qi, "Improved testing system for thermomechanical experiments on polymers using uniaxial compression equipment," Polym. Test. **29**(4), 503–512 (2010).

[133]R. Xiao, J. Choi, N. Lakhera, C. M. Yakacki, C. P. Frick, and T. D. Nguyen, "Modeling the glass transition of amorphous networks for shape-memory behavior," J. Mech. Phys. Solids **61**(7), 1612–1635 (2013).

[134]K. Yu, Y. Liu, Y. Liu, H. X. Peng, and J. S. Leng, "Mechanical and shape recovery properties of shape memory polymer composite embedded with cup-stacked carbon nanotubes," J. Intell. Mater. Syst. Struct. **25**(10), 1264–1275 (2013).

[135]F. Xie, L. W. Liu, X. B. Gong, L. N. Huang, J. S. Leng, and Y. J. Liu, "Effects of accelerated aging on thermal, mechanical and shape memory properties of cyanate-based shape memory polymer. I. Vacuum ultraviolet radiation," Polym. Degrad. Stab. **138**, 91–97 (2017).

[136]H. Gao, X. Lan, L. Liu, X. Xiao, Y. Liu, and J. S. Leng, "Study on performances of colorless and transparent shape memory polyimide film in space thermal cycling, atomic oxygen and ultraviolet irradiation environments," Smart Mater. Struct. **26**(9), 095001 (2017).

[137]Q. Tan, F. F. Li, L. W. Liu, H. T. Chu, Y. J. Liu, and J. S. Leng, "Effects of atomic oxygen on epoxy-based shape memory polymer in low earth orbit," J. Intell. Mater. Syst. Struct. **29**(6), 1081–1087 (2018).

[138]W. Zhao, Q. Wang, L. W. Liu, L. H. Zhu, J. S. Leng, and Y. J. Liu, "Structural response measurement of shape memory polymer components using digital image correlation method," Opt. Lasers Eng. **110**, 323–340 (2018).

[139]F. F. Li, F. Scarpa, X. Lan, L. W. Liu, Y. J. Liu, and J. S. Leng, "Bending shape recovery of unidirectional carbon fiber reinforced epoxy-based shape memory polymer composites," Compos. Part A **116**, 169–179 (2019).

[140]H. Tobushi, T. Hashimoto, S. Hayashi, and E. Yamada, "Thermomechanical constitutive modeling in shape memory polymer of polyurethane series," J. Intell. Mater. Syst. Struct. **8**(8), 711–718 (1997).

[141]H. Tobushi, K. Okumura, S. Hayashi, and N. Ito, "Thermomechanical constitutive model of shape memory polymer," Mech. Mater. **33**(10), 545–554 (2001).

[142]B. Zhou, Y. J. Liu, and J. S. Leng, "A macro-mechanical constitutive model for shape memory polymer," Sci. China-Phys. Mech. Astron. **53**(12), 2266–2273 (2010).

[143]B. Zhou, Y. J. Liu, X. Lan, J. S. Leng, and S. H. Yoon, "A glass transition model for shape memory polymer and its composite," Int. J. Mod. Phys. B **23**(6), 1248–1253 (2009).

[144]J. Morshedian, H. A. Khonakdar, and S. Rasouli, "Modeling of shape memory induction and recovery in heat-shrinkable polymers," Macromol. Theory Simul. **14**(7), 428–434 (2005).

[145]J. Diani, Y. Liu, and K. Gall, "Finite strain 3D thermoviscoelastic constitutive model for shape memory polymers," Polym. Eng. Sci. **46**(4), 486–492 (2006).

[146]S. J. Hong, W. R. Yu, and J. H. Youk, "Thermomechanical deformation analysis of shape memory polymers using viscoelasticity," AIP Conf. Proc. **907**, 853–858 (2007).

[147]J. G. Chen, L. W. Liu, Y. J. Liu, and J. S. Leng, "Thermoviscoelastic shape memory behavior for epoxy-shape memory polymer," Smart Mater. Struct. **23**, 055025 (2014).

[148]T. Nguyen, H. Jerryqi, F. Castro, and K. N. Long, "A thermoviscoelastic model for amorphous shape memory polymers: Incorporating structural and stress relaxation," J. Mech. Phys. Solids **56**(9), 2792–2814 (2008).

[149]S. Reese and S. Govindjee, "A theory of finite viscoelasticity and numerical aspects," Int. J. Solids Struct. **35**, 3455–3482 (1998).

[150]K. K. Westbrook, P. H. Kao, F. Castro, Y. F. Ding, and H. J. Qi, "A 3D finite deformation constitutive model for amorphous shape memory polymers: A multi-branch modeling approach for nonequilibrium relaxation processes," Mech. Mater. **43**(12), 853–869 (2011).

[151]K. Yu, A. J. W. Mcclung, G. P. Tandon, J. W. Baur, and H. J. Qi, "A thermomechanical constitutive model for an epoxy based shape memory polymer and its parameter identifications," Mech. Time-Depend. Mater. **18**(2), 453–474 (2014).

[152]F. Castro, K. K. Westbrook, K. N. Long, R. Shandas, and H. J. Qi, "Effects of thermal rates on the thermomechanical behaviors of amorphous shape memory polymers," Mech. Time-Depend. Mater. **14**(3), 219–241 (2010).

[153]V. Srivastava, S. A. Chester, N. M. Ames, and L. Anand, "A thermo-mechanically-coupled large-deformation theory for amorphous polymers in a temperature range which spans their glass transition," Int. J. Plast. **26**(8), 1138–1182 (2010).

[154]V. Srivastava, S. A. Chester, and L. Anand, "Thermally actuated shape-memory polymers: Experiments, theory, and numerical simulations," J. Mech. Phys. Solids **58**(8), 1100–1124 (2010).

[155]J. P. Gu, H. Y. Sun, and C. Q. Fang, "A finite deformation constitutive model for thermally activated amorphous shape memory polymers," J. Intell. Mater. Syst. Struct. **26**(12), 1530–1538 (2015).

[156]J. P. Gu, J. S. Leng, and H. Y. Sun, "A constitutive model for amorphous shape memory polymers based on thermodynamics with internal state variables," Mech. Mater. **111**, 1–14 (2017).

[157]C. Q. Fang, J. S. Leng, H. Y. Sun, and J. P. Gu, "A multi-branch thermoviscoelastic model based on fractional derivatives for free recovery behaviors of shape memory polymers," Mech. Mater. **120**, 34–42 (2018).

[158]H. Zeng, J. S. Leng, J. P. Gu, C. X. Yin, and H. Y. Sun, "Modeling the strain rate-, hold time-, and temperature-dependent cyclic behaviors of amorphous shape memory polymers," Smart Mater. Struct. **27**(7), 075050 (2018).

[159]H. Zeng, J. S. Leng, J. P. Gu, and H. Y. Sun, "A thermoviscoelastic model incorporated with uncoupled structural and stress relaxation mechanisms for amorphous shape memory polymers," Mech. Mater. **124**, 18–25 (2018).

[160]Y. P. Liu, K. Gall, M. L. Dunn, A. R. Greenberg, and J. Diani, "Thermomechanics of shape memory polymers: Uniaxial experiments and constitutive modeling," Int. J. Plast. **22**(2), 279–313 (2006).

[161]Y. C. Chen and D. C. Lagoudas, "A constitutive theory for shape memory polymers. I. Large deformations," J. Mech. Phys. Solids **56**(5), 1752–1765 (2008).

[162]Y. C. Chen and D. C. Lagoudas, "A constitutive theory for shape memory polymers. II. A linearized model for small deformations," J. Mech. Phys. Solids **56**(5), 1766–1778 (2008).

[163]H. J. Qi, T. D. Nguyen, F. Castro, C. M. Yakackia, and R. Shandas, "Finite deformation thermo-mechanical behavior of thermally induced shape memory polymers," J. Mech. Phys. Solids **56**(5), 1730–1751 (2008).

[164]G. Barot and I. J. Rao, "Constitutive modeling of the mechanics associated with crystallizable shape memory polymers," Z. Angew. Math. Phys. **57**(4), 652–681 (2006).

[165]W. Zhao, L. W. Liu, J. S. Leng, and Y. J. Liu, "Thermo-mechanical behavior prediction of shape memory polymers based on multiplicative decompositions of the deformation gradient," Mech. Mater. **143**, 103263 (2020).

[166]P. Gilormini and J. Diani, "On modeling shape memory polymers as thermoelastic two-phase composite materials," C.R. Mec. **340**(4–5), 338–348 (2012).

[167]X. Guo, L. Liu, B. Zhou, Y. J. Liu, and J. S. Leng, "Constitutive model for shape memory polymer based on the viscoelasticity and phase transition theories," J. Intell. Mater. Syst. Struct. **27**(3), 314–323 (2015).

[168]M. Bodaghi, A. Damanpack, and W. Liao, "Triple shape memory polymers by 4D printing," Smart Mater. Struct. **27**, 065010 (2018).

[169]Y. X. Li, Y. H. He, and Z. S. Liu, "A viscoelastic constitutive model for shape memory polymers based on multiplicative decompositions of the deformation gradient," Int. J. Plast. **91**, 300–317 (2017).

[170]Z. D. Wang, D. F. Li, Z. Y. Xiong, and R. N. Chang, "Modeling thermomechanical behaviors of shape memory polymer," J. Intell. Mater. Syst. Struct. **113**(1), 651–656 (2009).

[171]S. Reese, M. Böl, and D. Christ, "Finite element-based multi-phase modeling of shape memory polymer stents," Comput. Meth. Appl. Mech. Eng. **199**(21–22), 1276–1286 (2010).

[172]B. L. Volk, D. C. Lagoudas, Y. Chen, and K. S. Whitley, "Analysis of the finite deformation response of shape memory polymers. I. Thermomechanical characterization," Smart Mater. Struct. **19**(7), 75005 (2010).

[173]B. L. Volk, D. C. Lagoudas, and D. J. Maitland, "Characterizing and modeling the free recovery and constrained recovery behavior of a polyurethane shape memory polymer," Smart Mater. Struct. **20**(9), 094004 (2011).

[174]B. L. Volk, D. C. Lagoudas, and Y. Chen, "Thermomechanical characterization of the nonlinear rate-dependent response of shape memory polymers," Proc. SPIE **6929**, 69291B (2008).

[175]Q. Yang and G. Li, "Temperature and rate dependent thermomechanical modeling of shape memory polymers with physics based phase evolution law," Int. J. Plast. **80**, 168–186 (2016).

[176]J. H. Kim, T. J. Kang, and W. Yu, "Thermo-mechanical constitutive modeling of shape memory polyurethanes using a phenomenological approach," Int. J. Plast. **26**(2), 204–218 (2010).

[177]H. Park, P. Harrison, Z. Y. Guo, M. G. Lee, and W. R. Yu, "Three-dimensional constitutive model for shape memory polymers using multiplicative decomposition of the deformation gradient and shape memory strains," Mech. Mater. **93**, 43–62 (2016).

[178]J. M. Guo, J. B. A. Liu, Z. Q. Wang, X. F. He, L. F. Hu, L. Y. Tong, and X. J. Tang, "A thermodynamics viscoelastic constitutive model for shape memory polymers," J. Alloys Compd. **705**, 146–155 (2017).

[179]H. Lu, X. Wang, Y. Yao, and Y. Q. Fu, "A 'frozen volume' transition model and working mechanism for the shape memory effect in amorphous polymers," Smart Mater. Struct. **27**(6), 065023 (2018).

[180]R. Bouaziz, F. Roger, and K. Prashantha, "Thermomechanical modeling of semi-crystalline thermoplastic shape memory polymer under large strain," Smart. Mater. Struct. **26**, 055009 (2017).

[181]Z. Pan and Z. Liu, "A novel fractional viscoelastic constitutive model for shape memory polymers," J. Polym. Sci., Part B **56**, 1125–1134 (2018).

[182]G. Scalet, F. Auricchio, E. Bonetti, L. Castellani, D. Ferri, M. Pachera, and F. Scavello, "An experimental, theoretical and numerical investigation of shape memory polymers," Int. J. Plast. **67**, 127–147 (2015).

[183]A. I. Arvanitakis, "A constitutive level-set model for shape memory polymers and shape memory polymeric composites," Arch. Appl. Mech. **89**(9), 1939–1951 (2019).

[184]Q. S. Yang, X. Q. He, X. Liu, F. F. Leng, and Y. W. Mai, "The effective properties and local aggregation effect of CNT/SMP composites," Compos. Part B **43**, 33–38 (2012).

[185]C. Jaralia, M. Madhusudan, S. Vidyashankarc, and S. Rajaa, "A new micromechanics approach to the application of Eshelby's equivalent inclusion method in three phase composites with shape memory polymer matrix," Compos. Part B **152**, 17–30 (2018).

[186]W. Zhao, L. W. Liu, J. S. Leng, and Y. J. Liu, "Thermo-mechanical behavior prediction of particulate reinforced shape memory polymer composite," Compos. Part B **179**, 107455 (2019).

[187]N. F. Dow and B. W. Rosen, "Evaluations of filament-reinforced composites for aerospace structural applications," Report No. ADA305442 (General Electric Co., Philadelphia, PA, 1965), available at https://apps.dtic.mil/sti/citations/ADA305442.

[188]S. P. Timoshenko and J. M. Gere, *Theory of Elastic Stability* (Courier Dover Publications, 2009).

[189]D. Campbell, M. S. Lake, and K. Mallick, "A study of the compression mechanics of soft-resin composites," AIAA Paper No. 2004-1636, 2004.

[190]D. Campbell and A. Maji, "Failure mechanisms and deployment accuracy of elastic-memory composites," J. Aerosp. Eng. **19**(3), 184–193 (2006).

[191]D. Campbell and A. Maji, "Deployment precision and mechanics of elastic memory composites," AIAA Paper No. 2003-1495, 2003.

[192]Z. D. Wang, Z. Y. Xiong, Z. F. Li, and R. N. Chang, "Micromechanism of deformation in EMC laminates," Mater. Sci. Eng., A **496**(1), 323–328 (2008).

[193]X. Lan, L. Liu, Y. Liu *et al.*, "Post microbuckling mechanics of fiber-reinforced shape-memory polymers undergoing flexure deformation," Mech. Mater. **72**, 46–60 (2014).

[194]Q. Tan, L. W. Liu, Y. J. Liu, and J. S. Leng, "Post buckling analysis of the shape memory polymer composite laminate bonded with alloy film," Compos. Part B **53**, 218–225 (2013).

[195]W. Francis, M. Lake, M. Schultz, D. Campbell, M. Dumn, and H. J. Qi, "Elastic memory composite microbuckling mechanics: closed-form model with empirical correlation," AIAA Paper No. 2007-2164, 2007.

[196]W. H. Francis and M. S. Lake, "A review of classical fiber microbuckling analytical solutions for use with elastic memory composites," AIAA Paper No. 2006-1764, 2006.

[197]E. R. Abrahamson and M. S. Lake, "Shape memory mechanics of an elastic memory composite resin," J. Intell. Mater. Syst. Struct. **14**, 623–632 (2003).

[198]D. Campbell and A. Maji, "Failure mechanisms in the folding of unidirectional soft-resin composites," in *Proceedings of the Society for Experimental Mechanics SEM Annual Conference and Exposition of Experimental and Applied Mechanics* (Society for Experimental Mechanics, Charlotte, NC, 2003), pp. 1–10.

[199]M. R. Schultz, W. H. Francis, D. Campbell, and M. S. Lake, "Analysis techniques for shape-memory composites structure," AIAA Paper No. 2007-2401, 2007, p. 2401.

[200]K. Miura and Y. Miyazaki, "Concept of the tension truss antenna," AIAA J. **28**(6), 1098–1104 (1990).

[201]S. C. Arzberger, M. L. Tupper, M. S. Lake, R. Barrett, K. Mallick, and C. Hazelton, "Elastic memory composites (EMC) for deployable industrial and commercial applications," Proc. SPIE **5762**, 35–47 (2005).

[202]D. Campbell, M. S. Lake, M. S. Scherbarth, E. Nelson, and R. W. Six, "Elastic memory composite material: An enabling technology for future furlable space structures," AIAA Paper No. 2005-2362, 2005, pp. 18–21.

[203]M. S. Robert, J. P. Emil, W. T. Eric, and M. H. Jason, "Veritex (TM) struts for antenna application," AIAA Paper No. 2006-2038, 2006, pp. 1–4.

[204]X. Lan, Y. J. Liu, H. B. Lv, X. H. Wang, J. S. Leng, and S. Y. Du, "Fiber reinforced shape memory polymer composite and its application in a deployable hinge," Smart Mater. Struct. **18**(2), 024002 (2009).

[205]R. Zhang, X. Guo, Y. Liu, and J. S. Leng, "Theoretical analysis and experiments of a space deployable truss structure," Compos. Struct. **112**, 226–230 (2014).

[206]F. F. Li, L. W. Liu, L. Z. Du, Y. J. Liu, and J. S. Leng, "Mechanical analysis of a tip-loaded deployable truss based on shape memory polymer composite," Compos. Struct. **242**, 112196 (2020).

[207]Q. Chen, Z. Yao, Y. Hou, and H. Fang, "Design and testing of a space deployable mechanism," AIAA Paper No. 2017-0716, 2017.

[208]A. Rakow, K. Hedin, and B. Anthony, "Development of high specific power solar arrays with shape memory polymer hinge lines," AIAA Paper No. 2018-2206, 2018.

[209]X. Lan, L. W. Liu, F. H. Zhang, Z. X. Liu, L. L. Wang, Q. F. Li, F. Peng, S. D. Hao, W. X. Dai, X. Wan, Y. Tang, M. Wang, Y. Y. Hao, Y. Yang, C. Yang, Y. J. Liu, and J. S. Leng, "World's first spaceflight on-orbit demonstration of a flexible solar array system based on shape memory polymer composites," Sci. China-Technol. Sci. **63**, 1436–1451 (2020).

[210]A. W. Love, "Some highlights in reflector antenna development," Radio Sci. **11**, 671–684, https://doi.org/10.1029/RS011i008p00671 (1976).

[211]J. Huang, H. F. Fang, R. Lovick, and M. Lou, "The development of large flat inflatable antenna for deep-space communications," AIAA Paper No. 2004-6112, 2004.

[212]S. C. Arzberger, N. A. Munshia, M. S. Lakea, J. Wintergerst, S. J. Varlese, and M. P. Ulmer, "Elastic memory composite technology for thin, lightweight space and ground-based deployable mirrors," Proc. SPIE **5179**, 143–154 (2003).

[213]S. J. Varlese and L. R. Hardaway, "Laminated electroformed shape memory composite for deployable light weight optics," Proc. SPIE **5542**, 375–383 (2004).

[214]W. Francis, M. Lake, J. Hinkle, and L. Peterson, "Development of an EMC self-locking linear actuator for deployable optics," AIAA Paper No. 2004-1821, 2004, pp. 19–22.

[215]P. N. Keller, M. S. Lake, D. Codell, R. Barrett, R. Taylor, and M. R. Schultz, "Development of elastic memory composite stiffeners for a flexible precision reflector," AIAA Paper No. 2006-2179, 2006, p. 2179.

[216]J. K. H. Lin, C. F. Knoll, and C. E. Willey, "Shape memory rigidizable inflatable (Ri) structures for large space systems applications," AIAA Paper No. 2006-1896, 2006, pp. 1–4.

[217]F. F. Li, L. W. Liu, X. Lan, C. T. Pan, Y. J. Liu, J. S. Leng, and Q. Xie, "Ground and geostationary orbital qualification of a sunlight-stimulated substrate based on shape memory polymer composite," Smart Mater. Struct. **28**(7), 075023 (2019).

[218]Z. X. Liu, Q. F. Li, W. F. Bian, X. Lan, Y. J. Liu, and J. S. Leng, "Preliminary test and analysis of an ultralight lenticular tube based on shape memory polymer composites," Compos. Struct. **223**, 110936 (2019).

[219]D. W. Zhang, O. J. George, K. M. Petersen, A. C. Jimenez-Vergara, M. S. Hahn, and M. A. Grunlan, "A bioactive 'self-fitting' shape memory polymer scaffold with potential to treat cranio-maxillo facial bone defects," Acta Biomater. **10**(11), 4597–4605 (2014).

[220]X. Liu, K. Zhao, T. Gong, J. Song, C. Y. Bao, E. Luo, J. Weng, and S. B. Zhou, "Delivery of growth factors using a smart porous nanocomposite scaffold to repair a mandibular bone defect," Biomacromolecules **15**(3), 1019–1030 (2014).

[221]P. Rychter, E. Pamula, A. Orchel, U. Posadowska, M. Krok-Borkowicz, A. Kaps, N. Smigiel-Gac, A. Smola, J. Kasperczyk, W. Prochwicz, and P. Dobrzynski, "Scaffolds with shape memory behavior for the treatment of large bone defects," J. Biomed. Mater. Res. Part A **103**, 3503 (2015).

[222]F. S. Senatov, K. V. Niaza, M. Y. Zadorozhnyy, A. V. Maksimkin, S. D. Kaloshkin, and Y. Z. Estrin, "Mechanical properties and shape memory effect of 3D-printed PLA-based porous scaffolds," J. Mech. Behav. Biomed. Mater. **57**, 139–148 (2016).

[223]F. H. Zhang, L. L. Wang, Z. C. Zheng, Y. J. Liu, and J. S. Leng, "Magnetic programming of 4D printed shape memory composite structures," Compos. Part A **125**, 105571 (2019).

[224]H. Tamai, K. Igaki, E. Kyo, K. Kosuga, A. Kawashima, S. Matsui, H. Komori, T. Tsuji, S. Motohara, and H. Uehata, "Initial and 6-month results of biodegradable poly-l-lactic acid coronary stents in humans," Circulation **102**(4), 399–404 (2000).

[225]R. J. Morrison, S. J. Hollister, M. F. Niedner, M. G. Mahani, A. H. Park, D. K. Mehta, R. G. Ohye, and G. E. Greer, "Mitigation of tracheobronchomalacia with 3D-printed personalized medical devices in pediatric patients," Sci. Transl. Med. **7**(285), 285ra64 (2015).

[226]D. A. Zopf, C. L. Flanagan, M. Wheeler, J. H. Scott, and E. G. Glenn, "Treatment of severe porcine tracheomalacia with a 3-dimensionally printed, bioresorbable, external airway splint," JAMA Otolaryngol. **140**(1), 66–71 (2014).

[227]D. A. Zopf, S. J. Hollister, M. E. Nelson, R. G. Ohye, and G. E. Green, "Bioresorbable airway splint created with a three-dimensional printer," Sci. Transl. Med. **368**(21), 2043–2045 (2013).

[228]M. Zarek, N. Mansour, S. Shapira, and D. Cohn, "4D printing of shape memory-based personalized endoluminal medical devices," Macromol. Rapid Commun. **38**, 1600628 (2017).

[229]H. Q. Wei, Q. W. Zhang, Y. T. Yao, L. W. Liu, Y. J. Liu, and J. S. Leng, "Direct-write fabrication of 4D active shape-changing structures based on a shape memory polymer and its nanocomposite," ACS Appl. Mater. Interfaces **9**(1), 876–883 (2017).

[230]T. Kim and Y. Lee, "Shape transformable bifurcated stents," Sci. Rep. **8**, 13911 (2018).

[231]D. Liu, T. Xiang, T. Gong, T. Tian, X. Liu, and S. Zhou, "Bioinspired 3D multilayered shape memory scaffold with a hierarchically changeable micropatterned surface for efficient vascularization," ACS Appl. Mater. Interfaces **9**(23), 19725–19735 (2017).

[232]W. Zhao, F. H. Zhang, J. S. Leng, and Y. J. Liu, "Personalized 4D printing of bioinspired tracheal scaffold concept based on magnetic stimulated shape memory composites," Compos. Sci. Technol. **184**, 107866 (2019).

[233]W. Zhao, N. Li, L. W. Liu, J. S. Leng, and Y. J. Liu, "Origami derived self-assembly stents fabricated via 4D printing," Compos. Struct. **293**, 115669 (2022).

[234]W. M. Huang, C. L. Song, Y. Q. Fu, C. C. Wang, Y. Zhao, H. Purnawali, B. H. Lu, C. Tang, Z. Ding, and J. L. Zhang, "Shaping tissue with shape memory materials," Adv. Drug Delivery Rev. **65**(4), 515–535 (2013).

[235]Y. Niimi, J. Song, M. Madrid, and A. Berenstein, "Endosaccular treatment of intracranial aneurysms using matrix coils-early experience and midterm follow-up," Stroke **37**(4), 1028–1032 (2006).

[236]J. M. Hampikian, B. C. Heaton, F. C. Tong, Z. Q. Zhang, and C. P. Wong, "Mechanical and radiographic properties of a shape memory polymer composite for intracranial aneurysm coils," Mater. Sci. Eng., C **26**(8), 1373–1379 (2006).

[237]A. Metcalfe, A. C. Desfaits, I. Salazkin, L. Yahia, W. M. Sokolowski, and J. Raymond, "Cold hibernated elastic memory foams for endovascular interventions," Biomaterials **24**, 491 (2003).

[238]A. D. Lantada, P. Lafont, I. Rada, A. Jimenez, J. L. Hernandez, H. Lorenzo-Yustos, and J. Munoz-Garcia, "Active annuloplasty system for mitral valve insufficiency," in *Biostec, Biomedical Engineering Systems and Technologies* (Springer, Berlin, Heidelberg, 2008), Vol. 25, pp. 59–72.

[239]C. Lin, J. Lv, Y. Li, F. H. Zhang, J. R. Li, Y. J. Liu, and L. W. Liu, "4D-printed biodegradable and remotely controllable shape memory occlusion devices," Adv. Funct. Mater. **29**(51), 1906569 (2019).

[240]W. Zhao, L. W. Liu, X. Lan, B. Su, J. S. Leng, and Y. J. Liu, "Adaptive repair device concept with shape memory polymer," Smart Mater. Struct. **26**(2), 025027 (2017).

[241]M. C. Everhart and J. Stahl, "Reusable shape memory polymer mold," Proc. SPIE **5762**, 27–34 (2005).

[242]L. Zhang, H. Y. Du, L. W. Liu, Y. J. Liu, and J. S. Leng, "Analysis and design smart mold using shape memory polymers," Compos. Part B **59**, 230–237 (2014).

[243]H. Y. Du, L. W. Liu, F. H. Zhang, J. S. Leng, and Y. J. Liu, "Triple-shape memory effect in a styrene-based shape memory polymer: Characterization," Compos. Part B **173**, 106905 (2019).

[244]J. Wang, Q. L. Zhao, H. Q. Cui, Y. L. Wang, H. X. Chen, and X. M. Du, "Tunable shape memory polymer mold for multiple microarray replications," J. Mater. Chem. A **6**, 24748 (2018).

[245]M. Lucy, R. Hardy, E. Kist, J. Watson, and S. Wise, "Report on alternative devices to pyrotechnics on spacecraft," National Aeronautics and Space Administration Langley Research Center, Paper No. NASA-TM-110470, 1996. https://apps.dtic.mil/sti/citations/ADA327677

[246]W. Huang, "On the selection of shape memory alloys for actuators," Mater. Des. **23**(1), 11–19 (2002).

[247]K. GallMark, L. Mark, L. J. Harvey, and E. Ricca, "Development of a shockless thermally actuated release nut using elastic memory composite material," AIAA Paper No. 2003-1582, 2003, pp. 20191–4344.

[248]H. Q. Wei, L. W. Liu, Z. C. Zhang, H. Y. Du, Y. J. Liu, and J. S. Leng, "Design and analysis of smart release devices based on shape memory polymer composites," Compos. Struct. **133**, 642–651 (2015).

[249]H. X. Zhao, X. Lan, L. W. Liu, Y. J. Liu, and J. S. Leng, "Design and analysis of shockless smart releasing device based on shape memory polymer composites," Compos. Struct. **223**, 110958 (2019).

[250]D. Zhang, L. W. Liu, J. S. Leng, and Y. J. Liu, "Ultra-light release device integrated with screen-printed heaters for CubeSat's deployable solar arrays," Compos. Struct. **232**, 111561 (2020).